ANSYS FLUENT 12.0

Validation Guide

April 2009

VISIT…

LANZAROTE Caliente.com

Copyright © 2009 by ANSYS, Inc.
All Rights Reserved. No part of this document may be reproduced or otherwise used in any form without express written permission from ANSYS, Inc.

Airpak, Mechanical APDL, Workbench, AUTODYN, CFX, FIDAP, FloWizard, FLUENT, GAMBIT, Iceboard, Icechip, Icemax, Icepak, Icepro, Icewave, MixSim, POLYFLOW, TGrid, and any and all ANSYS, Inc. brand, product, service and feature names, logos and slogans are registered trademarks or trademarks of ANSYS, Inc. or its subsidiaries located in the United States or other countries. All other brand, product, service and feature names or trademarks are the property of their respective owners.

CATIA V5 is a registered trademark of Dassault Systèmes. CHEMKIN is a registered trademark of Reaction Design Inc.

Portions of this program include material copyrighted by PathScale Corporation 2003-2004.

ANSYS, Inc. is certified to ISO 9001:2008

See the on-line documentation for the complete Legal Notices for ANSYS proprietary software and third-party software. If you are unable to access the Legal Notice, contact ANSYS, Inc.

Contents

Introduction **Introduction-1**

1 Flow in a Rotating Cavity **1-1**

1.1 Purpose 1-1
1.2 Problem Description 1-1
1.3 References 1-1
1.4 Results 1-3
1.4.1 Validation-Specific Information 1-3
1.4.2 Plot Data 1-4

2 Natural Convection in an Annulus **2-1**

2.1 Purpose 2-1
2.2 Problem Description 2-1
2.3 References 2-2
2.4 Results 2-2
2.4.1 Validation-Specific Information 2-3
2.4.2 Plot Data 2-3

3 Flow in a 90° Planar Tee-Junction **3-1**

3.1 Purpose 3-1
3.2 Problem Description 3-1
3.3 References 3-1
3.4 Results 3-3
3.4.1 Validation-Specific Information 3-3
3.4.2 Plot Data 3-4

4 Flows in Driven Cavities 4-1

4.1 Purpose 4-1

4.2 Problem Description 4-1

4.3 References 4-1

4.4 Results 4-1

4.4.1 Trapezoidal Cavity 4-1

4.4.2 Triangular Cavity 4-1

4.4.3 Validation-Specific Information 4-3

4.4.4 Plot Data 4-4

5 Periodic Flow in a Wavy Channel 5-1

5.1 Purpose 5-1

5.2 Problem Description 5-1

5.3 References 5-1

5.4 Results 5-2

5.4.1 Validation-Specific Information 5-2

5.4.2 Plot Data 5-3

6 Heat Transfer in a Pipe Expansion 6-1

6.1 Purpose 6-1

6.2 Problem Description 6-1

6.3 References 6-2

6.4 Results 6-2

6.4.1 Validation-Specific Information 6-3

6.4.2 Plot Data 6-3

7 Propane Jet in a Coaxial Air Flow 7-1

7.1 Purpose 7-1

7.2 Problem Description 7-1

7.3 References 7-1

Release 12.0 © ANSYS, Inc. January 24, 2009

7.4 Results 7-3
7.4.1 Validation-Specific Information 7-3
7.4.2 Plot Data 7-4

8 Flow through an Engine Inlet Valve 8-1
8.1 Purpose 8-1
8.2 Problem Description 8-1
8.3 References 8-2
8.4 Results 8-2
8.4.1 Validation-Specific Information 8-2
8.4.2 Plot Data 8-3

9 Turbulent Flow in a Transition Duct 9-1
9.1 Purpose 9-1
9.2 Problem Description 9-1
9.3 References 9-1
9.4 Results 9-3
9.4.1 Validation-Specific Information 9-3
9.4.2 Plot Data 9-4

10 Transonic Flow Over an RAE 2822 Airfoil 10-1
10.1 Purpose 10-1
10.2 Problem Description 10-1
10.3 References 10-2
10.4 Results 10-2
10.4.1 Validation-Specific Information 10-3
10.4.2 Plot Data 10-4

11 Mid-Span Flow Over a Goldman Stator Blade 11-1
11.1 Purpose 11-1
11.2 Problem Description 11-1

11.3 References 11-1
11.4 Results 11-3
11.4.1 Validation-Specific Information 11-3
11.4.2 Plot Data 11-4

12 Reflecting Shock Waves **12-1**
12.1 Purpose 12-1
12.2 Problem Description 12-1
12.3 References 12-2
12.4 Results 12-2
12.4.1 Validation-Specific Information 12-2
12.4.2 Plot Data 12-3

13 Turbulent Bubbly Flows **13-1**
13.1 Purpose 13-1
13.2 Problem Description 13-1
13.3 References 13-1
13.4 Results 13-1
13.4.1 Validation-Specific Information 13-3
13.4.2 Plot Data 13-4

14 Adiabatic Compression and Expansion Inside an Idealized 2D Piston-Cylinder Engine **14-1**
14.1 Purpose 14-1
14.2 Problem Description 14-1
14.3 Results 14-2
14.3.1 Validation-Specific Information 14-3
14.3.2 Plot Data 14-3

 Release 12.0 © ANSYS, Inc. January 24, 2009

15 Cavitation Over a Sharp-Edged Orifice **15-1**
15.1 Purpose . . . 15-1
15.2 Problem Description . . . 15-1
15.3 References . . . 15-2
15.4 Results . . . 15-2
15.4.1 Validation-Specific Information . . . 15-2
15.4.2 Plot Data . . . 15-4

16 Oscillating Laminar Flow Around a Circular Cylinder **16-1**
16.1 Purpose . . . 16-1
16.2 Problem Description . . . 16-1
16.3 References . . . 16-2
16.4 Results . . . 16-2
16.4.1 Validation-Specific Information . . . 16-3
16.4.2 Plot Data . . . 16-3

17 Rotation of Two Immiscible Liquids **17-1**
17.1 Purpose . . . 17-1
17.2 Problem Description . . . 17-1
17.3 References . . . 17-1
17.4 Results . . . 17-3
17.4.1 Validation-Specific Information . . . 17-3
17.4.2 Plot Data . . . 17-4

18 Polyhedral and Tetrahedral Mesh Accuracy **18-1**
18.1 Purpose . . . 18-1
18.2 Problem Description . . . 18-1
18.3 References . . . 18-1
18.4 Results . . . 18-1
18.4.1 Validation-Specific Information . . . 18-2

18.4.2 Plot Data 18-4

19 Methane Jet Combustion in a Swirling Annular Shroud 19-1

19.1 Purpose 19-1

19.2 Problem Description 19-1

19.3 References 19-1

19.4 Results 19-1

19.4.1 Validation-Specific Information 19-3

19.4.2 Plot Data 19-4

20 Inviscid High Pressure Hydrogen Flow with Real Gas Effects 20-1

20.1 Purpose 20-1

20.2 Problem Description 20-1

20.3 References 20-2

20.4 Results 20-2

20.4.1 Validation-Specific Information 20-2

20.4.2 Plot Data 20-3

Release 12.0 © ANSYS, Inc. January 24, 2009

Introduction

The Contents of This Manual

The ANSYS FLUENT Validation Manual contains a number of validations that compare the results obtained with ANSYS FLUENT against experimental data.

Each Validation is organized to present the purpose of the validation, the problem description, references, and results.

Where to Find the Solution Files for the Validations

Solution files are listed in the Validation-Specific Information section for each validation. These solution files can be used to determine the details of solution settings used for the validation.

Solution files for the validations are available for download from the User Services Center (`www.fluentusers.com`). Click on the Documentation link on the ANSYS FLUENT product page, then on the Validation Solution Files link on the documentation page, and select the file to download. Unzip the file in a working directory and the solution files will be available to read into ANSYS FLUENT.

Release 12.0 © ANSYS, Inc. January 24, 2009

Validation 1. Flow in a Rotating Cavity

1.1 Purpose

The purpose of this validation is to compare numerical values of swirl and radial velocity in a rotating cavity with experimental data [2].

1.2 Problem Description

An enclosed cylindrical cavity of height $L = 1.0$ m and radius $R = 1.0$ m has a lid that spins at $\Omega = 1.0$ rad/s, as shown in Figure 1.2.1. The flow field is 2D axisymmetric, so only the region bounded by the dashed lines in Figure 1.2.1 needs to be modeled. The Reynolds number of the flow based on the cavity radius R and the tip-speed of the disk (ΩR) is 1800. The flow within the cavity is assumed to be laminar. The problem can be solved using either a stationary reference frame or a rotating reference frame.

1.3 References

1. Sorensen, J.N. and Loc, T.P., Higher-Order Axisymmetric Navier-Stokes Code: Description and Evolution of Boundary Conditions, *International Journal For Numerical Methods in Fluids*, 9:1517–1537, 1989.

2. Michelsen, J. A., *Modeling of Laminar Incompressible Rotating Fluid Flow*, AFM 86-05, Ph.D. thesis, Department of Fluid Mechanics, Technical University of Denmark, 1986.

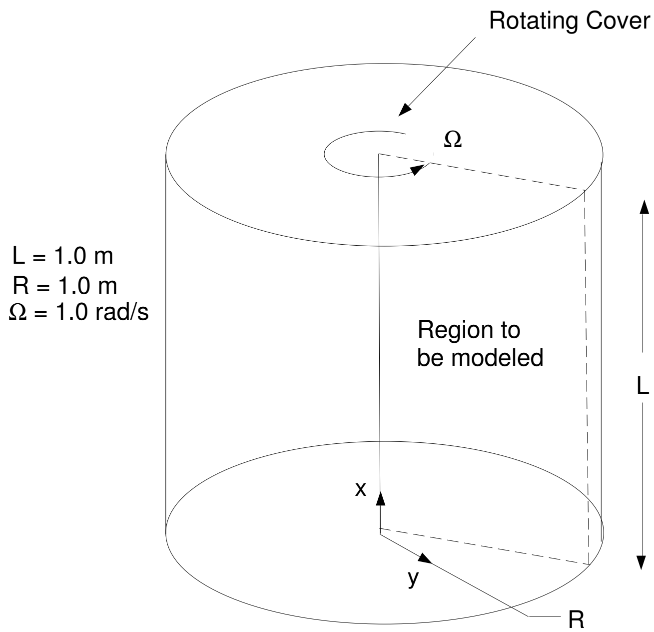


Figure 1.2.1: Problem Description

Release 12.0 © ANSYS, Inc. January 24, 2009

1.4 Results

Figures 1.4.1 - 1.4.4 compare the computed swirl and radial velocity profiles with measured data at $y = 0.6$ m (for both the stationary and the rotating reference frame). Figures 1.4.5 - 1.4.8 compare the computed and measured velocities at $y = 0.9$ m. The computed velocities in the rotating frame were transformed to the stationary reference frame of the measured data. The results obtained with ANSYS FLUENT match the measured velocity profiles and reproduce accurately the sharp gradients in swirl and radial velocity in the region of $x = 0.9$ m. The results show that the PRESTO! discretization scheme for pressure and QUICK discretization scheme for momentum and swirl velocity, produces good agreement with the data using a 41×41 non-uniform grid.

1.4.1 Validation-Specific Information

Solver:	ANSYS FLUENT 2D Double Precision
Version:	6.4.13
Solution Files:	1. `rotcv_r1.cas`, `rotcv_r1.dat` - stationary
	2. `rotcv_r2.cas`, `rotcv_r2.dat` - moving

These solution files are available from the User Services Center as described in the Introduction.

1.4.2 Plot Data

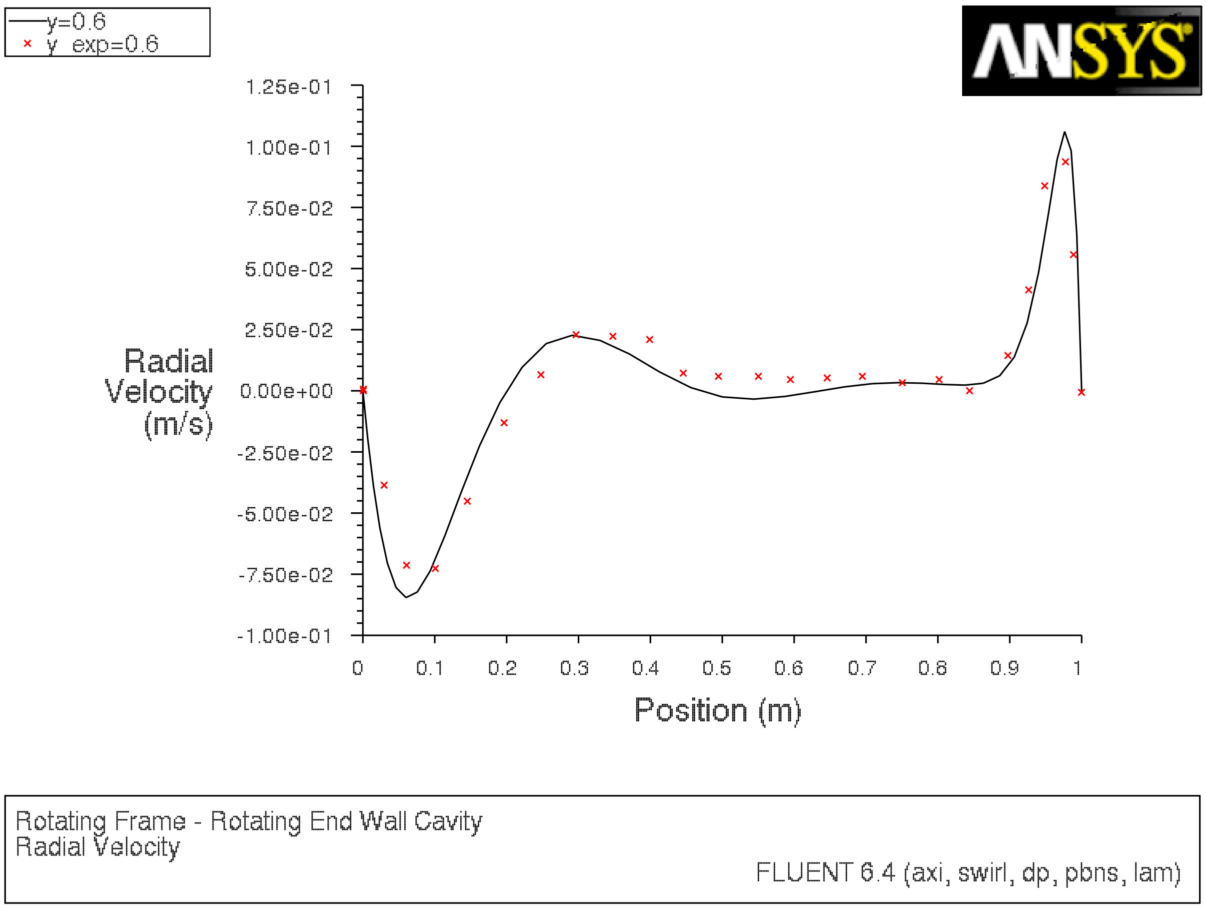


Figure 1.4.1: Comparison of Computed Radial Velocity Profile with Measured Data at $y = 0.6$ m (Rotating Reference Frame)

Release 12.0 © ANSYS, Inc. January 24, 2009

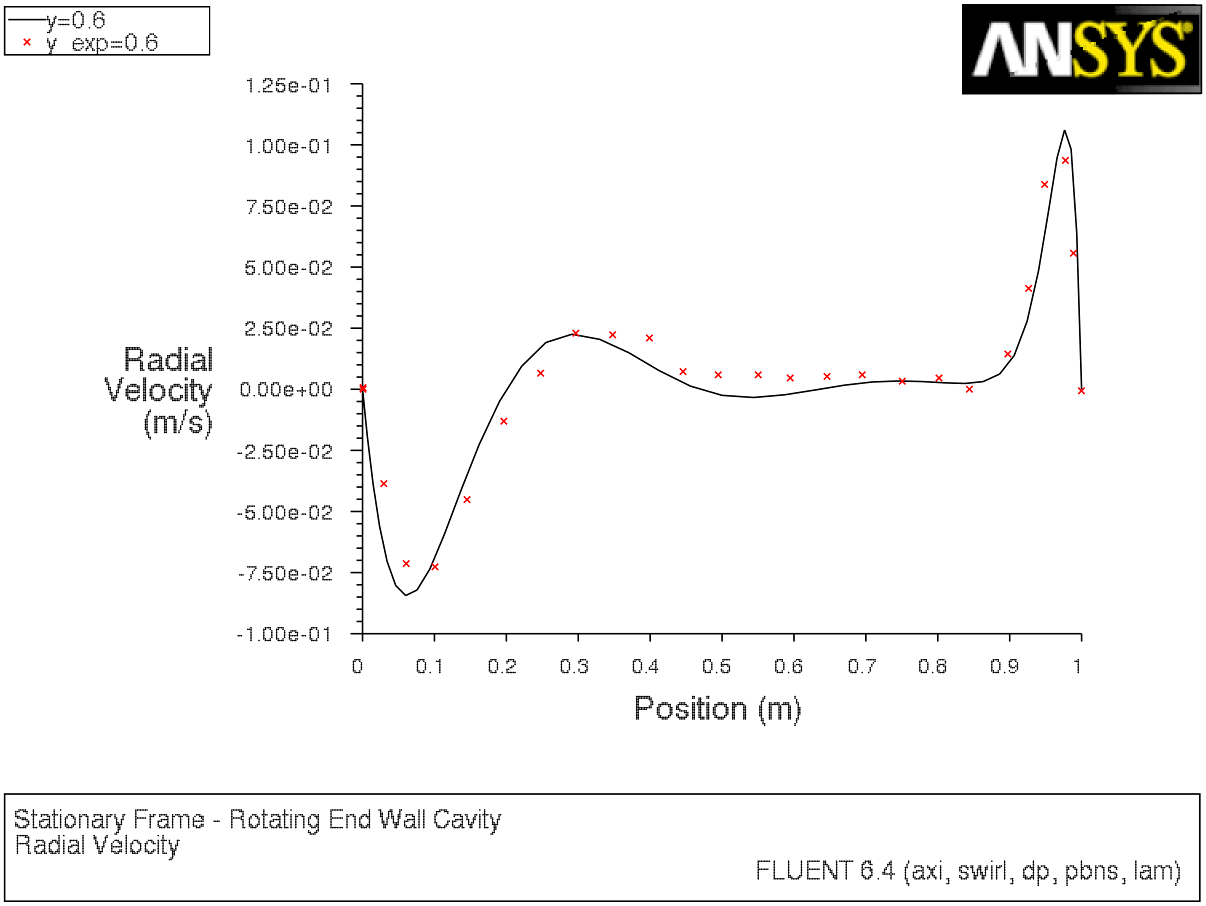


Figure 1.4.2: Comparison of Computed Radial Velocity Profile with Measured Data at $y = 0.6$ m (Stationary Reference Frame)

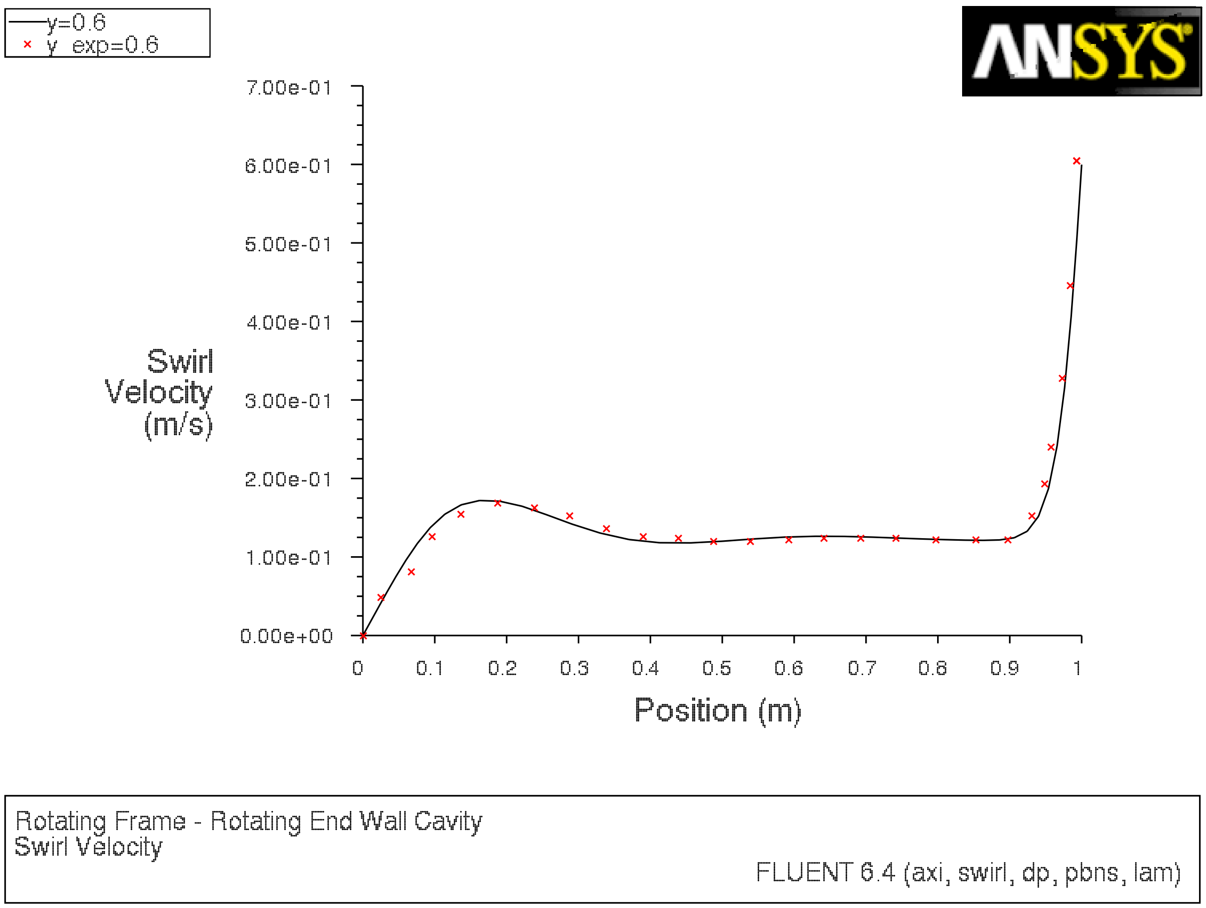


Figure 1.4.3: Comparison of Computed Swirl Velocity Profile with Measured Data at $y = 0.6$ m (Rotating Reference Frame)

Release 12.0 © ANSYS, Inc. January 24, 2009

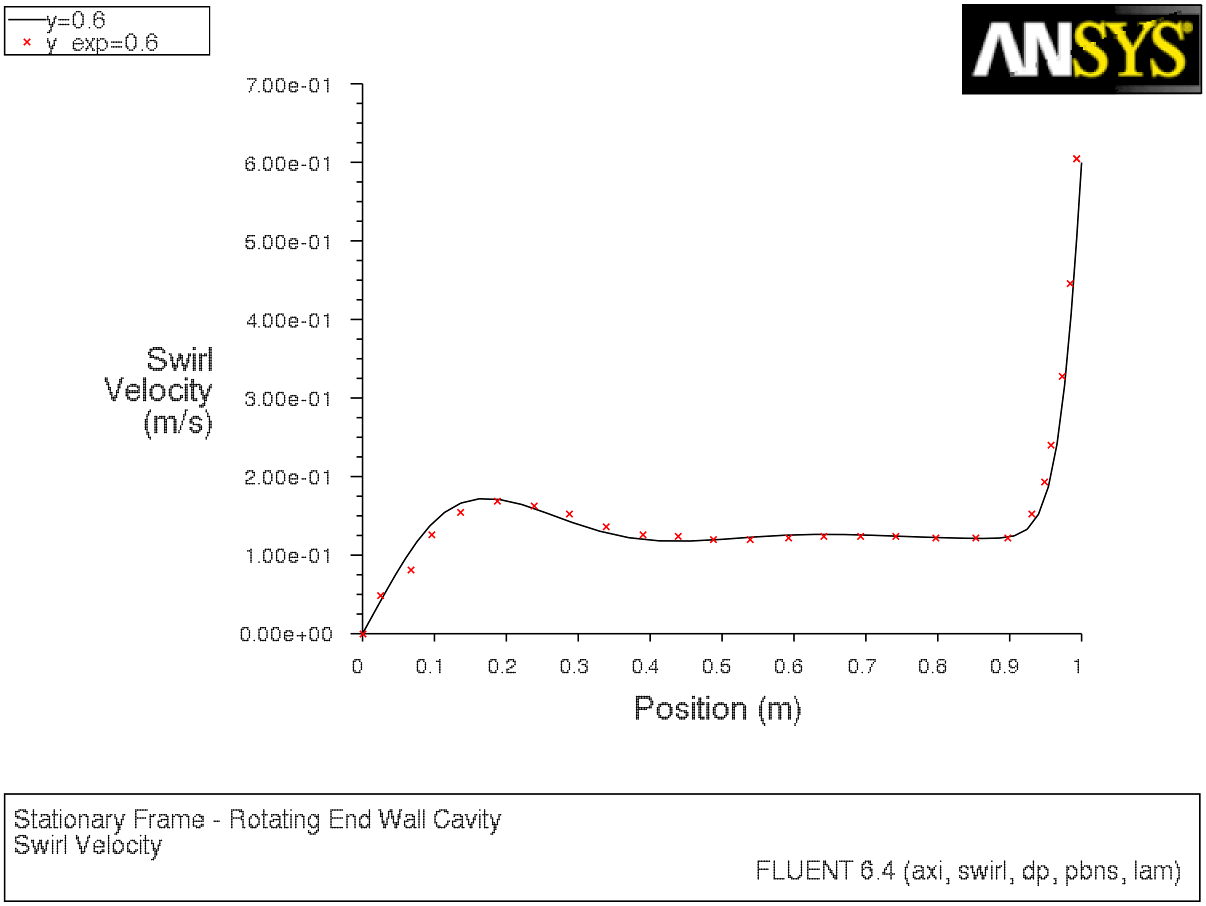


Figure 1.4.4: Comparison of Computed Swirl Velocity Profile with Measured Data at $y = 0.6$ m (Stationary Reference Frame)

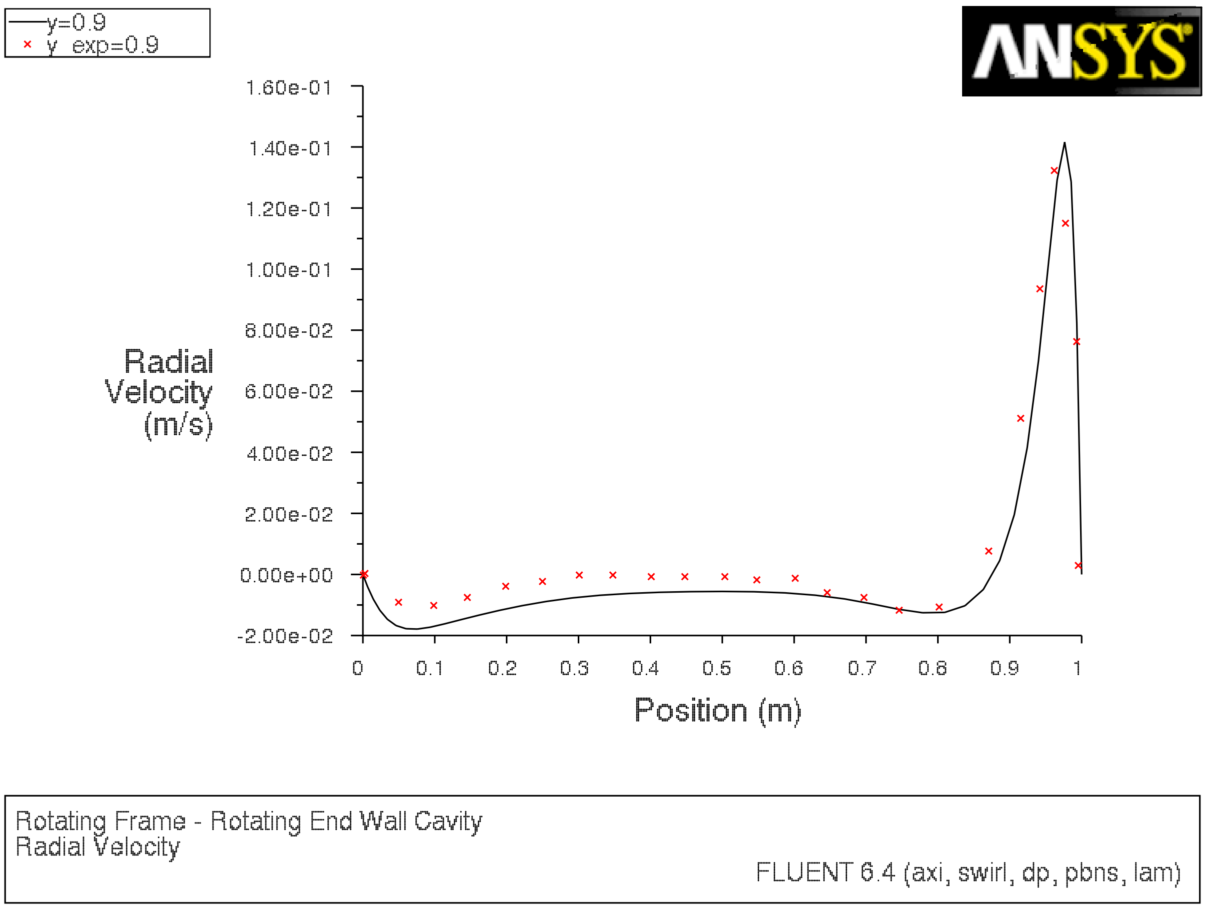


Figure 1.4.5: Comparison of Computed Radial Velocity Profile with Measured Data at $y = 0.9$ m (Rotating Reference Frame)

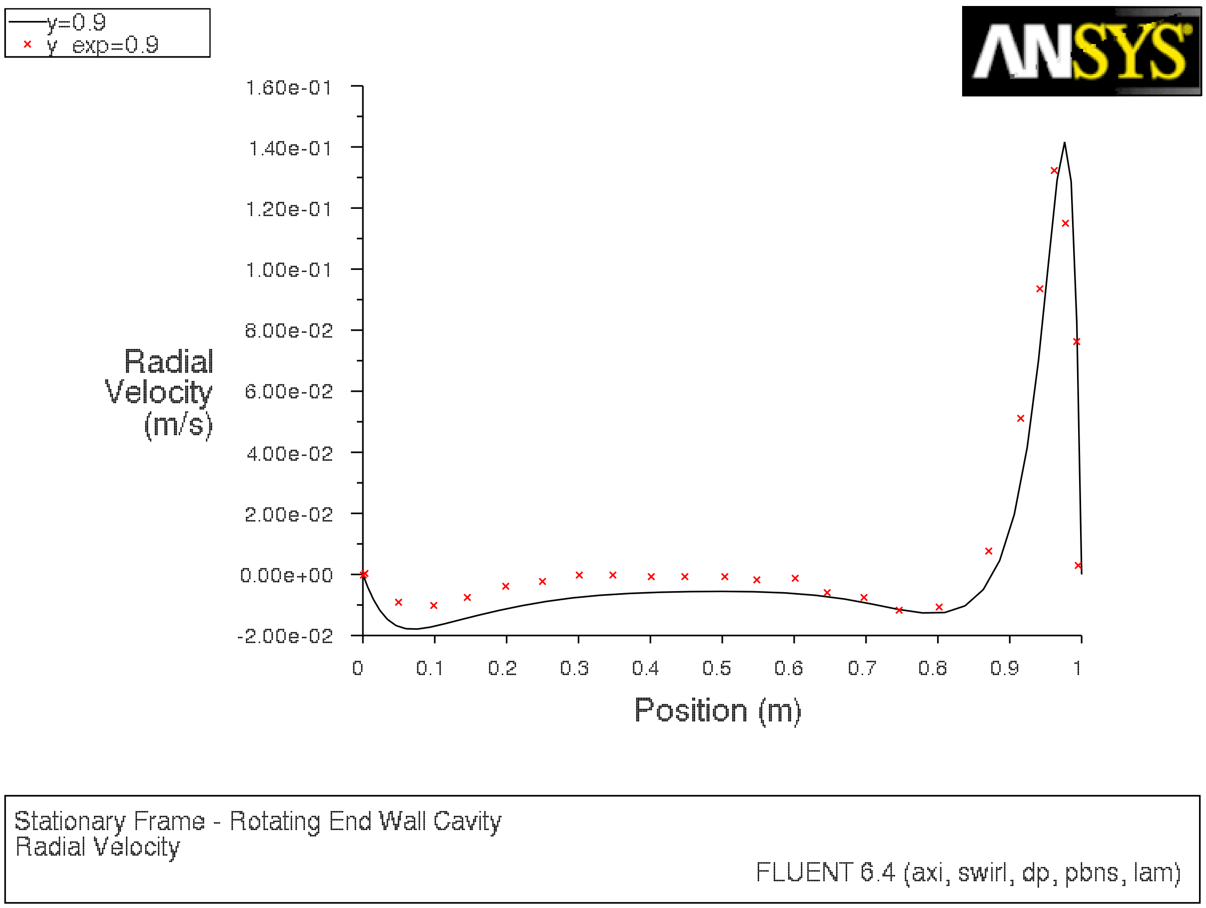


Figure 1.4.6: Comparison of Computed Radial Velocity Profile with Measured Data at $y = 0.9$ m (Stationary Reference Frame)

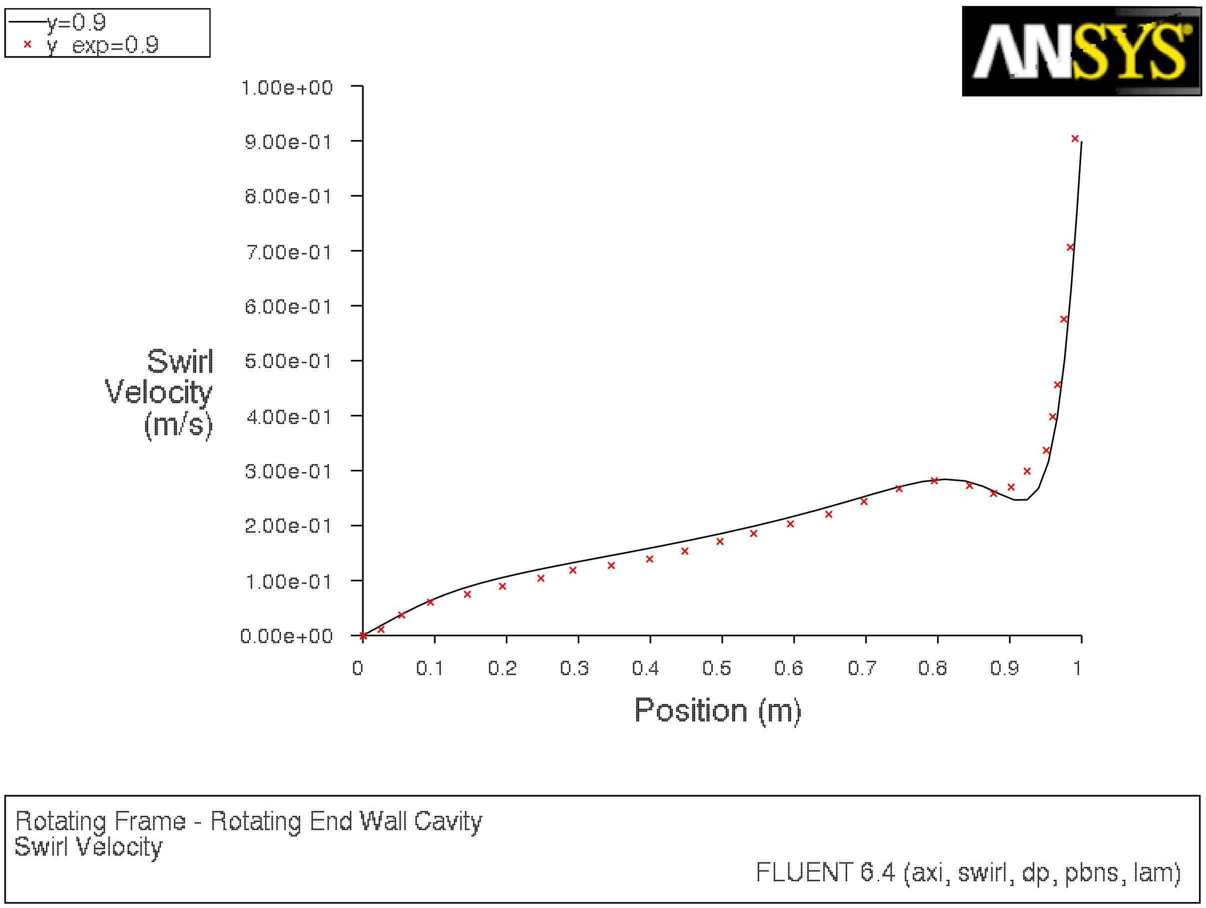


Figure 1.4.7: Comparison of Computed Swirl Velocity Profile with Measured Data at $y = 0.9$ m (Rotating Reference Frame)

Release 12.0 © ANSYS, Inc. January 24, 2009

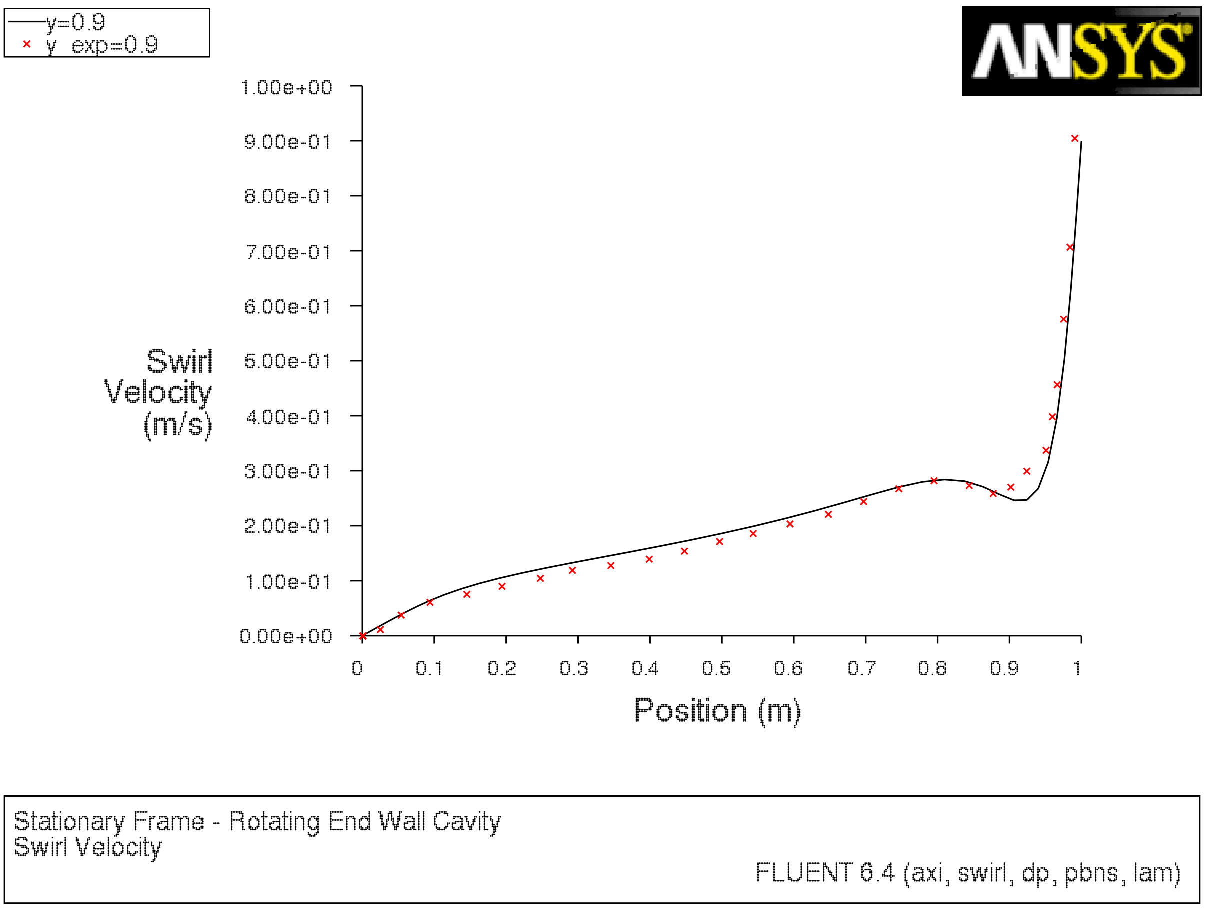


Figure 1.4.8: Comparison of Computed Swirl Velocity Profile with Measured Data at $y = 0.9$ m (Stationary Reference Frame)

Validation 2. Natural Convection in an Annulus

2.1 Purpose

The purpose of this test is to compare the numerical prediction of temperature profiles along the symmetry lines with the experimental results of Kuehn and Goldstein [1,2] for the eccentric and concentric case. The test also compares the numerically predicted heat flux from the surface of the inner and outer cylinders for the eccentric and concentric cases with the experimental results.

2.2 Problem Description

A heated cylinder is placed inside another cylinder, trapping air in the resulting annular cavity. The inner cylinder is placed in two configurations, one in which the cylinders are concentric and the other in which the inner cylinder is displaced downwards. As the inner cylinder is hotter than the outer, a buoyancy-induced flow results and natural convection occurs. Only half of the domain needs to be modeled from symmetry considerations. The geometry of the problem is shown in Figure 2.2.1.

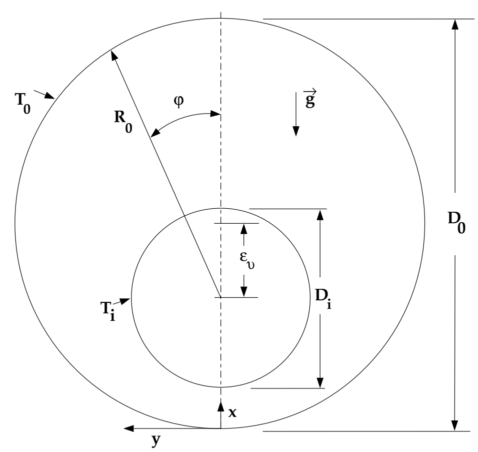


Figure 2.2.1: Problem Description

The radii of the outer and inner cylinders, respectively, are 46.3 mm and 17.8 mm. For the eccentric annulus case the eccentricity is $\epsilon = -0.6245$, which is very close to the value of -0.623 reported in the experiment. The eccentricity is the measure of the distance the inner cylinder is moved from the concentric position and is defined as

$$\epsilon = \epsilon_v / L \tag{2.2-1}$$

where

ϵ_v	=	the distance along the vertical axis the inner cylinder is moved from the concentric position (negative downwards)
	=	-17.8 mm
L	=	$\frac{D_o - D_i}{2}$
	=	28.5 mm
D_o	=	the diameter of the outer cylinder
	=	92.6 mm
D_i	=	the diameter of the inner cylinder
	=	35.6 mm

2.3 References

1. Kuehn, T.H. and Goldstein, R.J., An Experimental Study of Natural Convection Heat Transfer in Concentric and Eccentric Horizontal Cylindrical Annuli, *Journal of Heat Transfer*, 100:635–640, 1978.

2. Kuehn, T.H. and Goldstein, R.J., An Experimental and Theoretical Study of Natural Convection in the Annulus Between Horizontal Concentric Cylinders, *Journal of Fluid Mechanics*, 74:695–719, 1976.

2.4 Results

The temperature profiles along the symmetry lines for the eccentric and concentric cases are compared to the experimental data of Kuehn and Goldstein [1,2]. The agreement between the ANSYS FLUENT predictions and the experimental data is very good.

The heat flux from the inner and outer cylinder surfaces for the eccentric and concentric cases is compared with the experimental data. ANSYS FLUENT predictions of heat flux agree well with the benchmark experimental results, except for the outer wall heat flux prediction of the eccentric annulus. The relatively high grid skewness near the outer wall could be a possible reason for this marked deviation from the experimental data.

Release 12.0 © ANSYS, Inc. January 24, 2009

2.4.1 Validation-Specific Information

Solver: ANSYS FLUENT 2D Double Precision
Version: 6.4.13
Solution Files: 1. `concn_r1.cas`, `concn_r1.dat`
2. `ecc_r2.cas`, `ecc_r2.dat`

These solution files are available from the User Services Center as described in the Introduction.

2.4.2 Plot Data

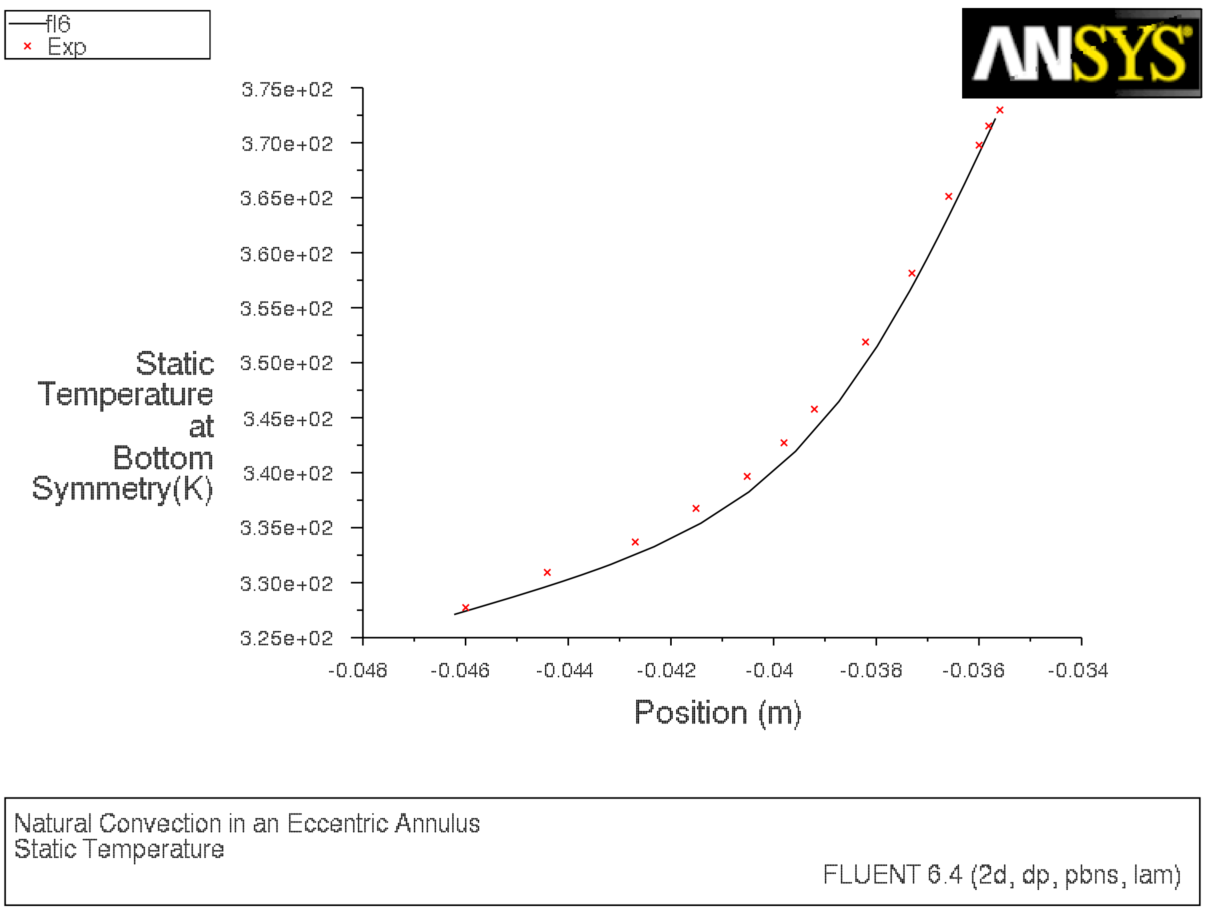


Figure 2.4.1: Temperature Profile Along the Bottom Symmetry Line for the Eccentric Case

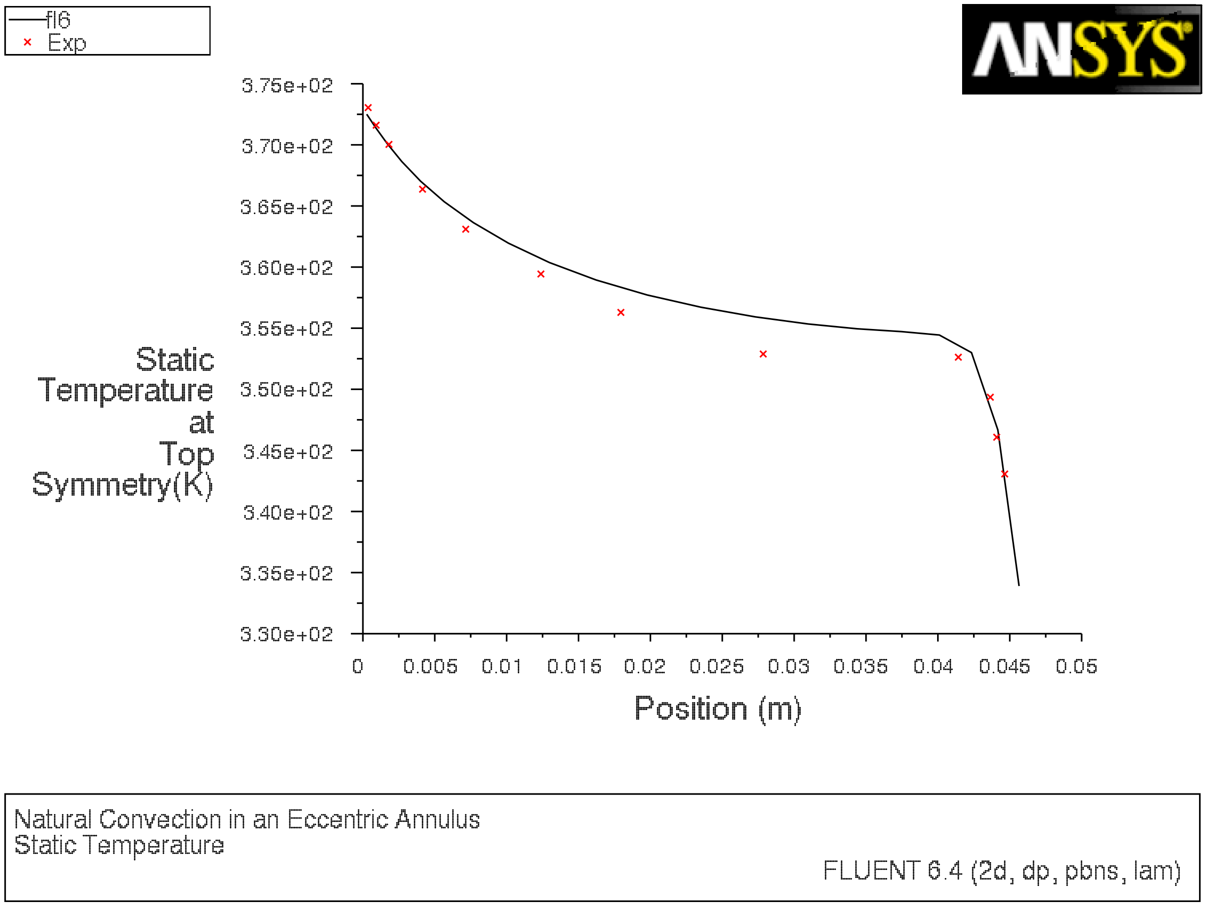


Figure 2.4.2: Temperature Profile Along the Top Symmetry Line for the Eccentric Case

Release 12.0 © ANSYS, Inc. January 24, 2009

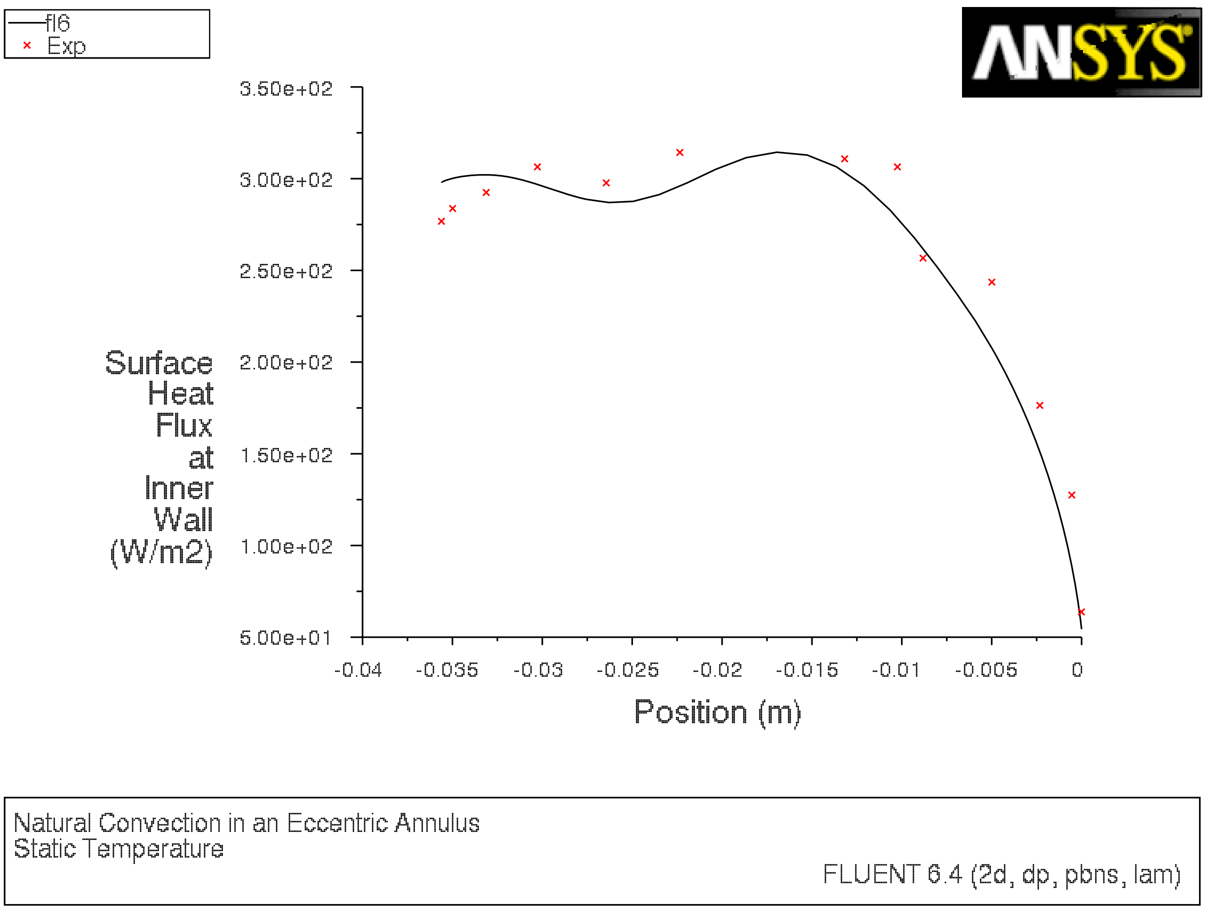


Figure 2.4.3: Comparison of Heat Flux from the Inner Cylinder Surface for the Eccentric Case

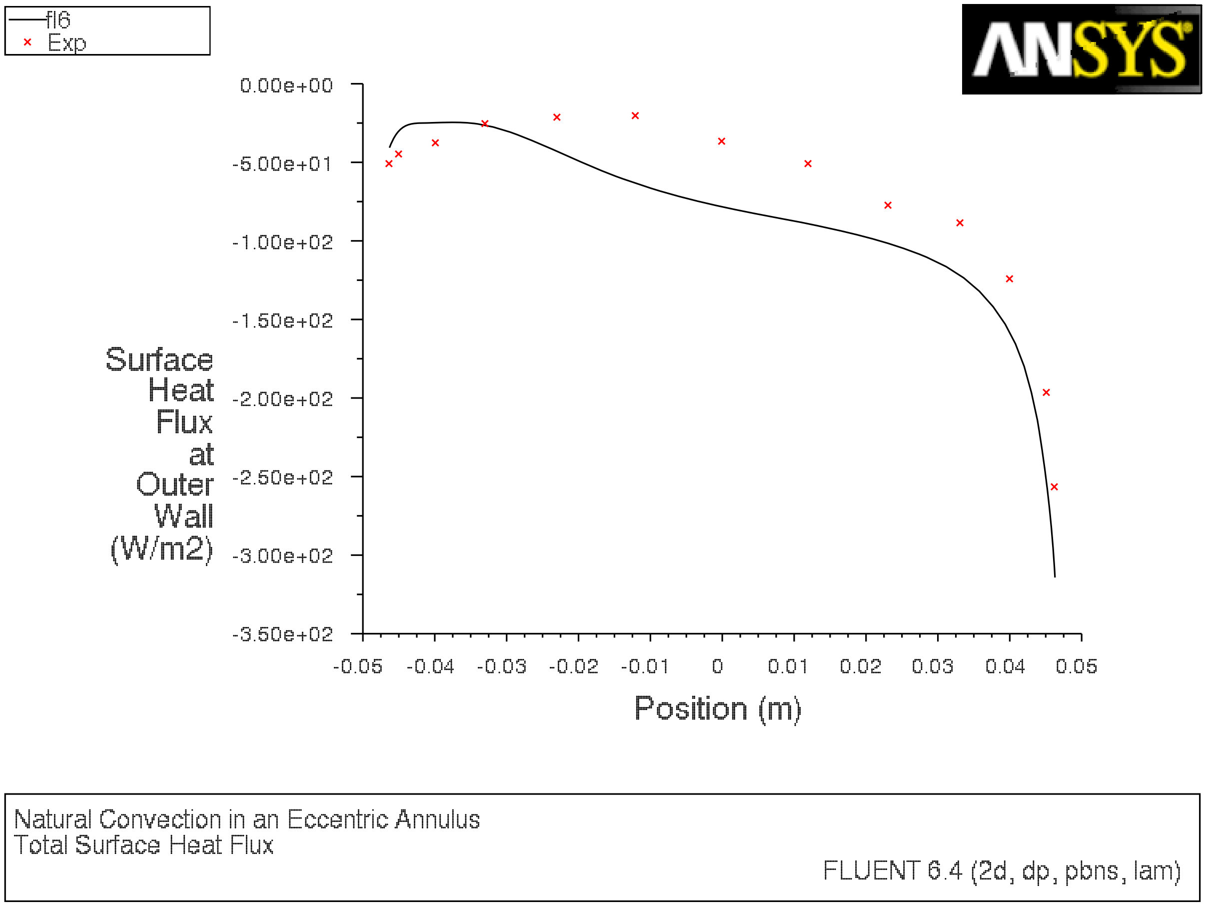


Figure 2.4.4: Comparison of Heat Flux from the Outer Cylinder Surface for the Eccentric Case

Release 12.0 © ANSYS, Inc. January 24, 2009

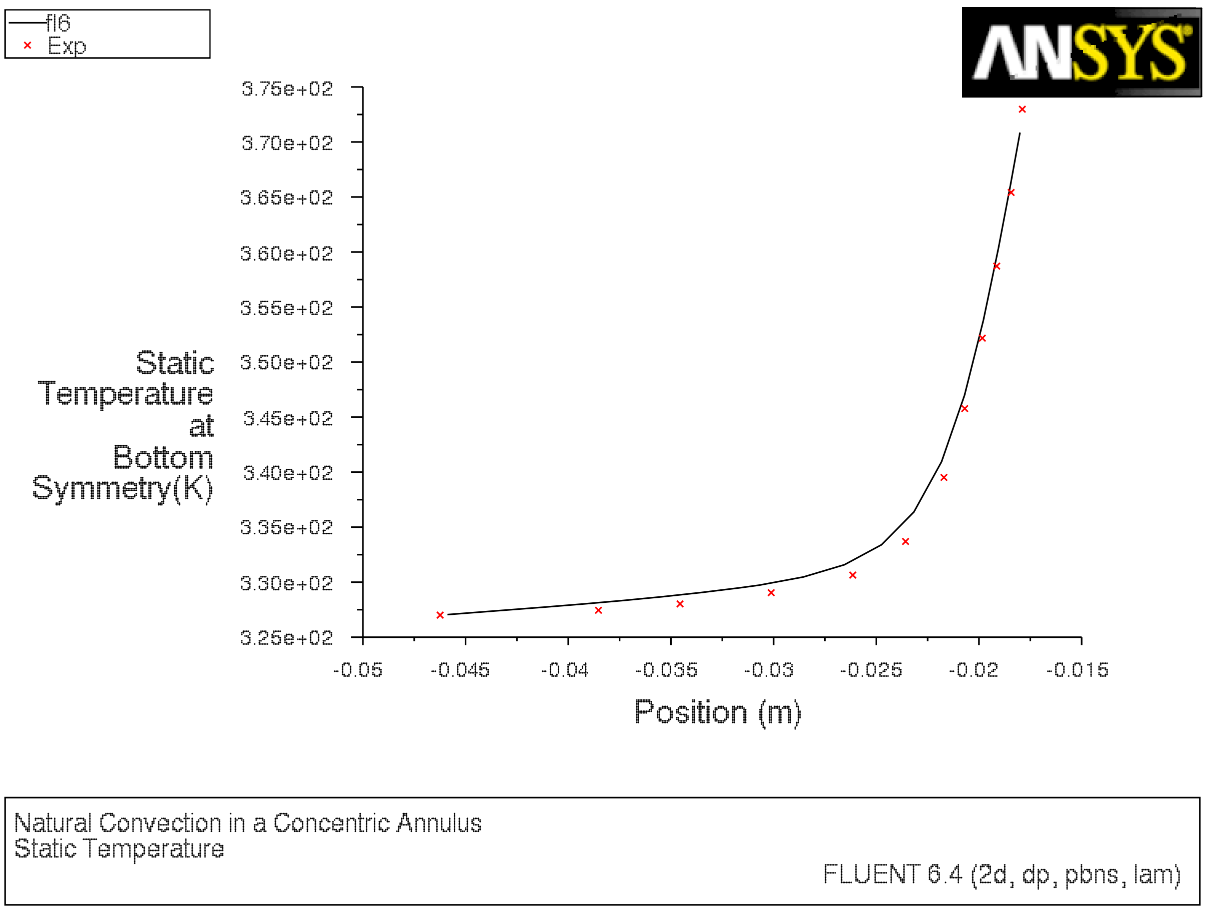


Figure 2.4.5: Temperature Profile Along the Bottom Symmetry Line for the Concentric Case

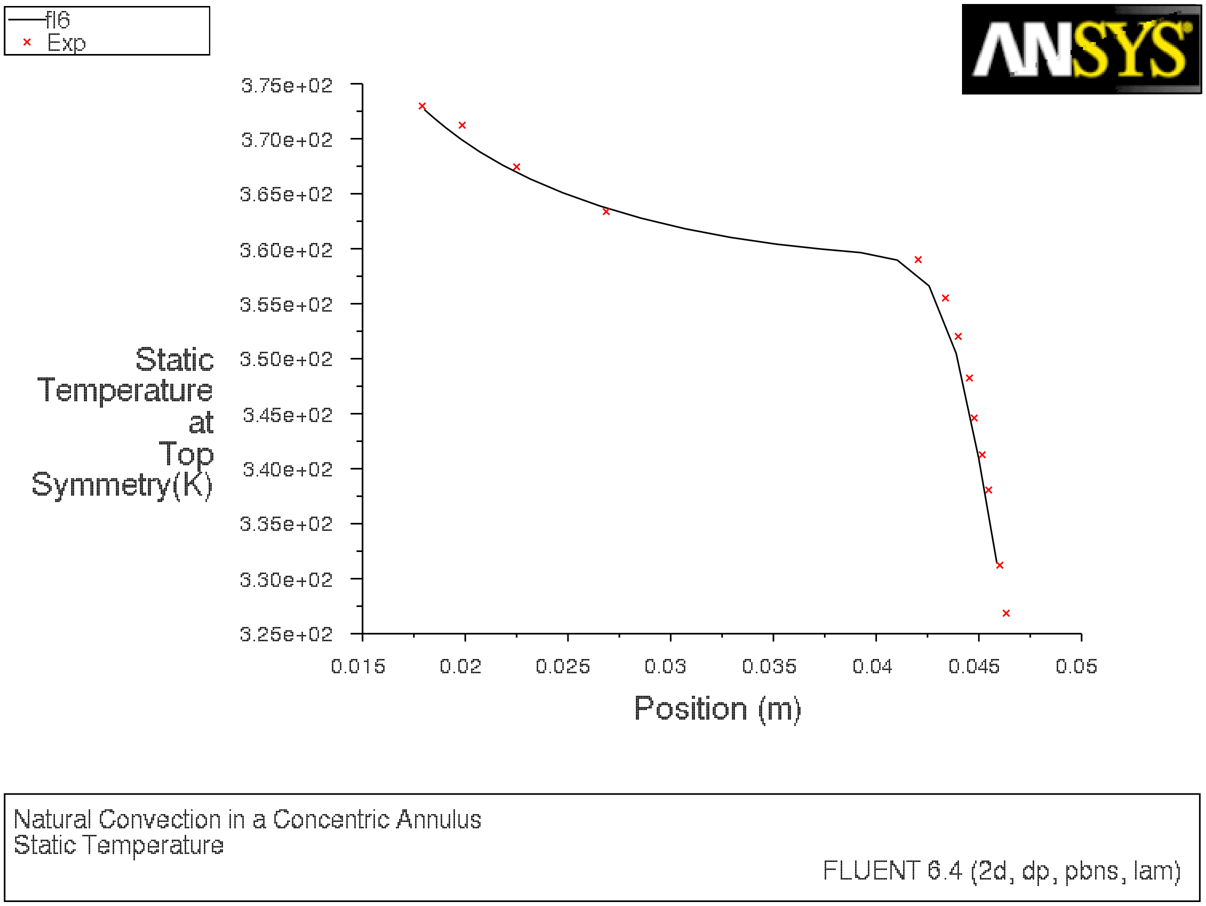


Figure 2.4.6: Temperature Profile Along the Top Symmetry Line for the Concentric Case

Release 12.0 © ANSYS, Inc. January 24, 2009

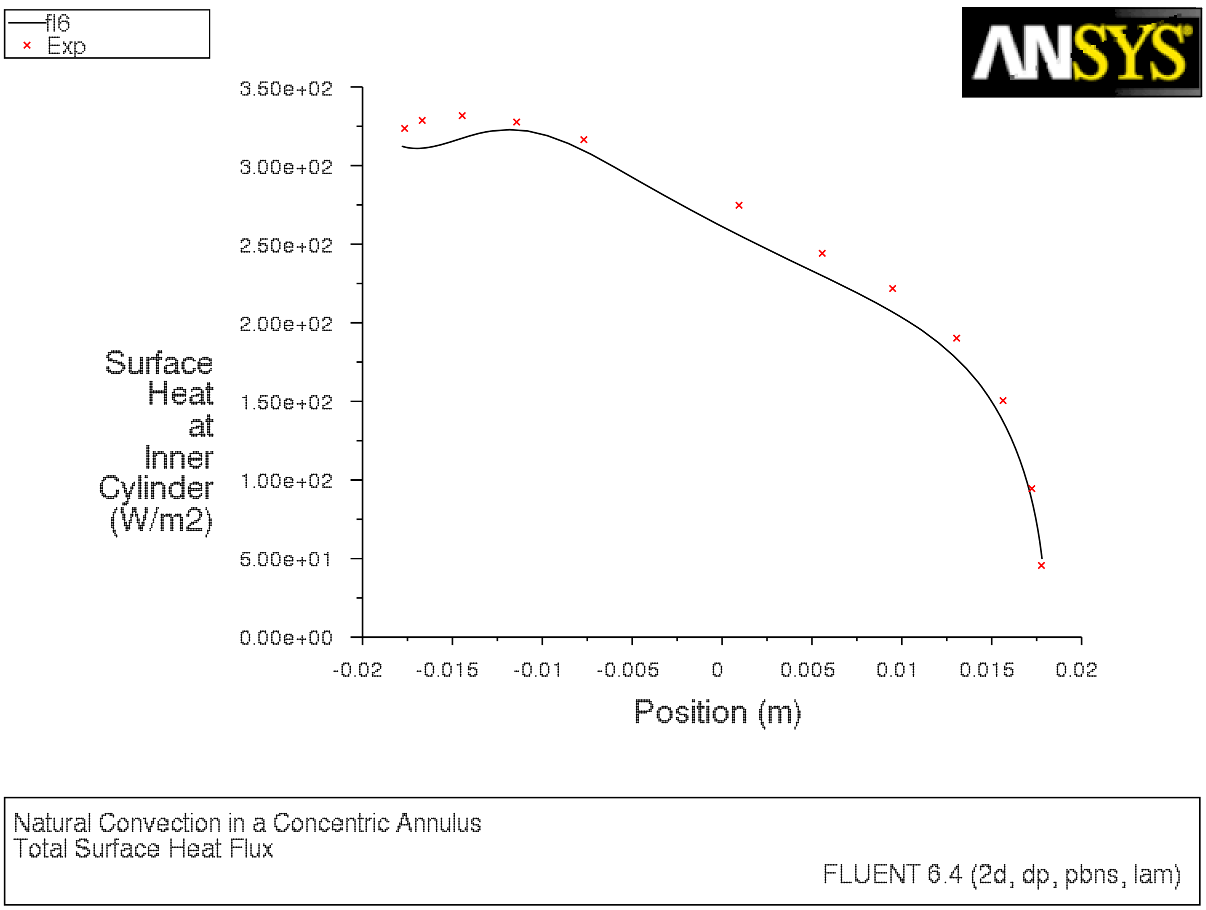


Figure 2.4.7: Comparison of Heat Flux from the Inner Cylinder Surface for the Concentric Case

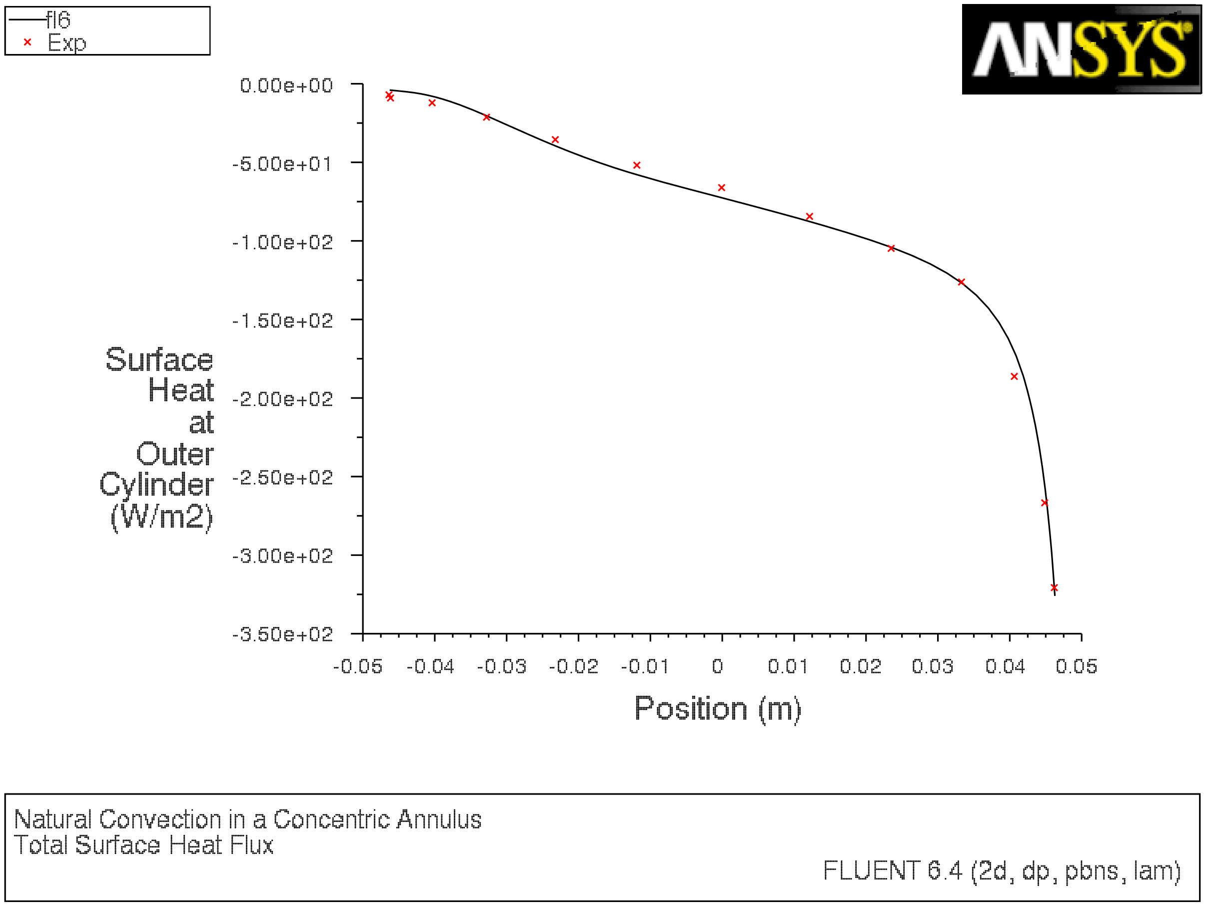


Figure 2.4.8: Comparison of Heat Flux from the Outer Cylinder Surface for the Concentric Case

Validation 3. Flow in a 90° Planar Tee-Junction

3.1 Purpose

The purpose of this test is to compare ANSYS FLUENT's prediction of the fractional flow in a dividing tee-junction with the experimental results of Hayes et al. [1].

3.2 Problem Description

The problem involves a planar 90° tee-junction as shown in Figure 3.2.1. The fluid enters through the bottom branch and divides into the two channels whose exit planes are held at the same static pressure.

The Reynolds number Re, based on the channel width and the centerline fluid velocity at the channel inlet, is given by

$$Re = \frac{\rho V_c W}{\mu} \tag{3.2-1}$$

where V_c is the inlet centerline velocity.

3.3 References

1. Hayes, R.E., Nandkumar, K., and Nasr-El-Din, H., Steady Laminar Flow in a 90 Degree Planar Branch, *Computers and Fluids*, 17(4): 537–553, 1989.

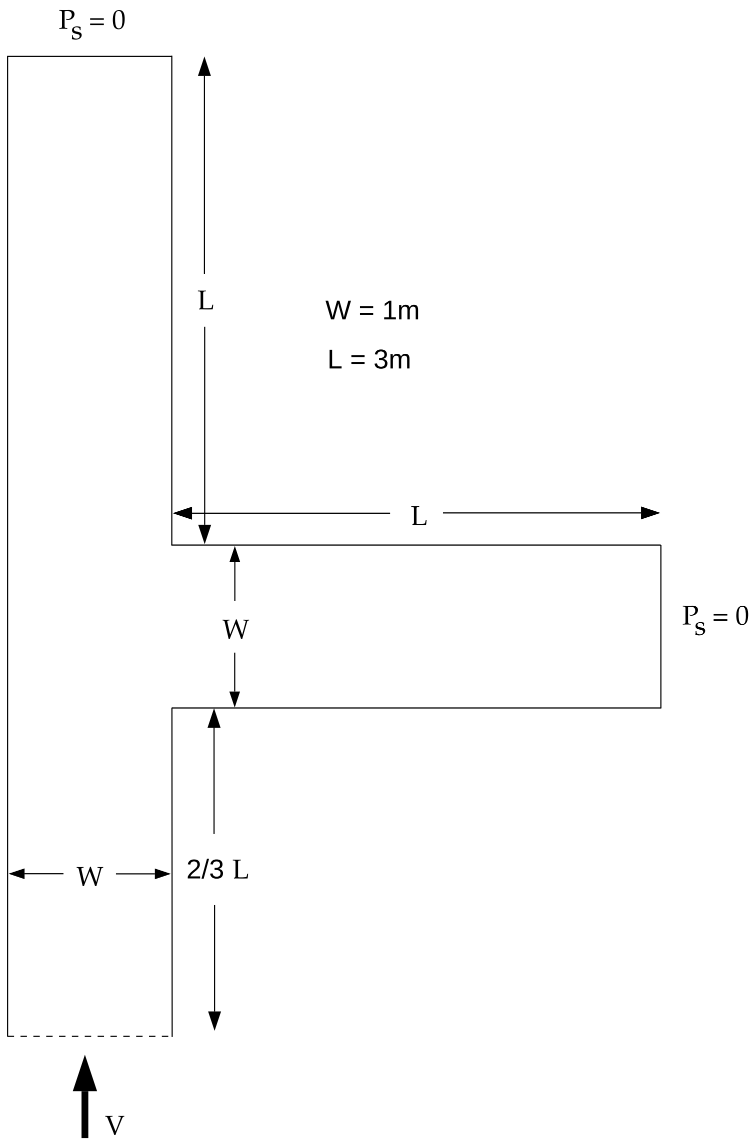


Figure 3.2.1: Problem Description

Release 12.0 © ANSYS, Inc. January 24, 2009

3.4 Results

The test runs were made for five different Reynold numbers ($Re = 10$, $Re = 100$, $Re = 200$, $Re = 300$, and $Re = 400$). The ANSYS FLUENT predictions are compared with the experimental results of Hayes et al.[1]. It is seen that with increasing flow rate in the main channel, less fluid escapes through the secondary (right) branch. The following table shows the fractional flow in the upper branch versus the Reynolds number. The ANSYS FLUENT predictions of fractional flow versus Re agree very well with the experiment.

Table 3.4.1: Flow Split

Reynolds No., Re	10	100	200	300	400
Upper branch mass flow rate, kg/s	0.349	0.481	0.556	0.591	0.611
Right branch mass flow rate, kg/s	0.319	0.188	0.113	0.077	0.058
Total mass flow rate, kg/s	0.668	0.668	0.668	0.668	0.668
Flow split in the upper branch	0.523	0.719	0.832	0.885	0.914

3.4.1 Validation-Specific Information

Solver: ANSYS FLUENT 2D Double Precision
Version: 6.4.13
Solution Files:
1. `plarb_r1.cas`, `plarb_r1.dat` ($Re = 10$)
2. `plarb_r2.cas`, `plarb_r2.dat` ($Re = 100$)
3. `plarb_r3.cas`, `plarb_r3.dat` ($Re = 200$)
4. `plarb_r4.cas`, `plarb_r4.dat` ($Re = 300$)
5. `plarb_r5.cas`, `plarb_r5.dat` ($Re = 400$)

These solution files are available from the User Services Center as described in the Introduction.

3.4.2 Plot Data

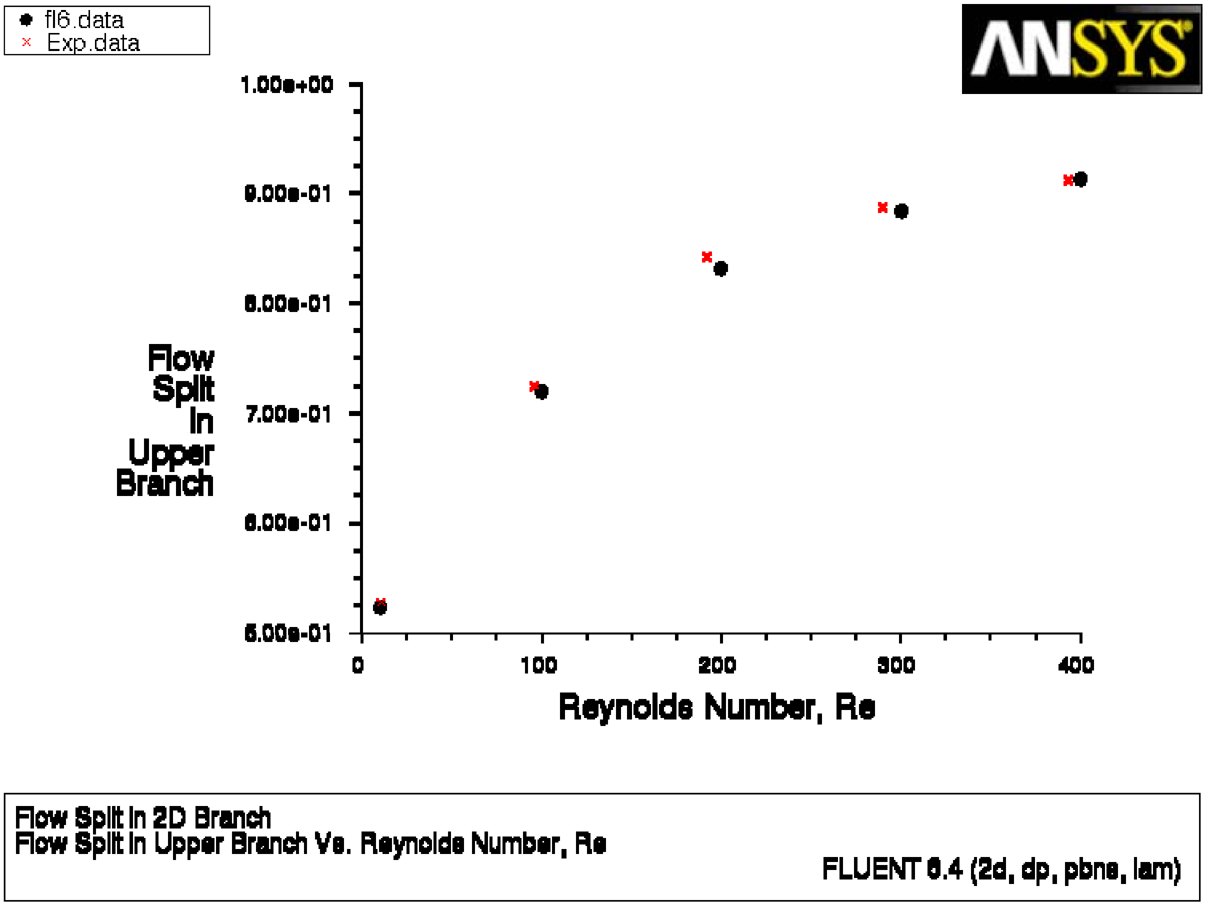


Figure 3.4.1: Flow Split in the Upper Branch vs. Reynolds Number

Release 12.0 © ANSYS, Inc. January 24, 2009

Validation 4. Flows in Driven Cavities

4.1 Purpose

The purpose of this test is to compare the prediction of u and v velocity profiles in the 2D laminar driven trapezoidal cavity flow against the calculations by Darr and Vanka [1], and to compare u velocity profiles in the 2D laminar driven triangular cavity flow against the calculations of Jyotsna and Vanka [2].

4.2 Problem Description

Two types of cavities are considered. The first cavity is a trapezoidal cavity in which the top and bottom walls move but the side walls are stationary. The height of the cavity h is 1 m; the widths of the top and bottom walls are 1 m and 2 m, respectively (see Figure 4.2.1).

The second cavity is a triangular cavity with a driven top wall and stationary side walls. The height of the cavity h is 4 m; the width of the top wall is 2 m (see Figure 4.2.2).

4.3 References

1. Darr, J.H. and Vanka, S.P., Separated Flow in a Driven Trapezoidal Cavity, *Phys. Fluids A*, 3(3):385–392, March 1991.
2. Jyotsna, R. and Vanka, S.P., Multigrid Calculation of Steady, Viscous Flow in a Triangular Cavity, *J. Comp. Phys.*, 122:107–117, 1995.

4.4 Results

4.4.1 Trapezoidal Cavity

The u velocity profile at the vertical centerline of the cavity and the v velocity profile at the horizontal centerline of the cavity are compared to Darr and Vanka [1] results for both types of meshes.

4.4.2 Triangular Cavity

The normalized u velocity profiles at the vertical centerline of the cavity for the coarse and fine meshes are compared with Jyotsna and Vanka [2] data.

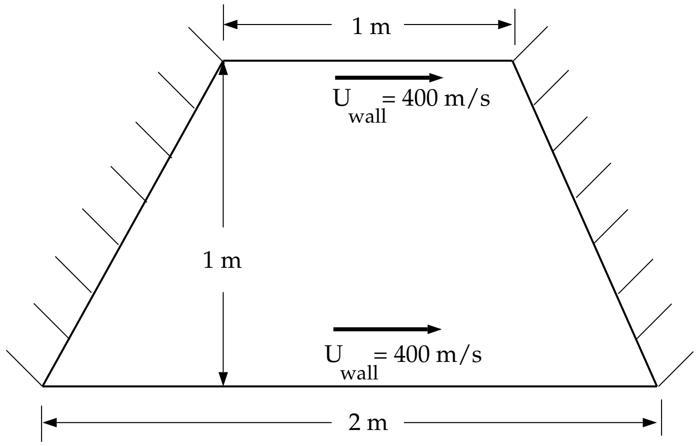


Figure 4.2.1: Problem Description: Trapezoidal Cavity

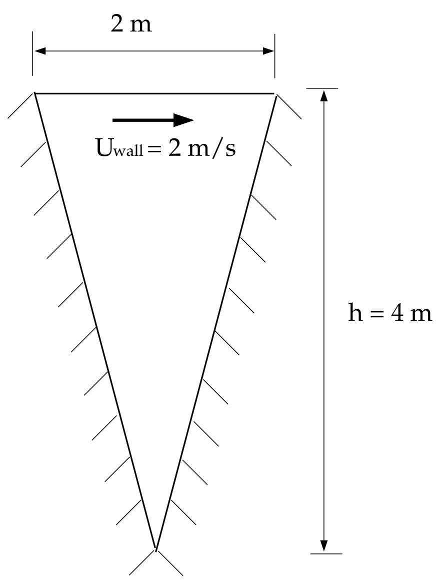


Figure 4.2.2: Problem Description: Triangular Cavity

Release 12.0 © ANSYS, Inc. January 24, 2009

4.4.3 Validation-Specific Information

Solver:	ANSYS FLUENT 2D Double Precision
Version:	6.4.13
Solution Files:	1. driv-trpz-tri_r1.cas, driv-trpz-tri_r1.dat
	2. driv-trpz-quad_r2.cas, driv-trpz-quad_r2.dat
	3. driv-tri-crs_r3.cas, driv-tri-crs_r3.dat
	4. driv-tri-fine_r3.cas, driv-tri-fine_r3.dat

These solution files are available from the User Services Center as described in the Introduction.

4.4.4 Plot Data

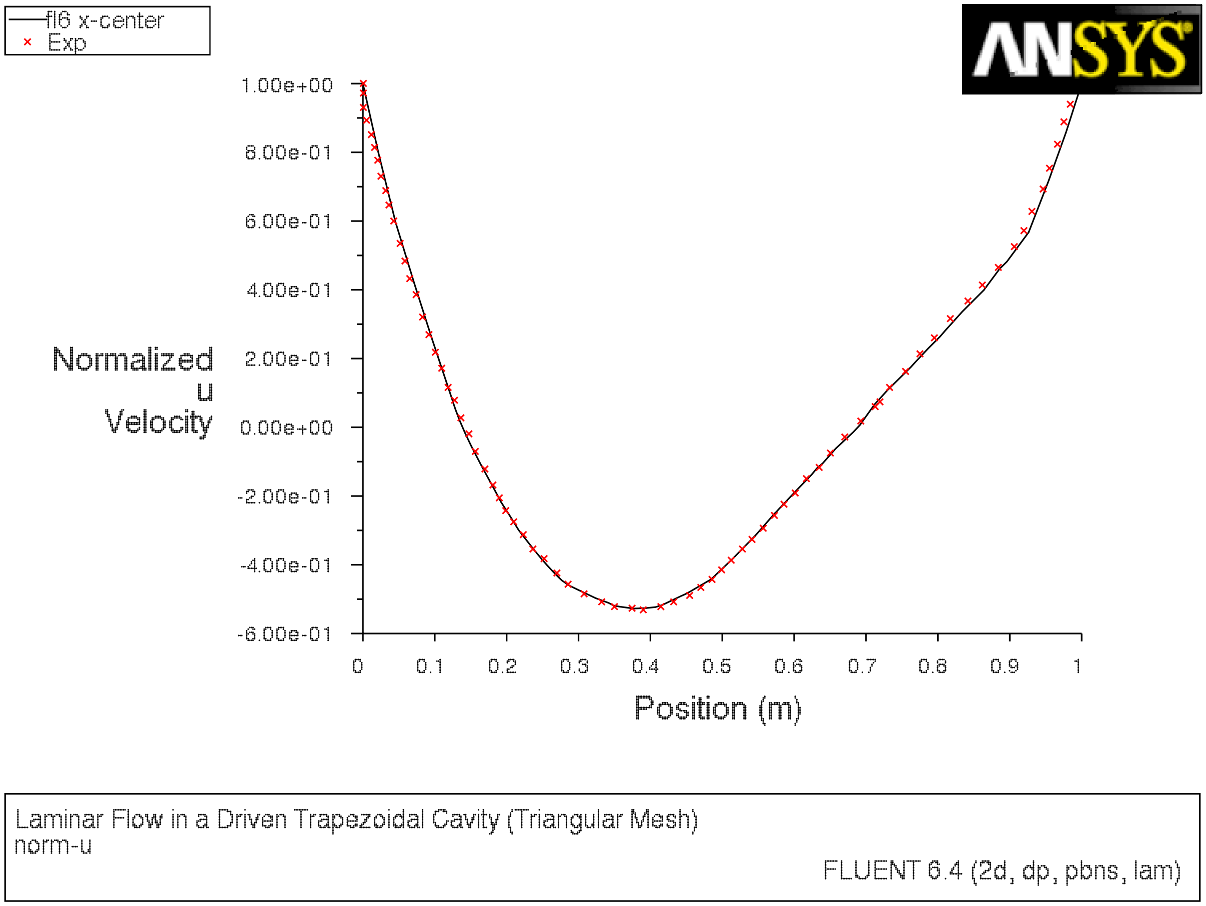


Figure 4.4.1: Normalized u Velocity at the Vertical Centerline of the Cavity (Triangular Mesh)

 Release 12.0 © ANSYS, Inc. January 24, 2009

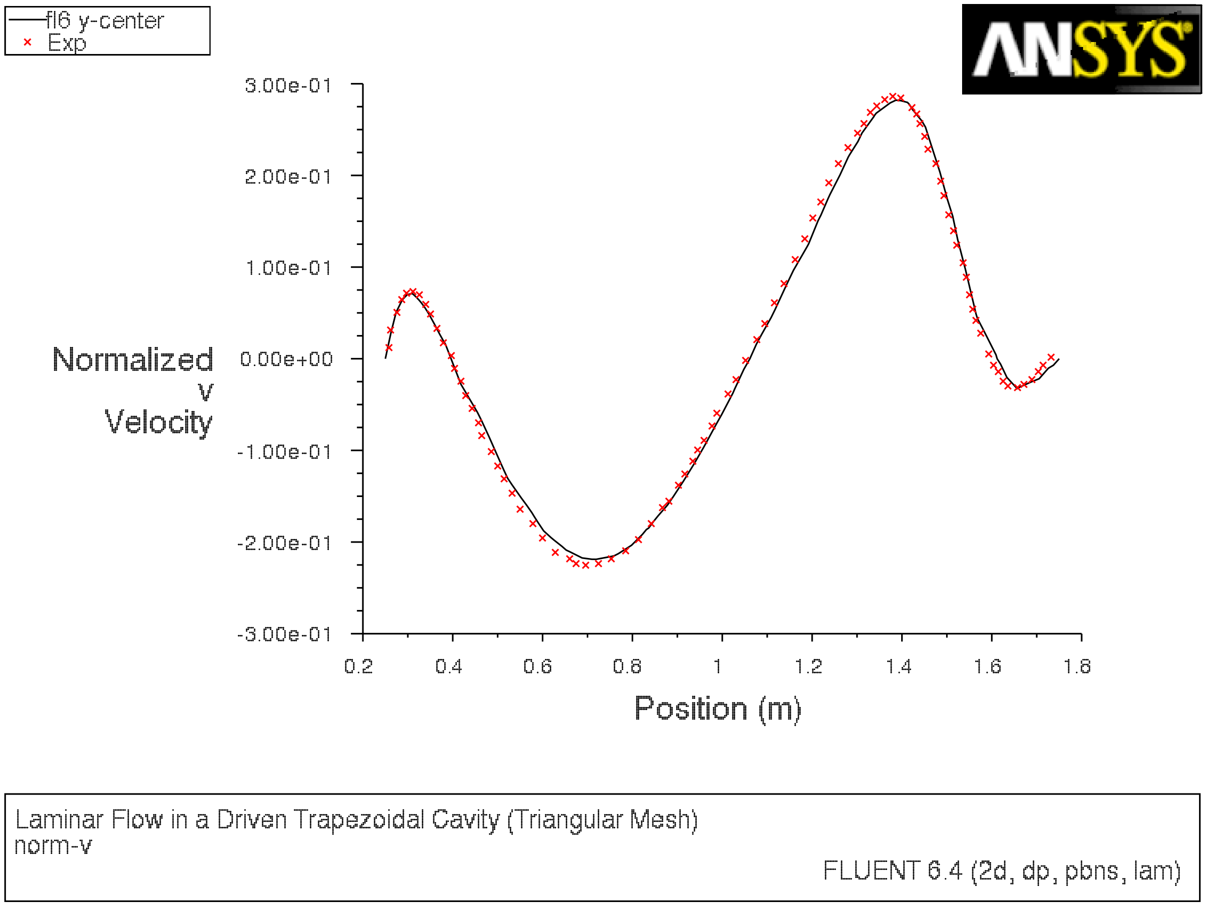


Figure 4.4.2: Normalized v Velocity at the Horizontal Centerline of the Cavity (Triangular Mesh)

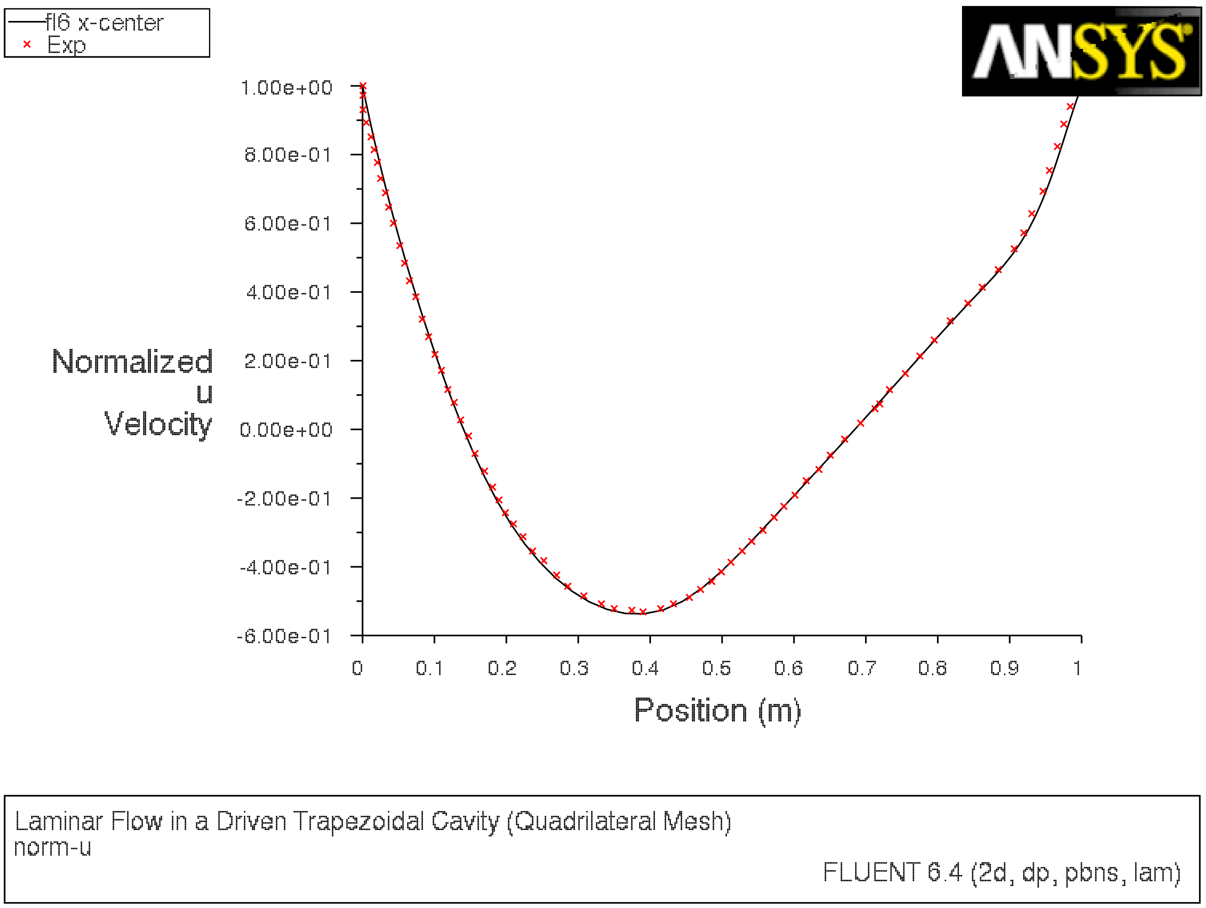


Figure 4.4.3: Normalized u Velocity at the Vertical Centerline of the Cavity (Quadrilateral Mesh)

Release 12.0 © ANSYS, Inc. January 24, 2009

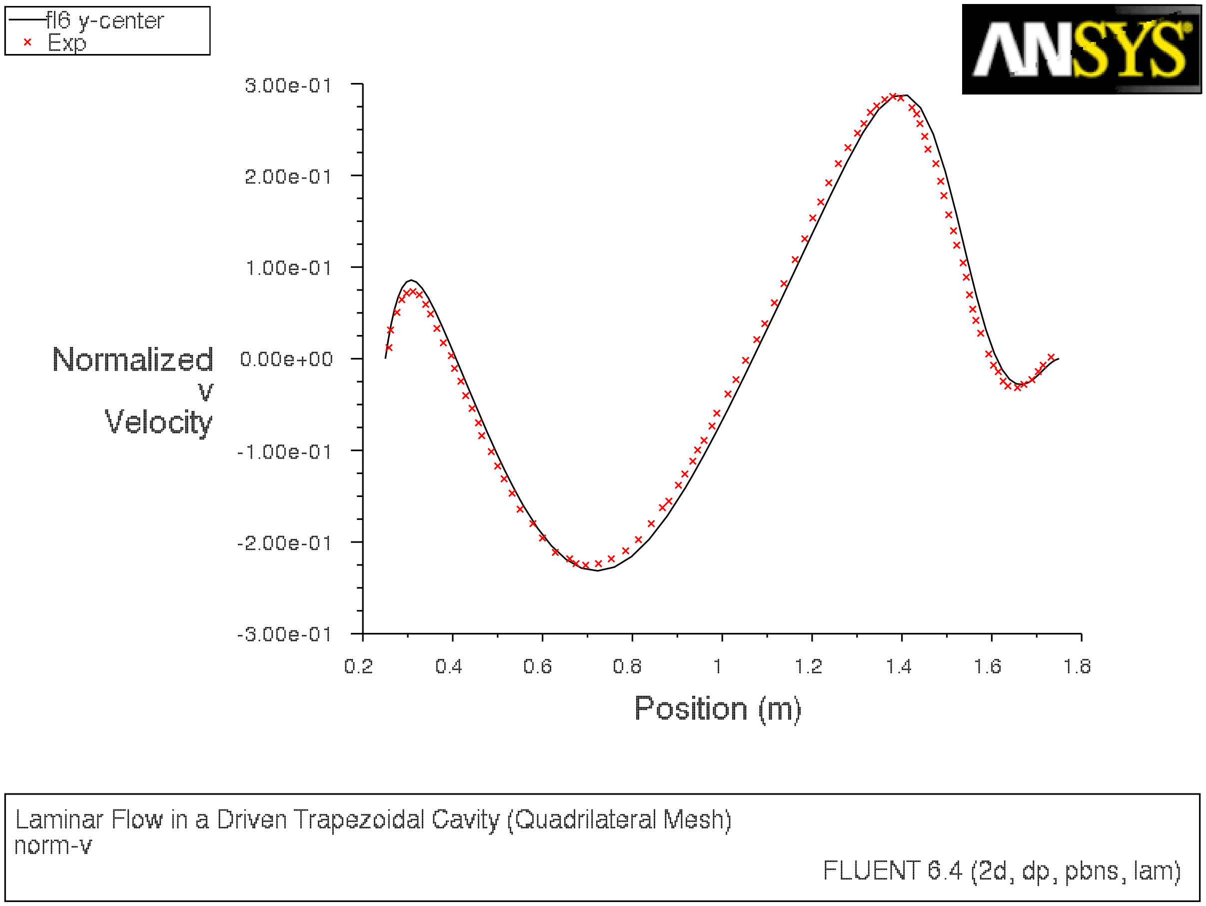


Figure 4.4.4: Normalized v Velocity at the Horizontal Centerline of the Cavity (Quadrilateral Mesh)

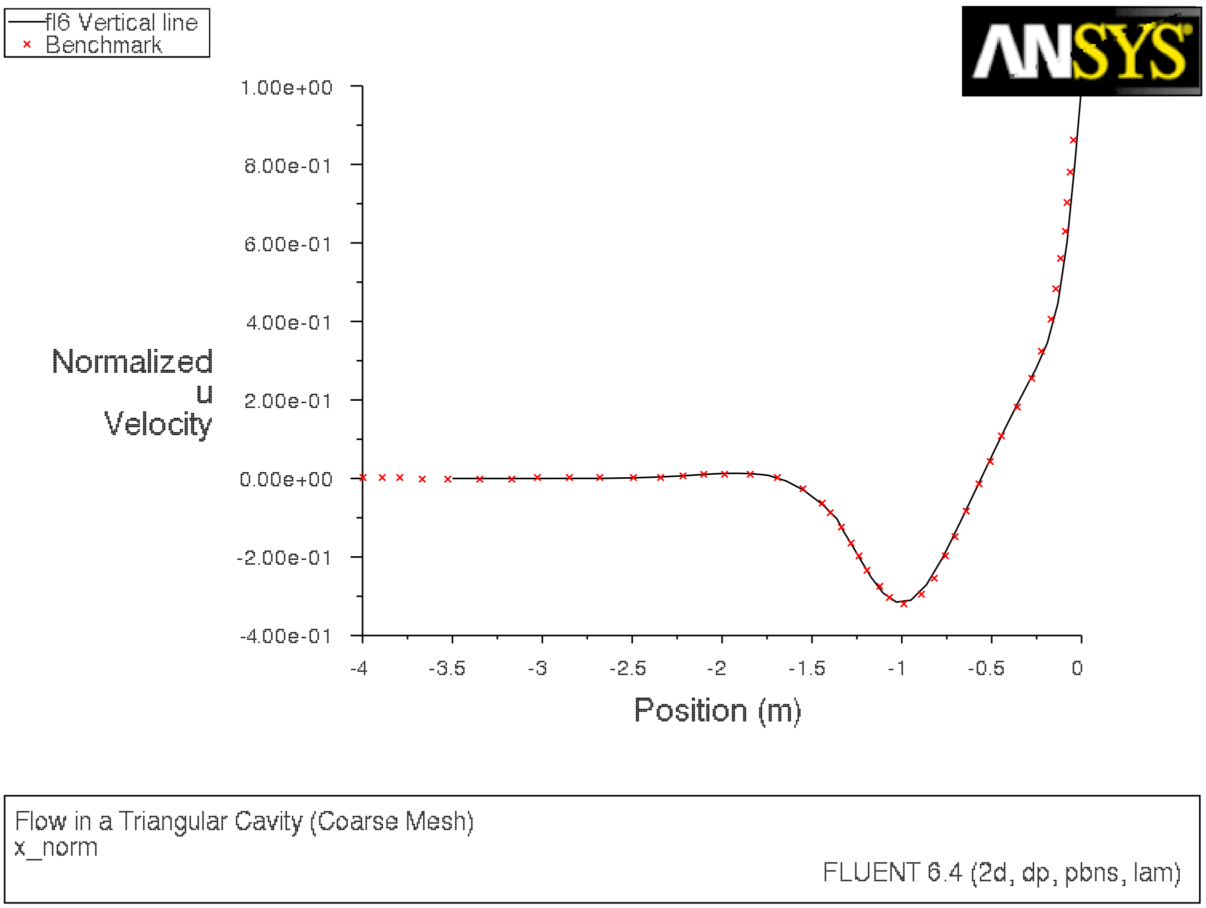


Figure 4.4.5: Normalized u Velocity at the Vertical Centerline of the Triangular Cavity (Mixed Coarse Mesh)

Release 12.0 © ANSYS, Inc. January 24, 2009

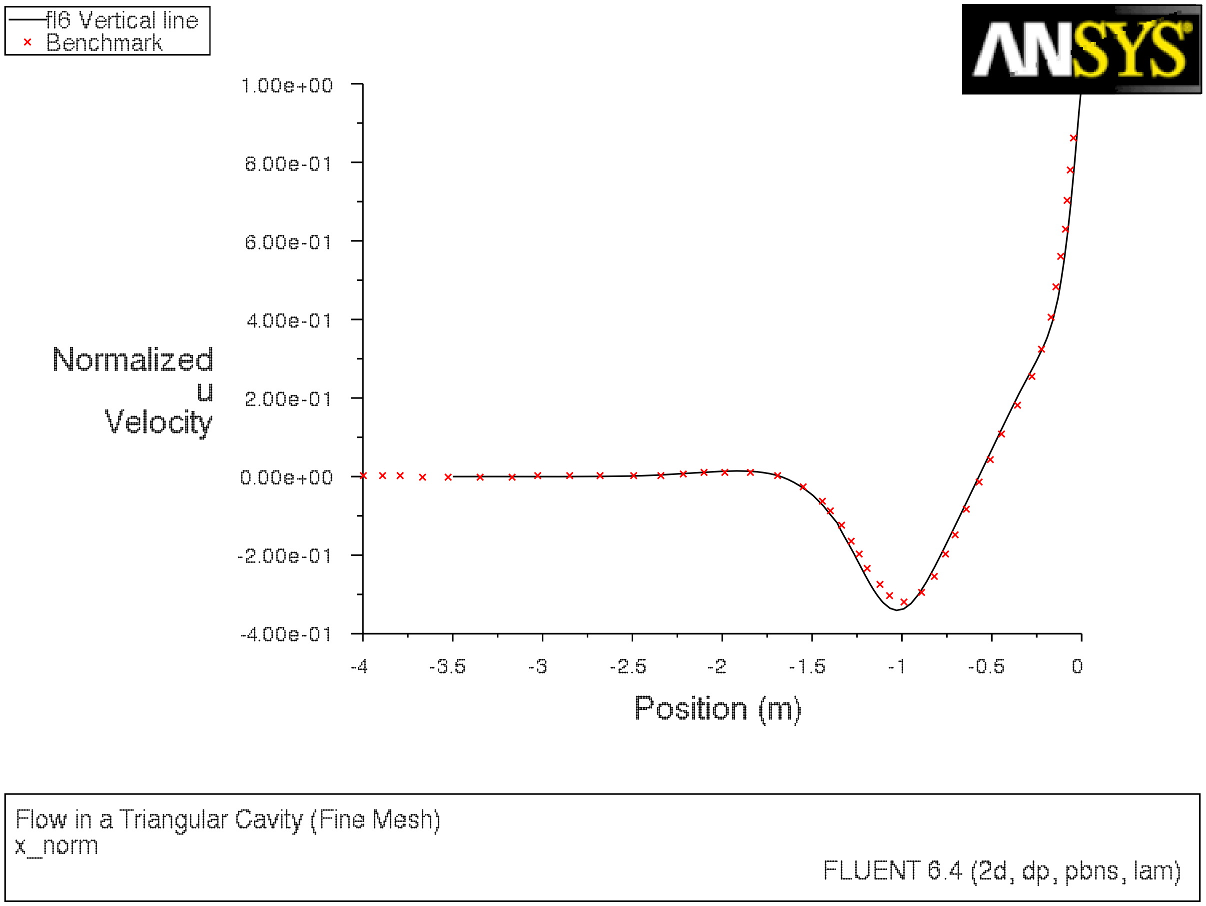


Figure 4.4.6: Normalized u Velocity at the Vertical Centerline of the Triangular Cavity (Mixed Fine Mesh)

 Release 12.0 © ANSYS, Inc. January 24, 2009

Validation 5. Periodic Flow in a Wavy Channel

5.1 Purpose

The purpose of this test is to compare the predictions of ANSYS FLUENT's realizable k-ε, SST k-ω and RSM turbulence models against the experimental results of Kuzan [1] for the x-velocity profiles.

5.2 Problem Description

The wavy bottom wall has a sinusoidal shape whose amplitude and wave length are 0.1 m and 1.0 m, respectively. The Reynolds Number based on channel height Re_H is 8,160. Since the flow is periodic, the computational domain can be chosen to cover only one period of the wavy channel, as shown in Figure 5.2.1. The length of the periodic domain is 1 m.

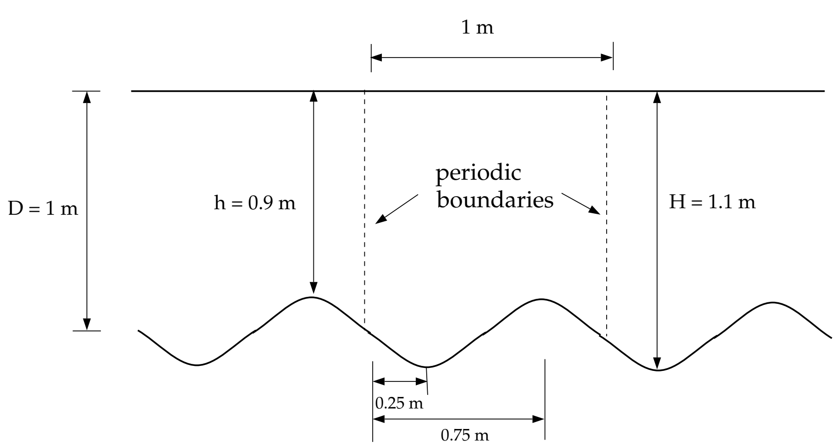


Figure 5.2.1: Problem Description

5.3 References

1. Kuzan, J.D., *Velocity Measurements for Turbulent Separated and Near-Separated Flows Over Solid Waves*, Ph.D. thesis, Dept. Chem. Eng., Univ. Illinois, Urbana,

IL, 1986.

5.4 Results

Figures 5.4.1 - 5.4.2 compare the x velocity profiles at the wave crest and at the wave trough with Kuzan's [1] experimental results for realizable k-ε, SST k-ω and RSM models. (The x velocity is normalized by the average fluid velocity at the mean channel height, $U = 0.816$ m/s.)

The velocity profiles at the wave trough confirm that the flow reversal occurs in the wave hollow, thus creating a recirculation zone. Near the top straight wall, velocity profiles remain attached to the wall. The predictions are in very close agreement with the experimental data.

5.4.1 Validation-Specific Information

Solver:	ANSYS FLUENT 2D Double Precision
Version:	12.0.5
Solution Files:	1. `rke-ewt.cas.gz`, `rke-ewt.dat.gz`
	2. `rsm-ewt.cas.gz`, `rsm-ewt.dat.gz`
	3. `sst.cas.gz`, `sst.dat.gz`

These solution files are available from the User Services Center as described in the Introduction.

Release 12.0 © ANSYS, Inc. January 24, 2009

5.4.2 Plot Data

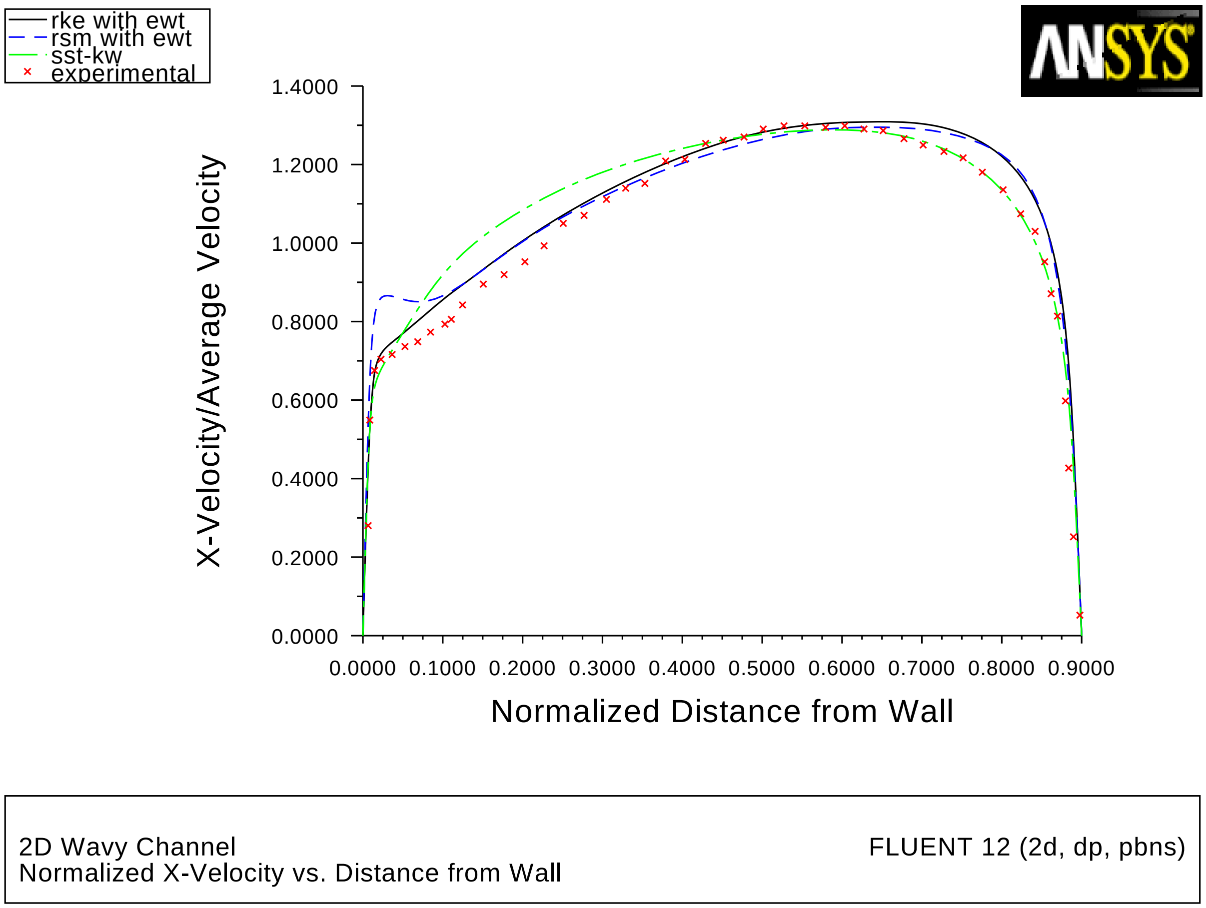


Figure 5.4.1: Normalized x Velocity at the Wave Crest (RNG k-ε Model)

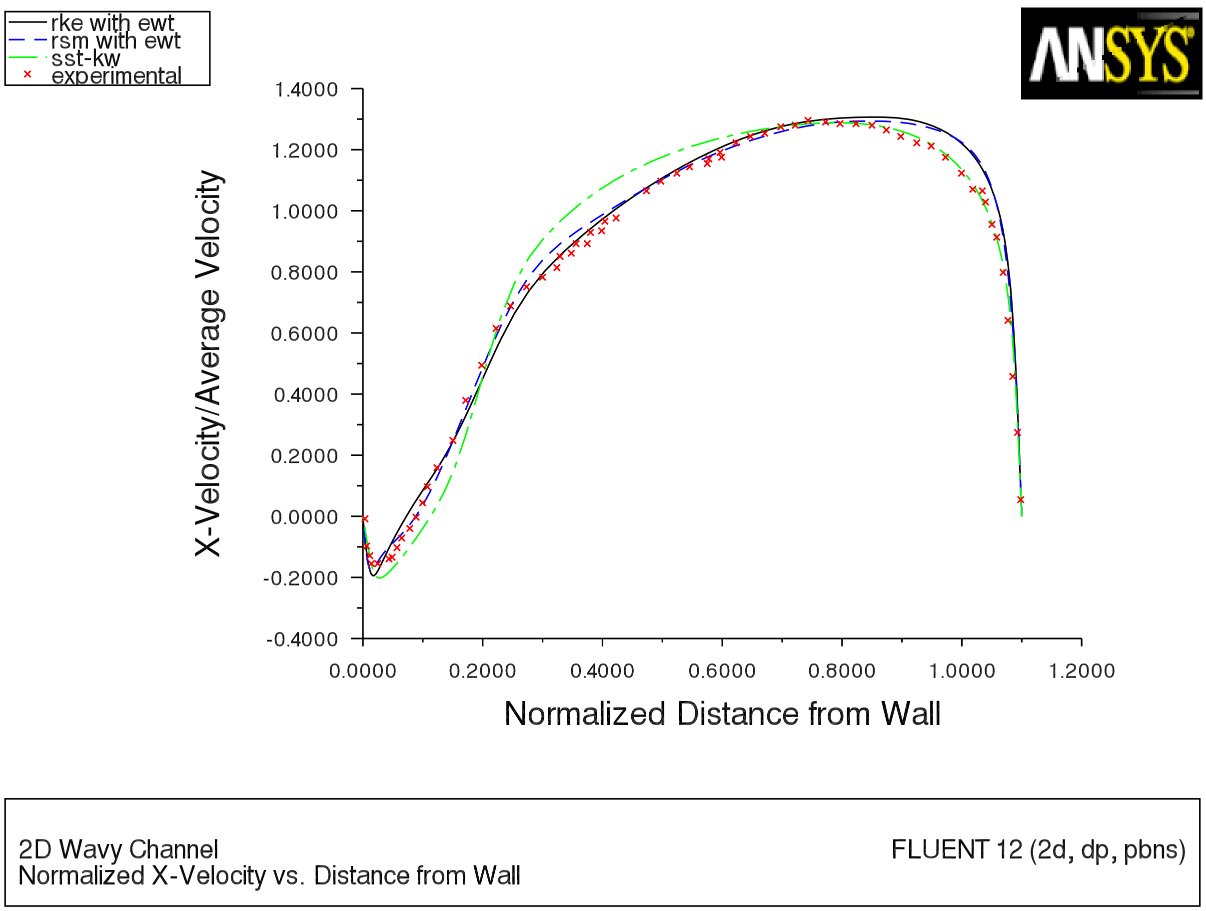


Figure 5.4.2: Normalized x Velocity at the Wave Trough

Validation 6. Heat Transfer in a Pipe Expansion

6.1 Purpose

The purpose of this test is to validate ANSYS FLUENT's SST k-ω turbulence model against the experimental data [1].

6.2 Problem Description

Figure 6.2.1 shows the geometry of the expansion considered. The inlet is placed $1H$ upstream of the step. The exit boundary is located $40H$ downstream of the step. The expansion ratio is $d/D = 0.400$, where $d = 1.33$ m is the inlet pipe diameter and $D = 3.33$ m is the downstream pipe diameter.

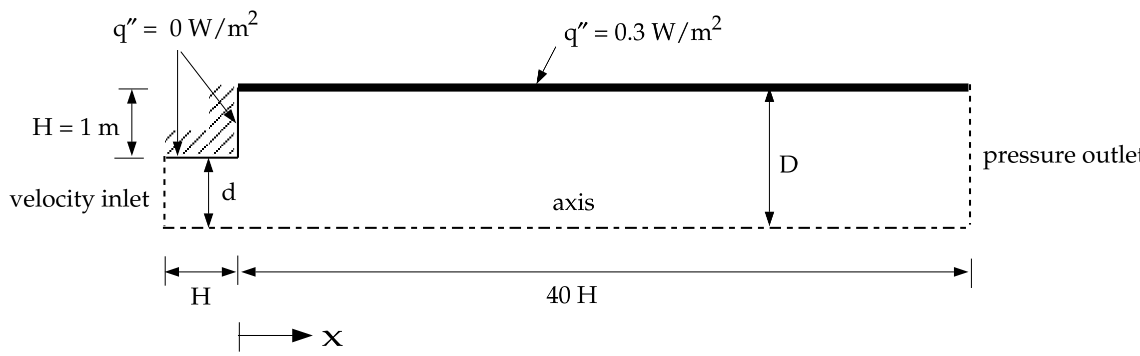


Figure 6.2.1: Problem Description

6.3 References

1. Baughn et al., Local Heat Transfer Downstream of an Abrupt Expansion in a Circular Channel With Constant Wall Heat Flux, *Journal of Heat Transfer*, 106:789–796, 1984.

2. Patel, C., Rodi, W., and Scheuerer, G., Turbulence Models for Near-Wall and Low-Reynolds-Number Flows: A Review, *AIAA Journal*, 23(9), 1984.

3. Schlichting, H., *Boundary-Layer Theory*, McGraw-Hill Series in Mechanical Engineering, 1979.

6.4 Results

The quantity of interest for comparison with the measurements of [1] is the Nusselt number, Nu, along the heated wall. The Nusselt number was calculated from the bulk temperature and the heat transfer coefficient. (See Figure 6.2.1 for the location of x.)

The bulk temperature is

$$T_B(x) = \frac{\dot{q}''(x)4x}{Re\mu c_p} + 273 \tag{6.4-1}$$

where $\dot{q}''(x)$ is the local heat flux (constant, in this case). The local heat transfer coefficient is

$$h(x) = \frac{\dot{q}''(x)}{T_{\text{wall}}(x) - T_B(x)} \tag{6.4-2}$$

Finally, the local Nusselt number is

$$Nu(x) = \frac{h(x)D}{k} \tag{6.4-3}$$

where D is the diameter of the pipe and k is the thermal conductivity of the fluid.

Data of [1] are in terms of Nu/Nu_{DB} where Nu_{DB} is the Nusselt number calculated with the Dittus-Boelter formula.

The variation of the ratio Nu/Nu_{DB} along the heated wall for the SST-k-ω turbulence model is presented here.

The ANSYS FLUENT results are compared to the experimental results of [1]. The agreement is satisfactory for all cases.

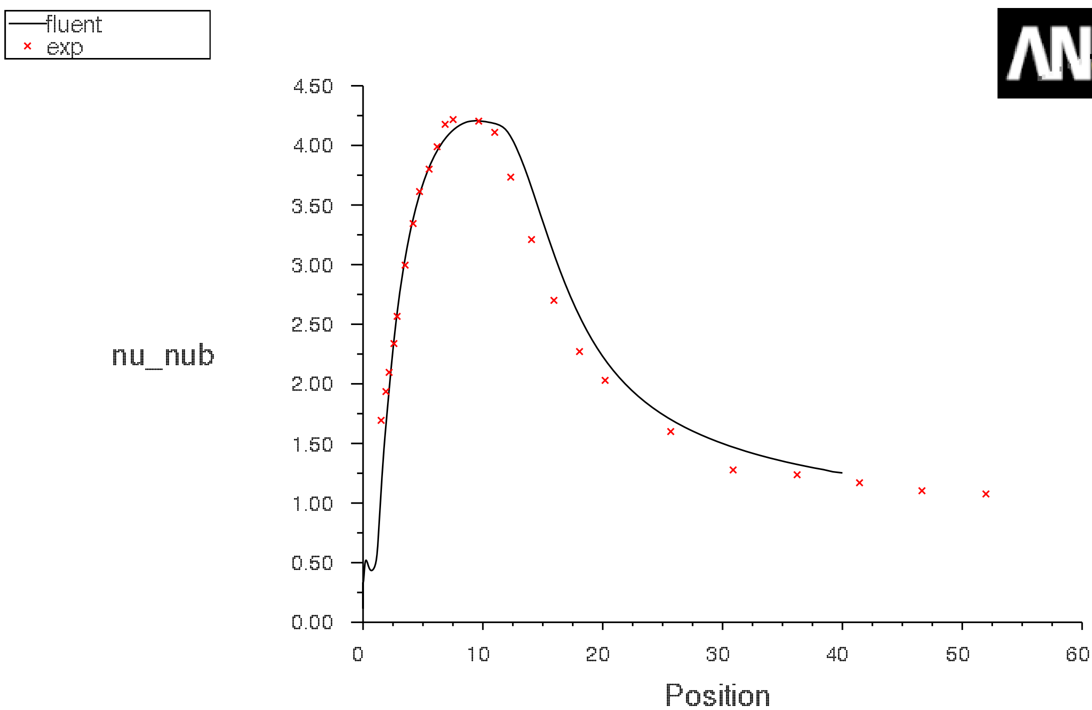
Release 12.0 © ANSYS, Inc. January 24, 2009

6.4.1 Validation-Specific Information

Solver: ANSYS FLUENT 2D Double Precision
Version: 12.0.5
Solution Files: `sst-kw-final.cas`, `sst-kw-final.dat`

These solution files are available from the User Services Center as described in the Introduction.

6.4.2 Plot Data



bghnexp (Baughn's Pipe Expansion, Re_D = 40,750)
nu_nub
SST k-omega FLUENT 12.0 (axi, dp, pbns, sstkw)

Figure 6.4.1: Nu/Nu_{DB} Along the Downstream Pipe Wall (SST k-ω Turbulence Model)

 Release 12.0 © ANSYS, Inc. January 24, 2009

Validation 7. Propane Jet in a Coaxial Air Flow

7.1 Purpose

The aim of this validation is to compare ANSYS FLUENT's predictions for the mean mixture fraction and the axial velocity along the jet axis with the experimental data [1,2,3]. The test was conducted using two methods: the non-reacting species transport model and the mixture fraction/PDF model. It also incorporated two types of meshes: a quadrilateral mesh and a triangular mesh.

7.2 Problem Description

The flow considered is a propane turbulent round jet in a coaxial air tunnel flow. The problem is axisymmetric. The tunnel has a length $L = 2$ m and a diameter $D = 0.3$ m. The inner diameter of the jet tube exit is $d = 5.2$ mm, and the outer diameter is $d' = 11$ mm. Figure 7.2.1 shows the geometry of the problem.

This problem involves three different species: propane (C_3H_8), oxygen (O_2), and nitrogen (N_2). The turbulent jet at the pipe exit contains only C_3H_8. The air that enters the tunnel is free of C_3H_8. There is no chemical reaction between species, and the flow is adiabatic.

7.3 References

1. Strahle, W.C., and Lekoudis, S.G., *Evaluation of Data on Simple Turbulent Reacting Flows*, AFOSR TR-85 0880, Chapter 2, School of Aerospace Engineering, Georgia Institute of Technology, Atlanta, GA.

2. Schefer, R.W., and Dibble, R.W., Simultaneous Measurements of Velocity and Density in a Turbulent Nonpremixed Flame, *AIAA Journal*, 23:1070–1078, 1985.

3. Schlichting, H., *Boundary-Layer Theory*, McGraw-Hill Series in Mechanical Engineering, 1979.

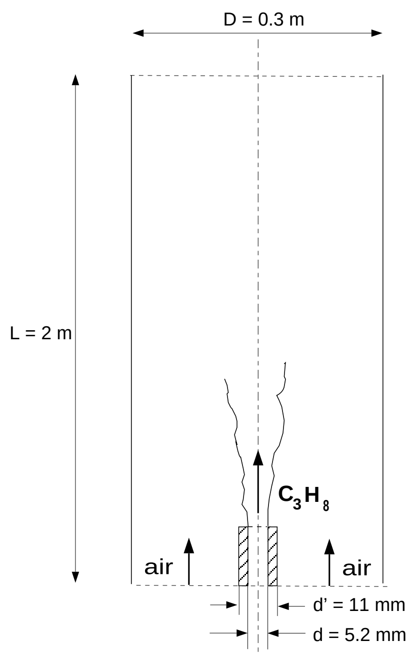


Figure 7.2.1: Problem Description

Release 12.0 © ANSYS, Inc. January 24, 2009

7.4 Results

ANSYS FLUENT's results for the four runs are compared to the data from [1] in Figures 7.4.1 and 7.4.2, as measured along the symmetry axis of the tunnel, downstream of the jet pipe exit. Figure 7.4.1 compares the propane mass fraction (for the nonreacting species transport model) or the mean mixture fraction (for the mixture fraction/PDF model). Figure 7.4.2 compares the axial velocities of the mixing flow.

Predictions of the mixture fraction or the propane mass fraction are very good for all the runs. The axial velocity distribution is in very close agreement with the benchmark.

7.4.1 Validation-Specific Information

Solver:	ANSYS FLUENT 2D Double Precision
Version:	6.4.13
Solution Files:	1. `mixing_quad.cas`, `mixing_quad.dat` (non-reacting species model)
	2. `mixing_tri.cas`, `mixing_tri.dat` (non-reacting species model)
	3. `mixing_pdf_quad.cas`, `mixing_pdf_quad.dat` (and `mixing.pdf`) (mixture fraction/PDF model)
	4. `mixing_pdf_tri.cas`, `mixing_pdf_tri.dat` (and `mixing.pdf`) (mixture fraction/PDF model)

These solution files are available from the User Services Center as described in the Introduction.

7.4.2 Plot Data

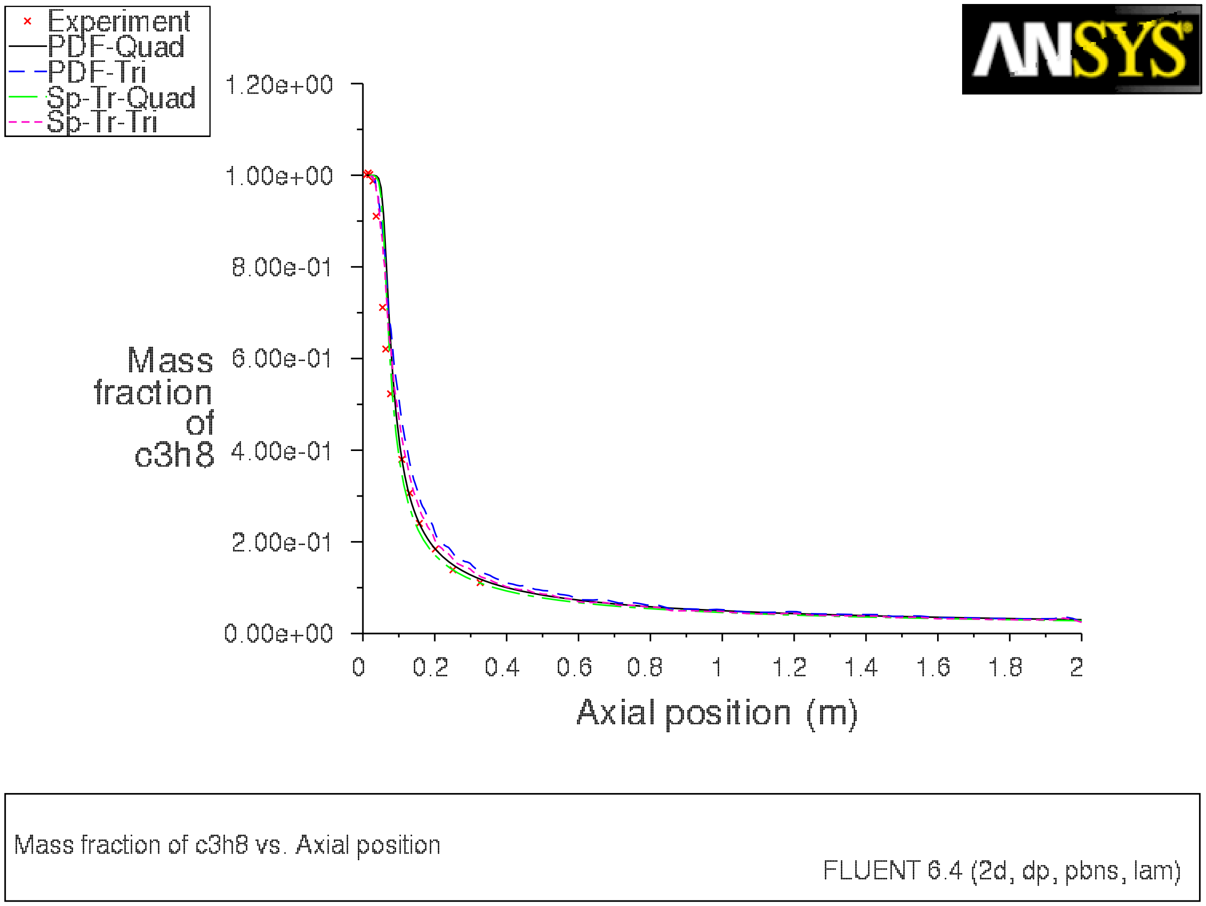


Figure 7.4.1: Propane Mass Fraction (Non-Reacting Species Transport Model Solutions) and Mixture Fraction (Mixture Fraction/PDF Model Solutions) Along the Symmetry Axis

Release 12.0 © ANSYS, Inc. January 24, 2009

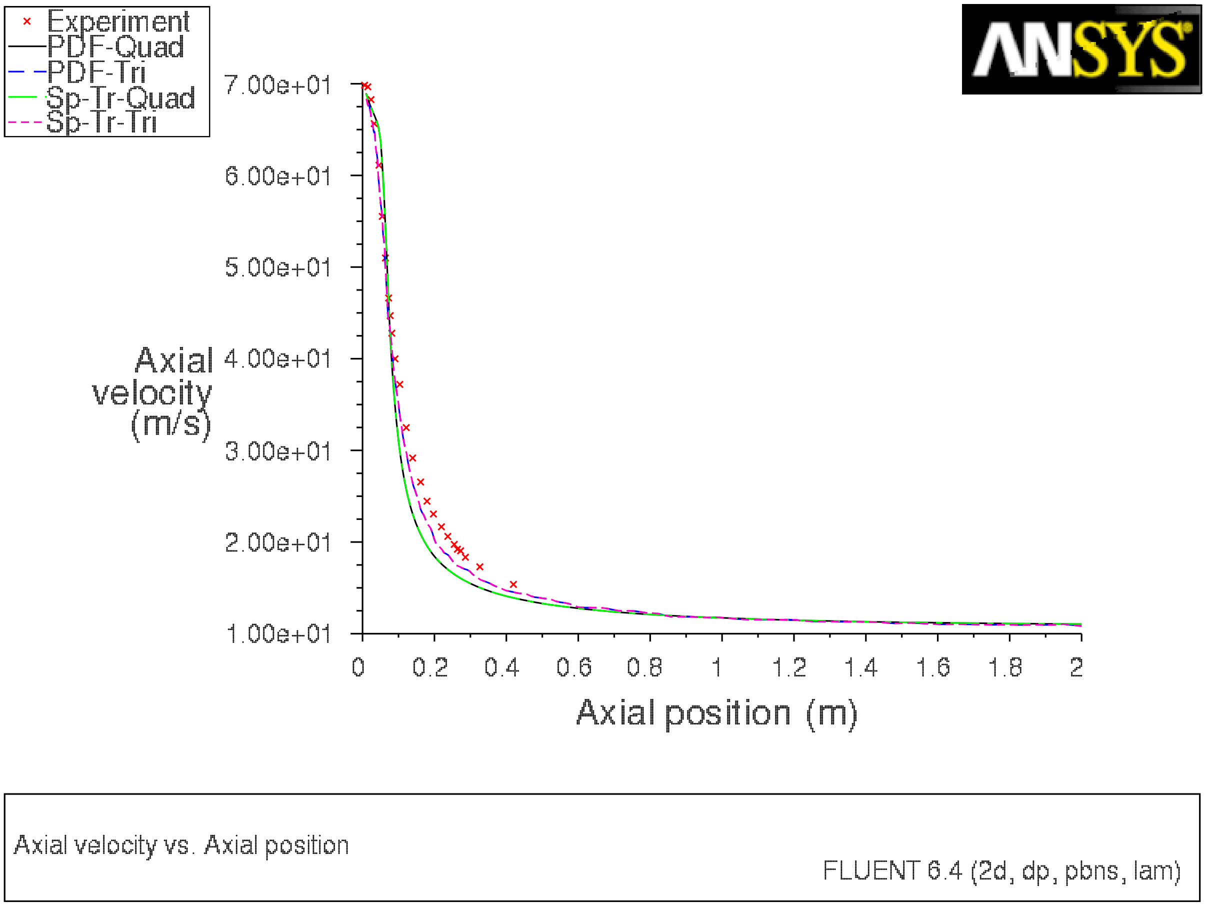


Figure 7.4.2: Axial Velocity Along the Symmetry Axis

Validation 8. Flow through an Engine Inlet Valve

8.1 Purpose

The purpose of this test is to compare the ANSYS FLUENT prediction of the local velocity field against experimental data of Chen et al. [1].

8.2 Problem Description

A flow in an idealized engine cylinder with a straight inlet port and a valve lift of 10 mm (the distance from the top of the cylinder to the bottom of the valve) is examined in this case. The length of the cylinder is chosen to be large enough that it will not affect the flow in the cylinder. The configuration of the inlet port, valve, and cylinder is shown in Figure 8.2.1.

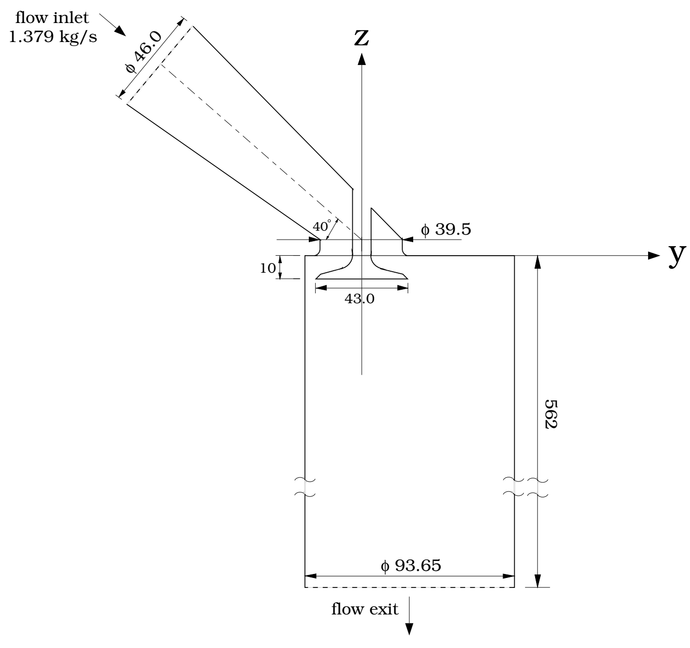


Figure 8.2.1: Problem Description (all dimensions in millimeters)

8.3 References

1. Chen, A., Lee, K.C., Yianneskis, M., and Ganti, G., Velocity Characteristics of Steady Flow Through a Straight Generic Inlet Port, *International Journal for Numerical Methods in Fluids*, 21:571–590, 1995.

8.4 Results

Figures compare ANSYS FLUENT's results with the experimental data (z component of velocity at different heights). All the characteristics of the flow (the angle of the inlet jet, the vortices at the far right and the far left side of the cylinder, and the little vortex to the left of the valve) are correctly predicted by ANSYS FLUENT.

8.4.1 Validation-Specific Information

Solver:	ANSYS FLUENT 3D Double Precision
Version:	12.0.1
Solution Files:	1. `valve10_1st.cas.gz`, `valve10_1st.dat.gz` - 1st order discretization 2. `valve10_2nd.cas.gz`, `valve10_2nd.dat.gz` - 2nd order discretization 3. `valve10_2nd_adapt.cas.gz`, `valve10_2nd_adapt.dat.gzt` - 2nd order + adaption

These solution files are available from the User Services Center as described in the Introduction.

 Release 12.0 © ANSYS, Inc. January 24, 2009

8.4.2 Plot Data

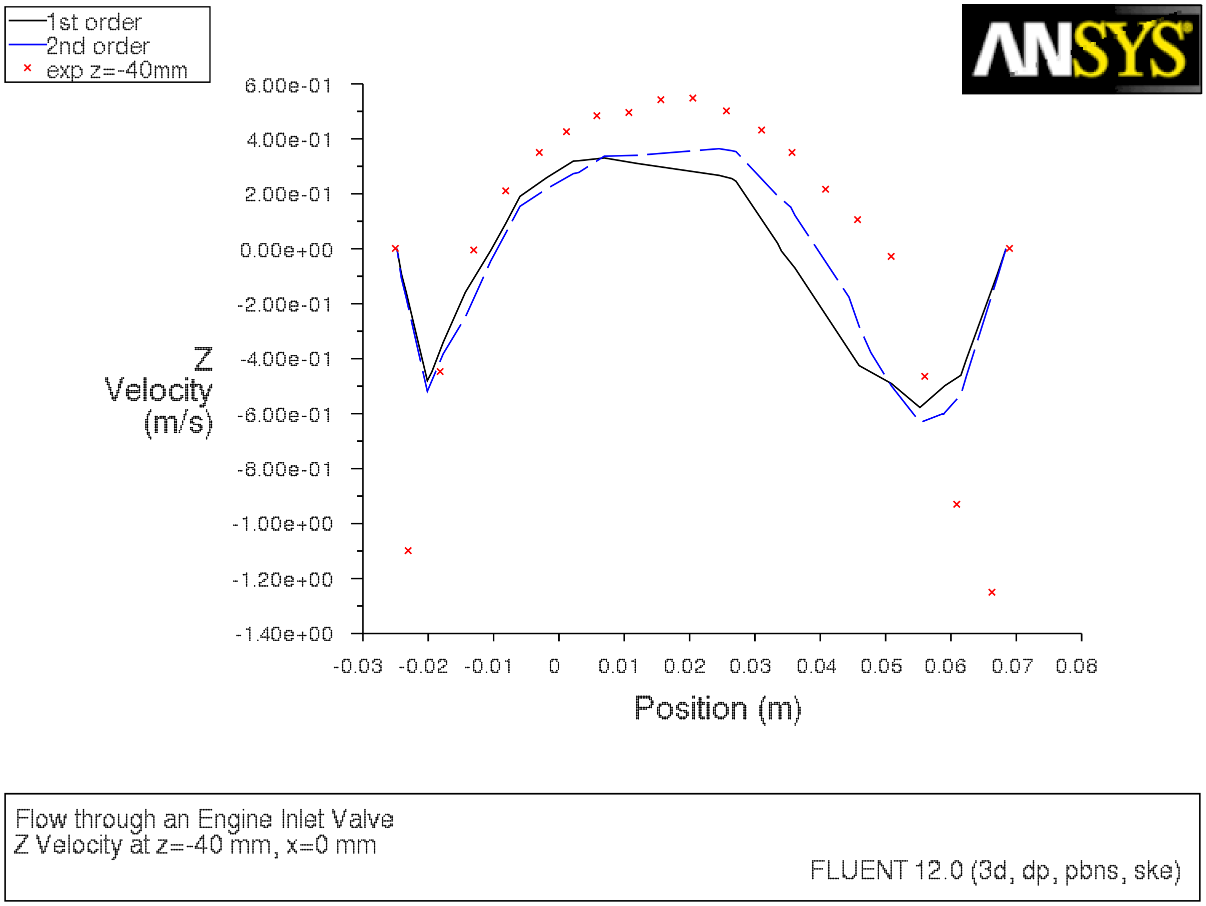


Figure 8.4.1: z-Velocity Components at $z = -40$ mm

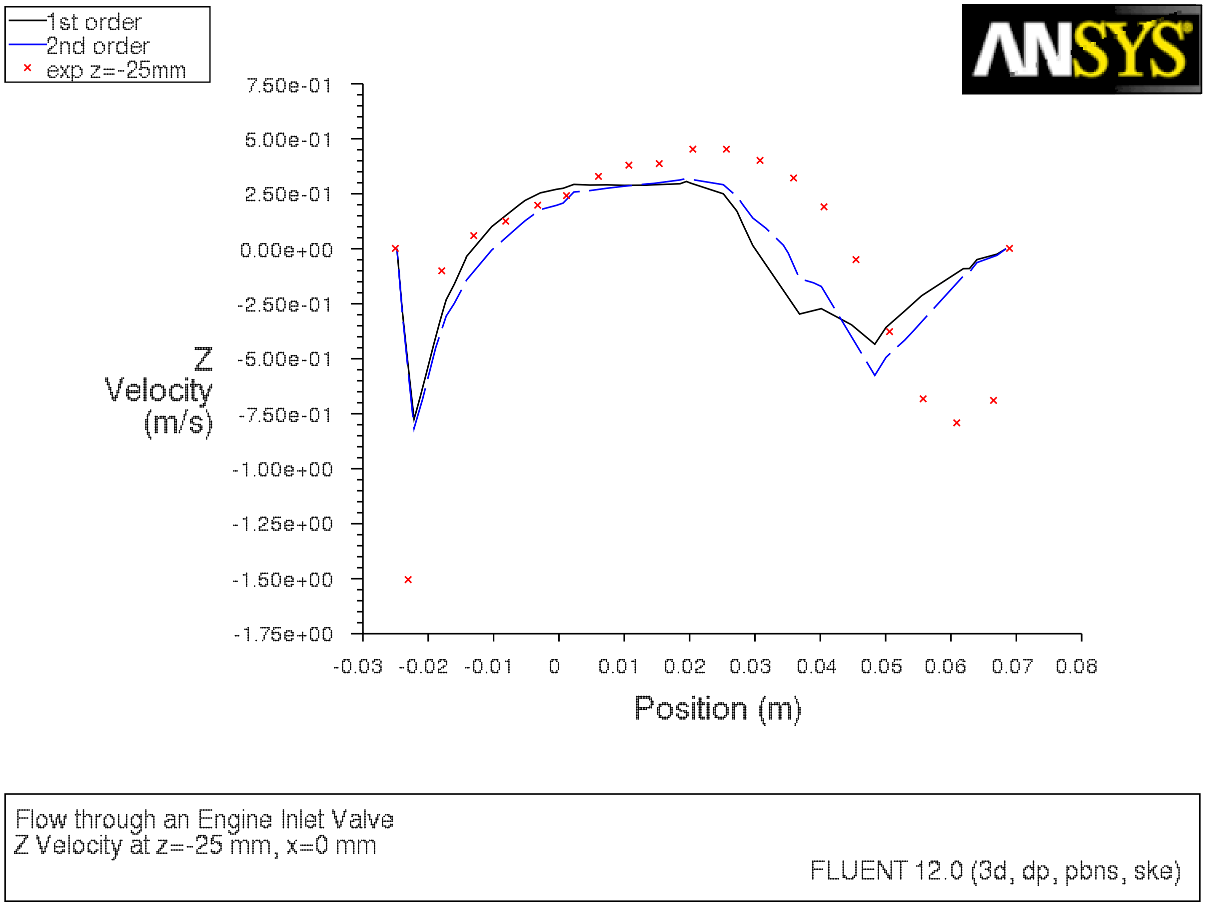


Figure 8.4.2: z-Velocity Components at $z = -25$ mm

Release 12.0 © ANSYS, Inc. January 24, 2009

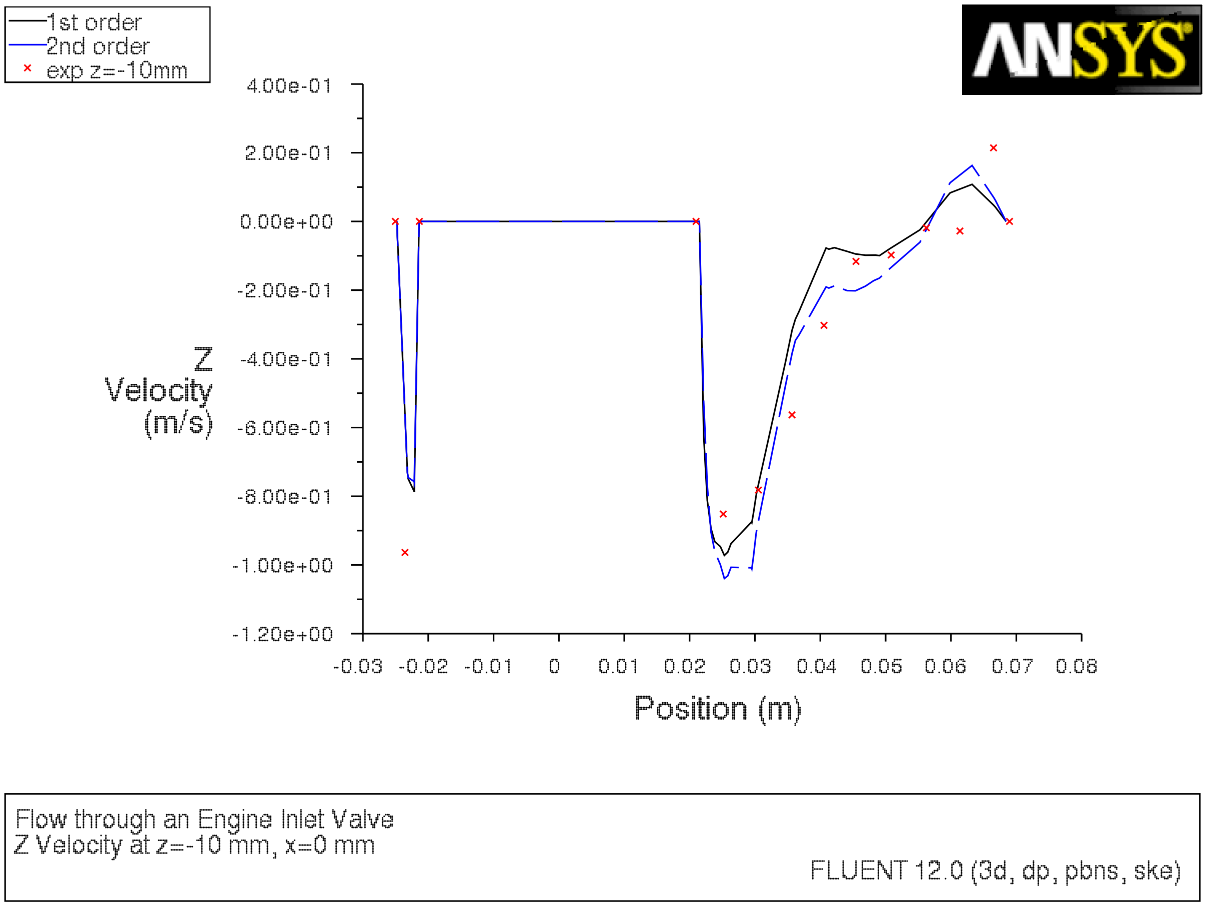


Figure 8.4.3: z-Velocity Components at $z = -10$ mm

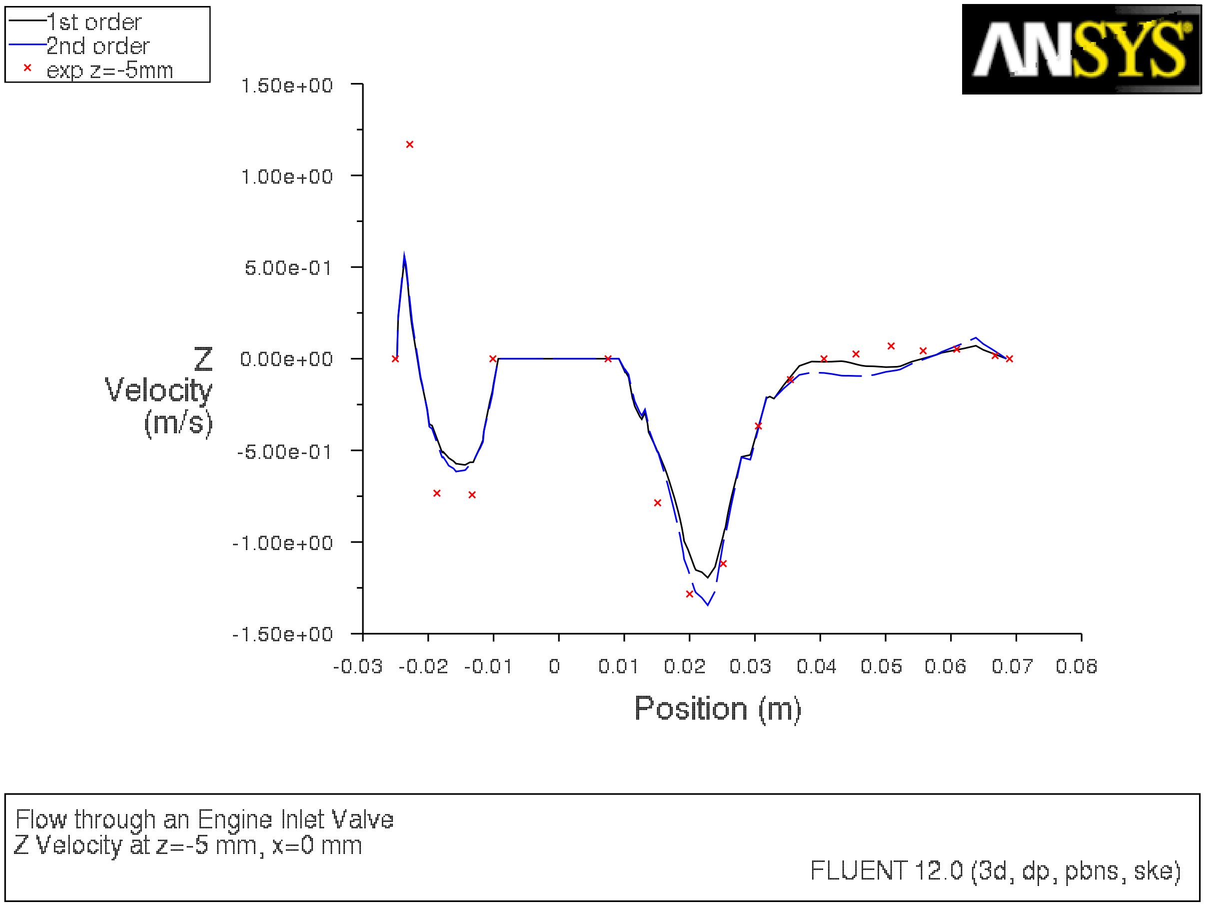


Figure 8.4.4: z-Velocity Components at $z = -5$ mm

Release 12.0 © ANSYS, Inc. January 24, 2009

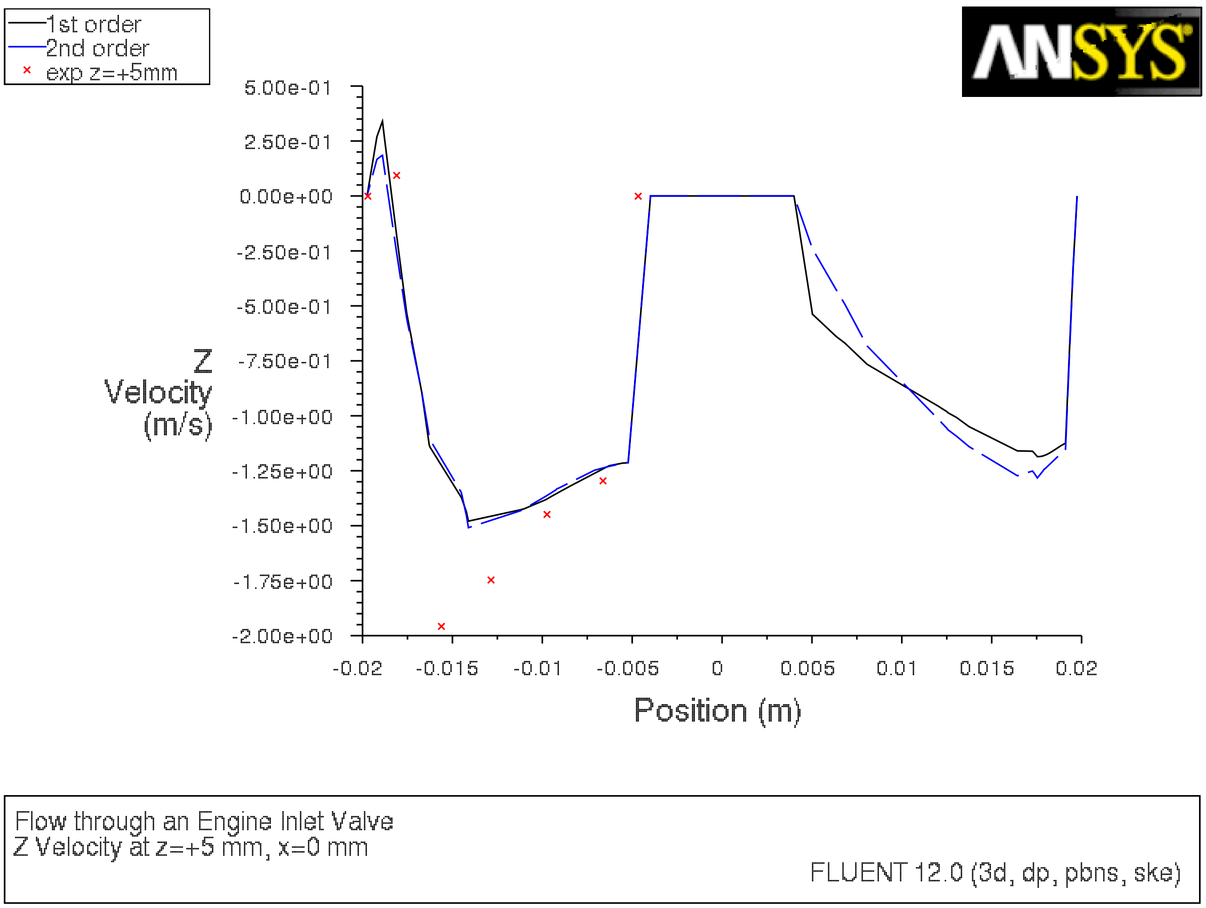


Figure 8.4.5: z-Velocity Components at $z = +5$ mm

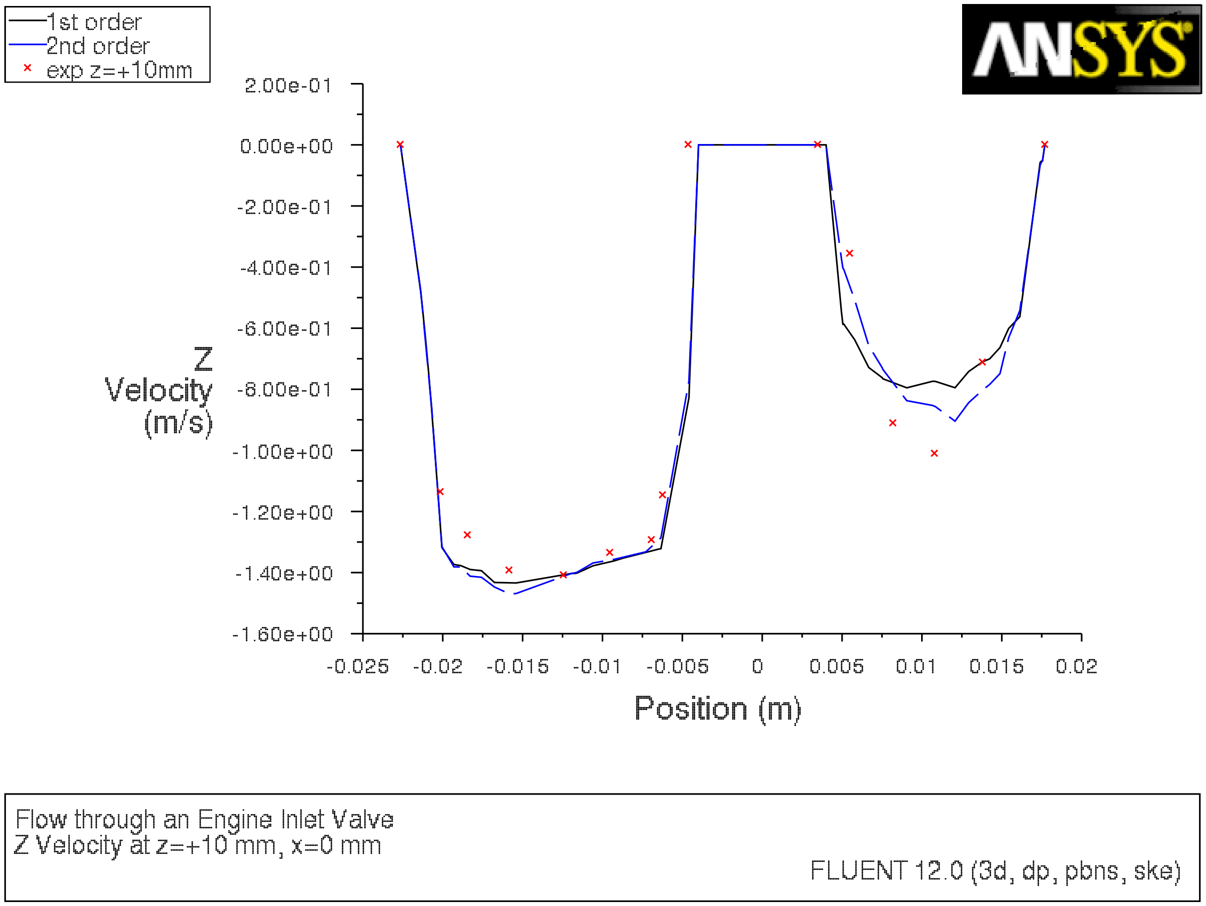


Figure 8.4.6: z-Velocity Components at $z = +10$ mm

Release 12.0 © ANSYS, Inc. January 24, 2009

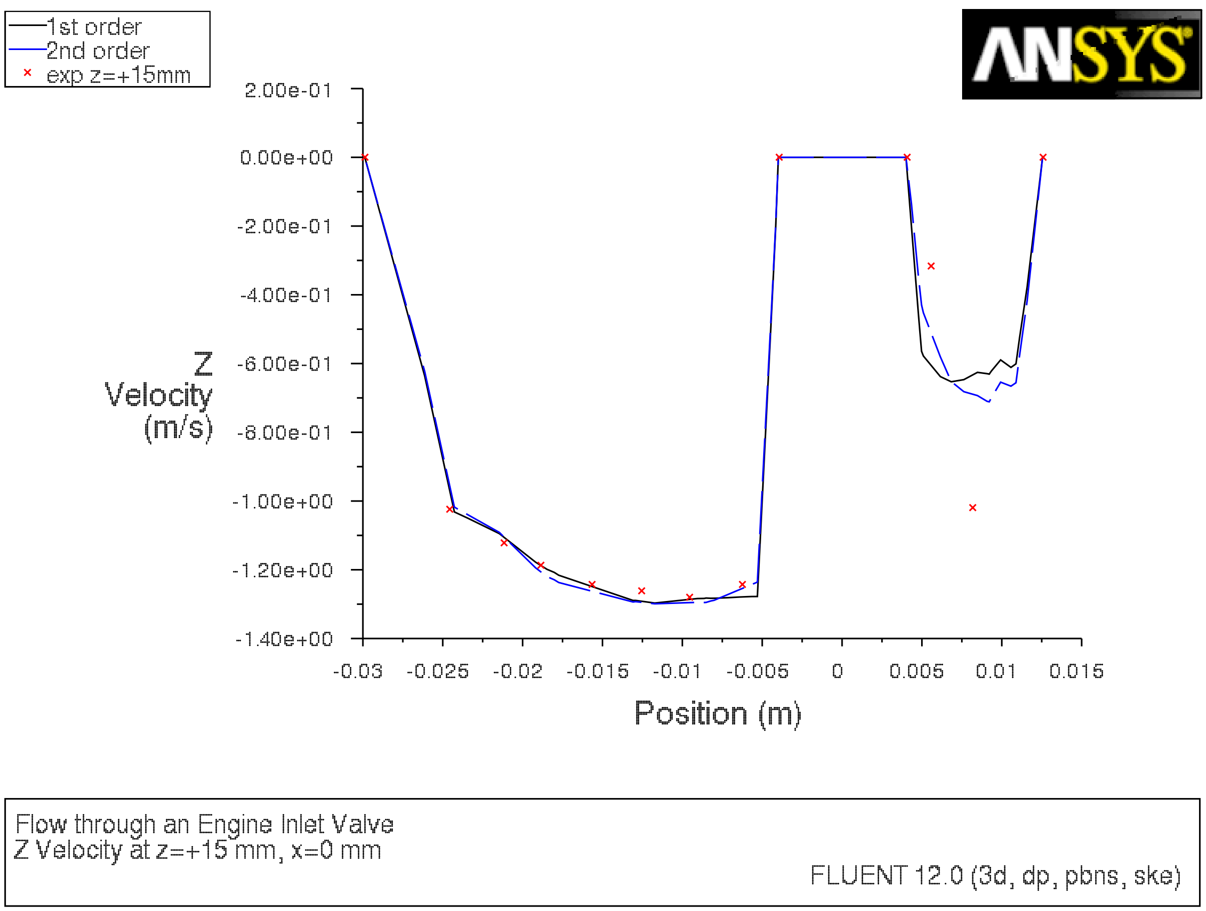


Figure 8.4.7: z-Velocity Components at $z = +15$ mm

Release 12.0 © ANSYS, Inc. January 24, 2009

Validation 9. Turbulent Flow in a Transition Duct

9.1 Purpose

The purpose of this test is to assess the ability of ANSYS FLUENT to reproduce the complicated three-dimensional features of a flow in a circular to rectangular transition duct. ANSYS FLUENT predictions for the following quantities are compared with the experimental data of Davis and Gessner [1]:

1. Distribution of pressure coefficient, C_p, and skin friction coefficient, C_f, at two different cross-sections along the duct wall as a function of the non-dimensional girth length
2. Distribution of static pressure coefficient along the centerline

9.2 Problem Description

The problem under consideration involves a flow through a circular-to-rectangular transition duct having the same inlet and outlet cross-sectional areas. The curvature of the duct walls induces a strong pressure-driven crossflow that develops into a counter-rotating vortex pair near the short side walls of the duct. This vortex pair significantly distorts both the primary mean velocity and the Reynolds stress fields. Taking into account the symmetry of the flow field, only one fourth of the duct is modeled (as shown in Figure 9.2.1). Station 5 and Station 6 are the cross-sections at $x/\rho = 4$ and $x/\rho = 8$, respectively, where ρ is the inlet radius and x is the axial direction ($x/\rho = -1$ at the inlet, and $x/\rho = 16$ at the outlet).

The computational domain shown in Figure 9.2.1 reproduces the test setup outlined by Davis and Gessner [1]. A uniform, low turbulence level flow enters a straight pipe ($L_{pipe}/D = 9$). A fully turbulent boundary layer is assumed along the entire pipe length, which is consistent with the experimental data where the boundary layer was tripped at the inlet.

9.3 References

1. Davis, D.O., and Gessner, F.B., Experimental Investigation of Turbulent Flow Through a Circular-to-Rectangular Transition Duct, *AIAA Journal*, 30(2):367–375, 1992.

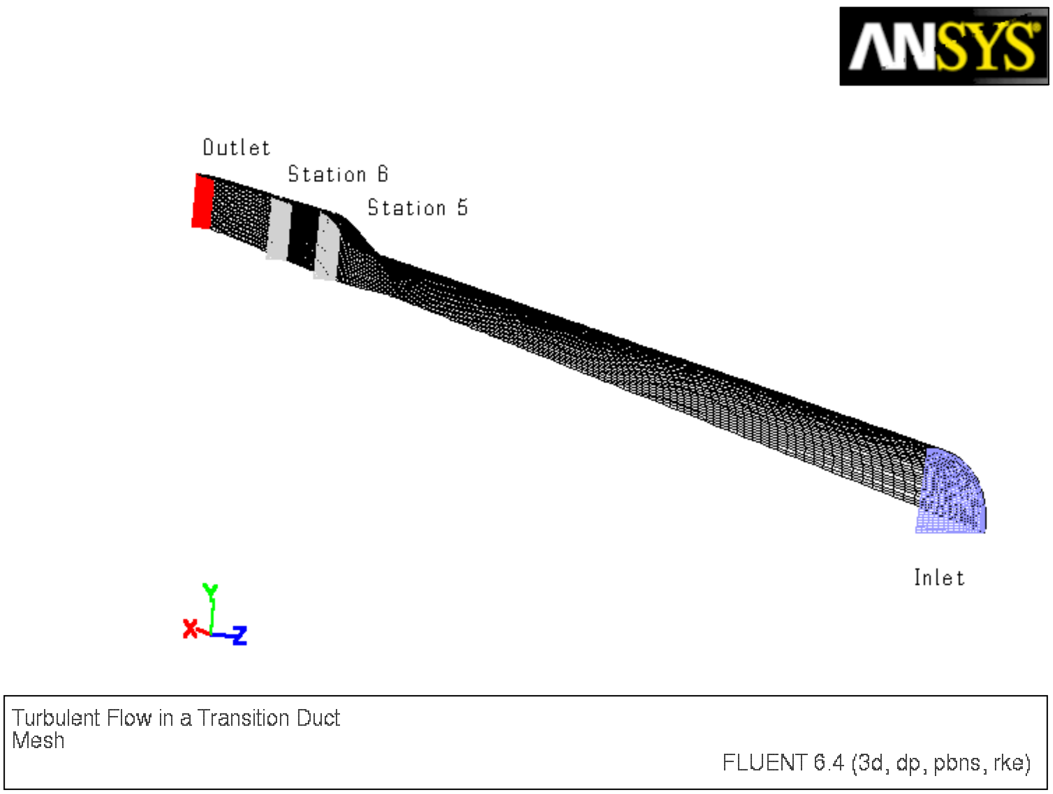


Figure 9.2.1: Problem Mesh

Release 12.0 © ANSYS, Inc. January 24, 2009

9.4 Results

Figures show comparison of the following profiles for all three turbulence models:

1. Pressure coefficient, C_p, and skin friction coefficient, C_f, at two different cross-sections along the duct wall as a function of the non-dimensional girth length.

   In the XY plots, the data is plotted against projected quarter of the duct boundary, where a position of 0 m corresponds to the center of the longer side of the duct, and a position of 1 m corresponds to the center of the shorter side.

2. Static pressure coefficient along the centerline.

9.4.1 Validation-Specific Information

Solver:	ANSYS FLUENT 3D, 3D Double Precision
Version:	6.4.13
Solution Files:	1. `hex_rke_r1.cas.gz`, `hex_rke_r1.dat.gz` - Realizable$k$-ϵ
	2. `hex_sst_r2.cas.gz`, `hex_sst_r2.dat.gz` - SST k-ω
	3. `hex_rsm_r3.cas.gz`, `hex_rsm_r3.dat.gz` - Reynolds Stress Model (RSM)

These solution files are available from the User Services Center as described in the Introduction.

9.4.2 Plot Data

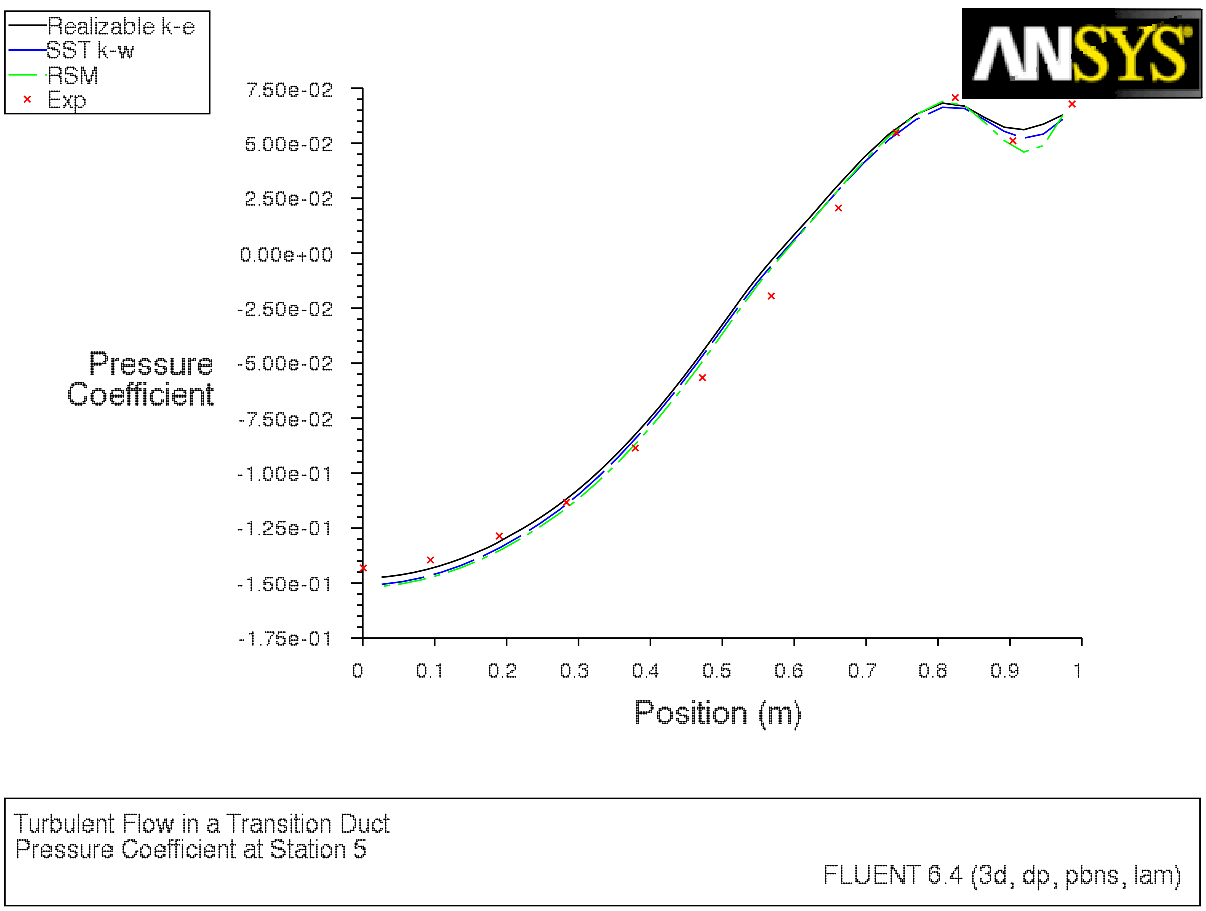


Figure 9.4.1: Comparison of Wall Pressure Coefficient at Station 5

Release 12.0 © ANSYS, Inc. January 24, 2009

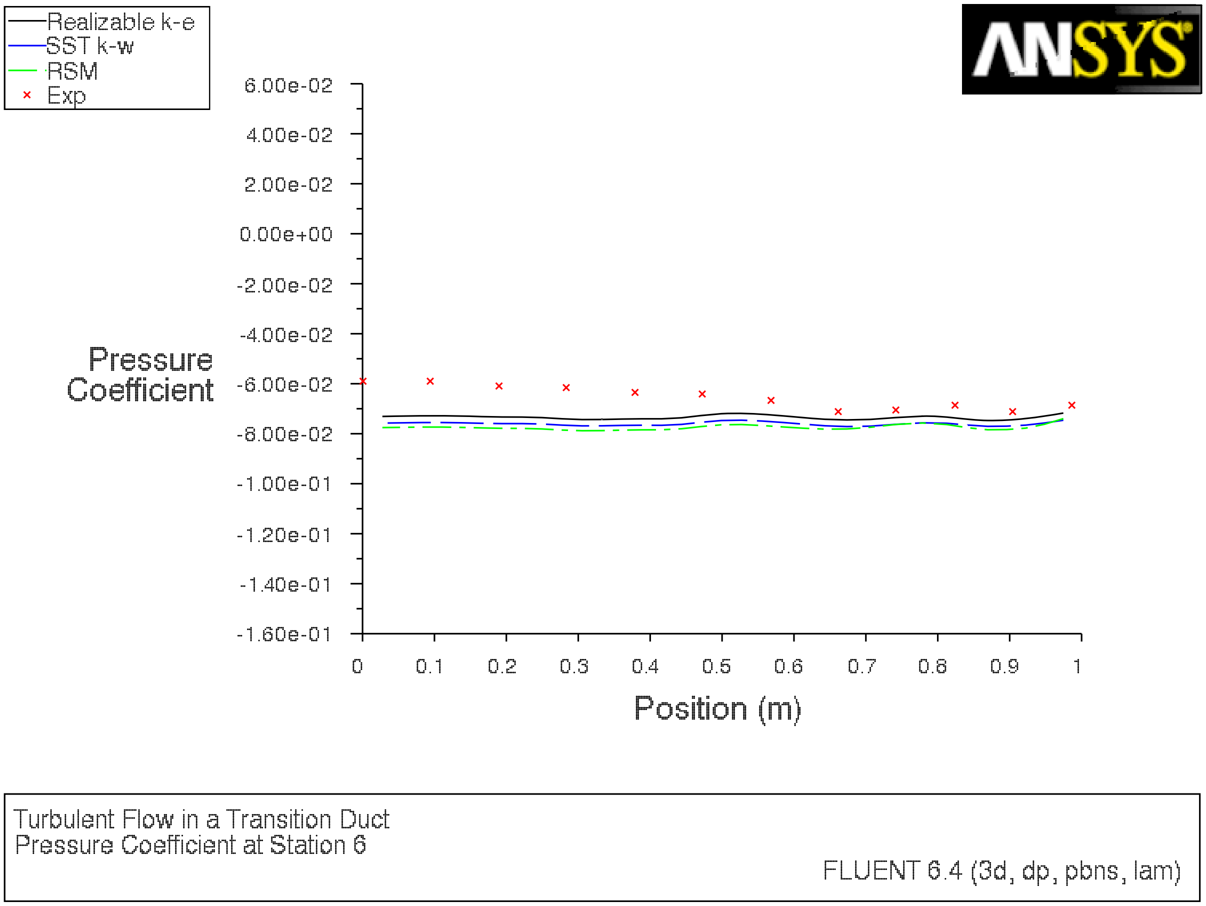


Figure 9.4.2: Comparison of Wall Pressure Coefficient at Station 6

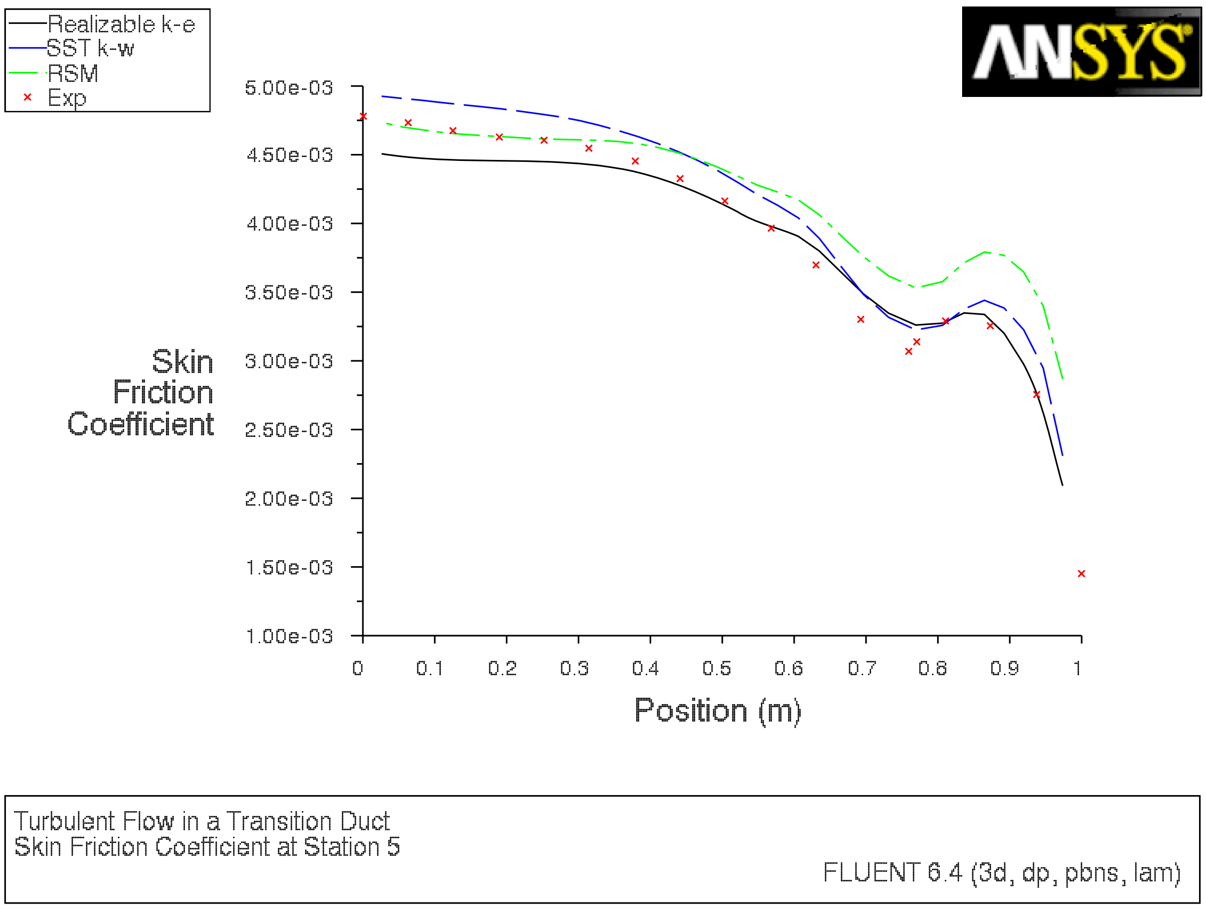


Figure 9.4.3: Comparison of Skin Friction Coefficient at Station 5

Release 12.0 © ANSYS, Inc. January 24, 2009

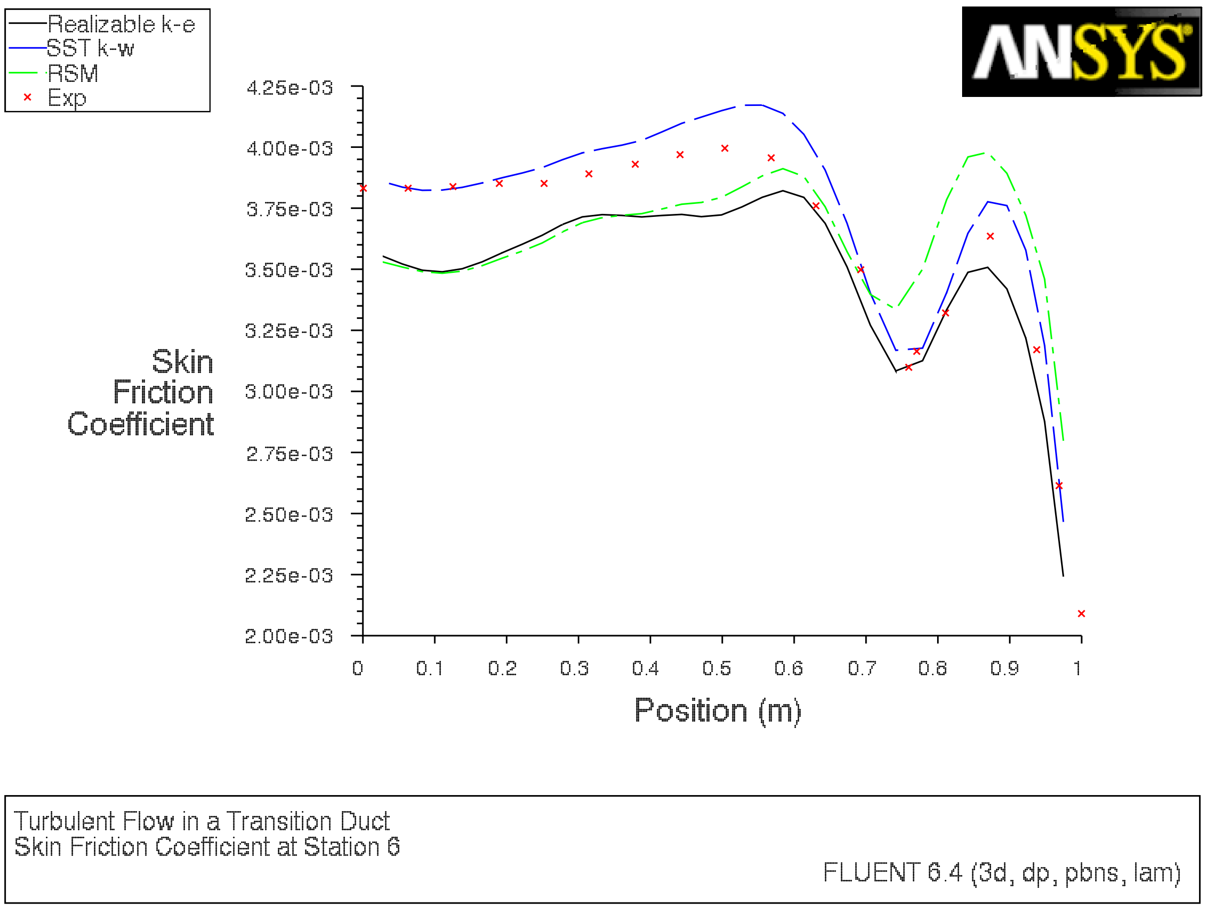


Figure 9.4.4: Comparison of Skin Friction Coefficient at Station 6

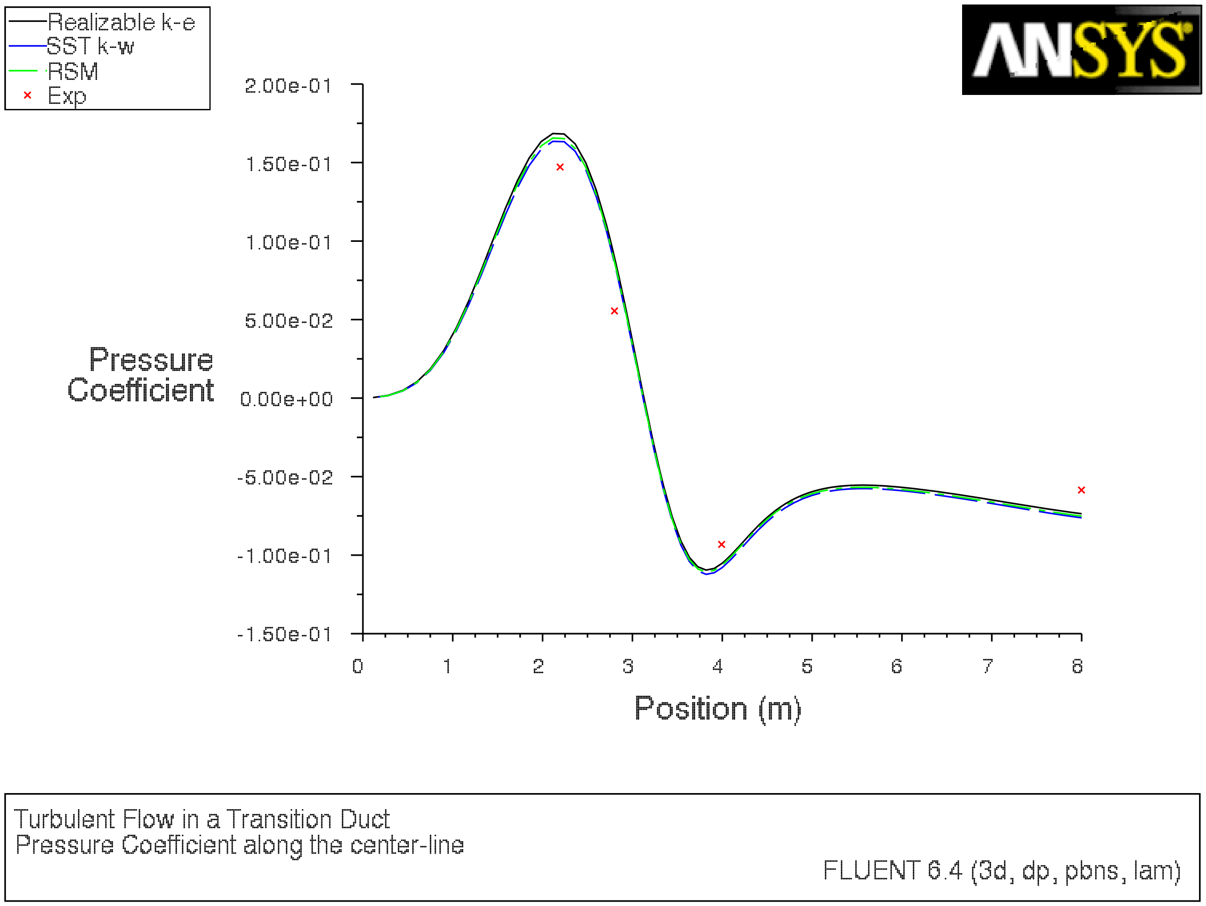


Figure 9.4.5: Comparison of Pressure Coefficient Along the Centerline

Release 12.0 © ANSYS, Inc. January 24, 2009

Validation 10. Transonic Flow Over an RAE 2822 Airfoil

10.1 Purpose

The purpose of this validation is to compare the predictions of ANSYS FLUENT with the experimental data of Cook et al. [1] for flow over an RAE 2822 airfoil. The quantities examined are:

1. Static pressure coefficient, C_p.
2. Lift and drag coefficients.
3. Shock position on the airfoil.

10.2 Problem Description

The problem under consideration involves flow over an RAE 2822 airfoil at a free-stream Mach number of 0.73. The angle of attack is 3.19 degrees, which corresponds to case 9 in the experimental data of Cook et al. [1]. Since the calculations were done in free-stream conditions, the angle of attack has been modified to account for the wind-tunnel wall effects. An angle of attack equal to 2.79 degrees was used in the calculations, as suggested by Coakley [2].

The geometry of the RAE 2822 airfoil is shown in Figure 10.2.1. It is a thick airfoil with a chord length, c, of 1.00 m and a maximum thickness, d, of 0.121 m. The domain extends $55c$ from the airfoil, so that the presence of the airfoil is not felt at the outer boundary.

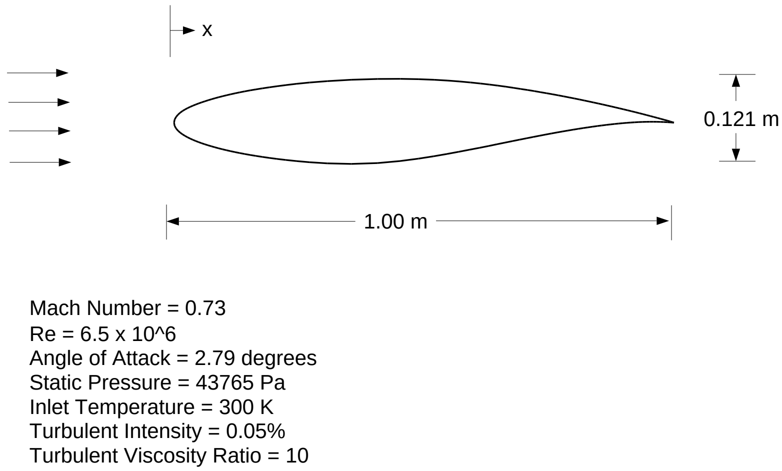


Figure 10.2.1: Geometry of the RAE 2822 Airfoil

10.3 References

1. Cook, P.H., McDonald, M.A., and Firmin, M.C.P., *AEROFOIL RAE 2822 Pressure Distribution and Boundary Layer and Wake Measurements*, AGARD Advisory Report No. 138, 1979.

2. Thomas J. Coakley., *Numerical Simulation of Viscous Transonic Airfoil Flows*, AIAA 25th Aerospace Sciences Meeting, 1987.

10.4 Results

A comparison of ANSYS FLUENT's predictions of the static pressure coefficient C_p with experimental data has been done for a hybrid and a quadrilateral mesh. In general, ANSYS FLUENT's predictions agree well with the experimental data.

The shock location over the airfoil is quantified as the location where the top surface pressure coefficient increases or decreases rapidly. Table 10.4.1 compares the numerical predictions of the shock location, the lift coefficients, and the drag coefficients for the six cases are compared with the experimental values and shown in the following table:

From Table 10.4.1, the predicted shock locations are accurately predicted within engineering accuracy for all six runs.

Release 12.0 © ANSYS, Inc. January 24, 2009

Table 10.4.1: Comparison of the Predictions of Shock Location

Mesh	**Model**	**Drag** (C_D)	**Lift** (C_L)	**Shock** (x/c)
	Experiment	0.803	0.0168	0.52
Hybrid	Realizable k-ϵ	0.830	0.0176	0.52
Hybrid	SST k-ω	0.781	0.0164	0.50
Hybrid	Spalart-Allmaras	0.815	0.0171	0.52
	Experiment	0.803	0.0168	0.52
Quadrilateral	Realizable k-ϵ	0.834	0.0177	0.52
Quadrilateral	SST k-ω	0.785	0.0162	0.50
Quadrilateral	Spalart-Allmaras	0.822	0.0170	0.52

10.4.1 Validation-Specific Information

Solver: ANSYS FLUENT 2D Double Precision
Version: 12.0.1
Solution Files:
1. `rae_hybrid_rke_nb.cas.gz`, `rae_hybrid_rke_nb.dat.gz`
2. `rae_hybrid_sst_nb.cas.gz`, `rae_hybrid_sst_nb.dat.gz`
3. `rae_hybrid_sa_nb.cas.gz`, `rae_hybrid_sa_nb.dat.gz`
4. `rae_quad_rke_nb.cas.gz`, `rae_quad_rke_nb.dat.gz`
5. `rae_quad_sst_nb.cas.gz`, `rae_quad_sst_nb.dat.gz`
6. `rae_quad_sa_nb.cas.gz`, `rae_quad_sa_nb.dat.gz`

These solution files are available from the User Services Center as described in the Introduction.

10.4.2 Plot Data

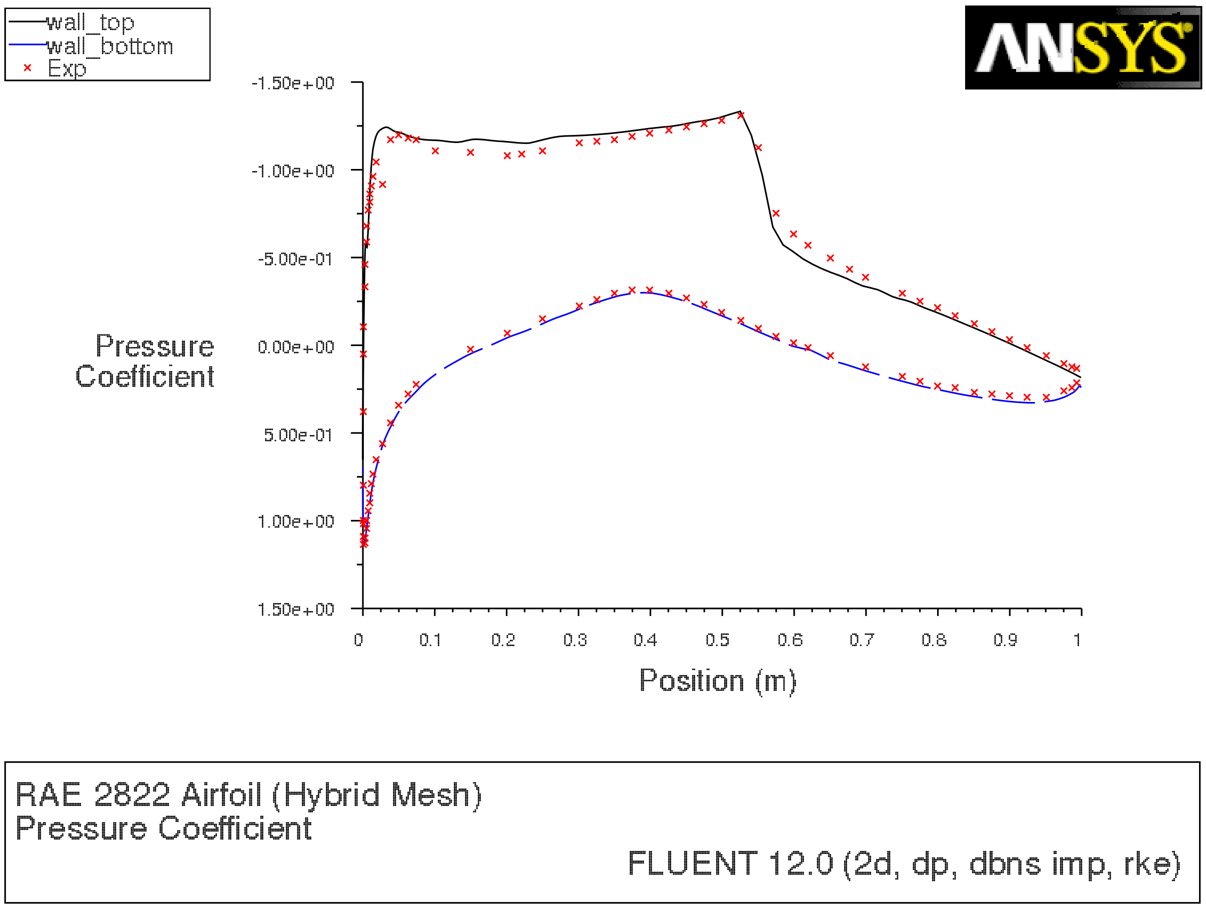


Figure 10.4.1: Comparison of ANSYS FLUENT's Predictions of the Static Pressure Coefficient C_p With the Experimental Data for the Hybrid Mesh, Realizable k-ϵ Case

Release 12.0 © ANSYS, Inc. January 24, 2009

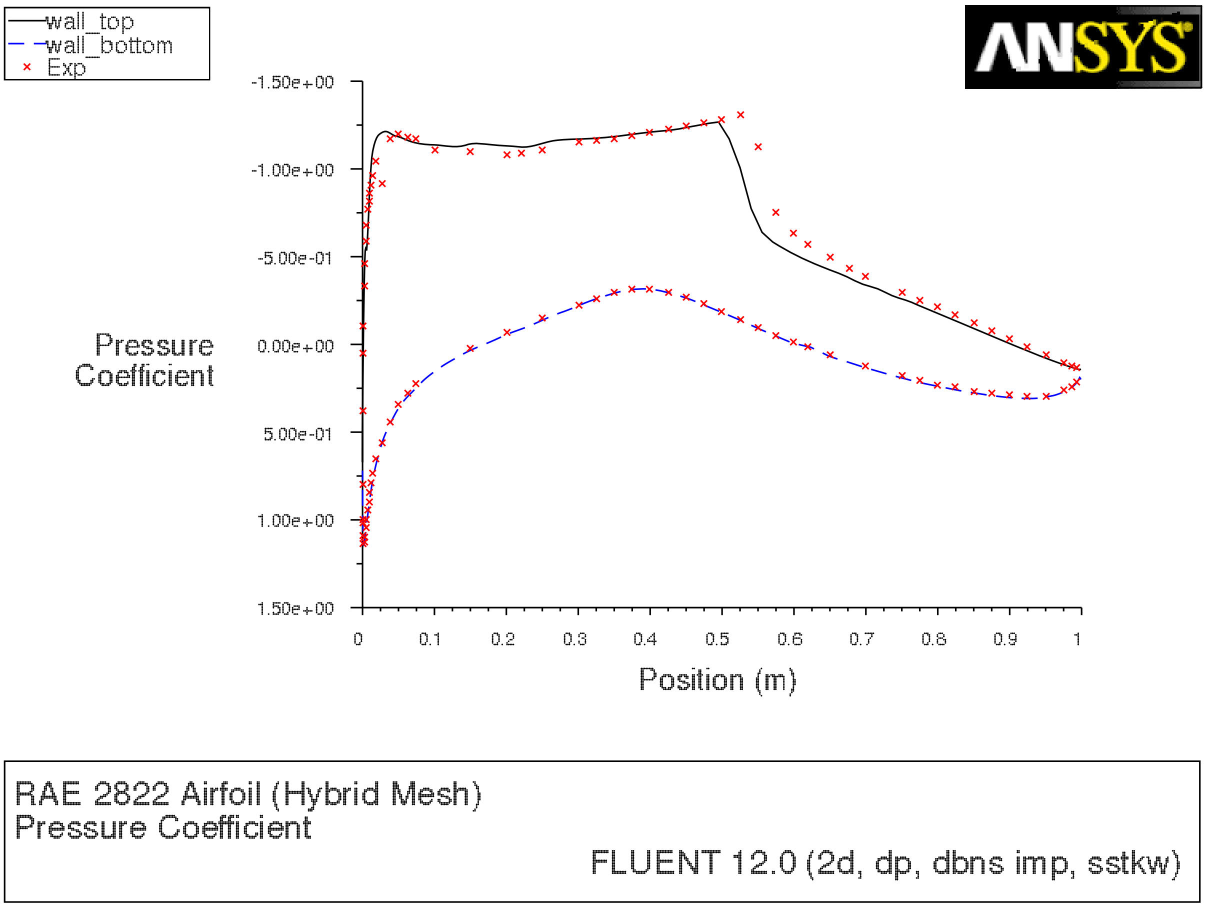


Figure 10.4.2: Comparison of ANSYS FLUENT's Predictions of the Static Pressure Coefficient C_p With the Experimental Data for the Hybrid Mesh, SST k-ω Case

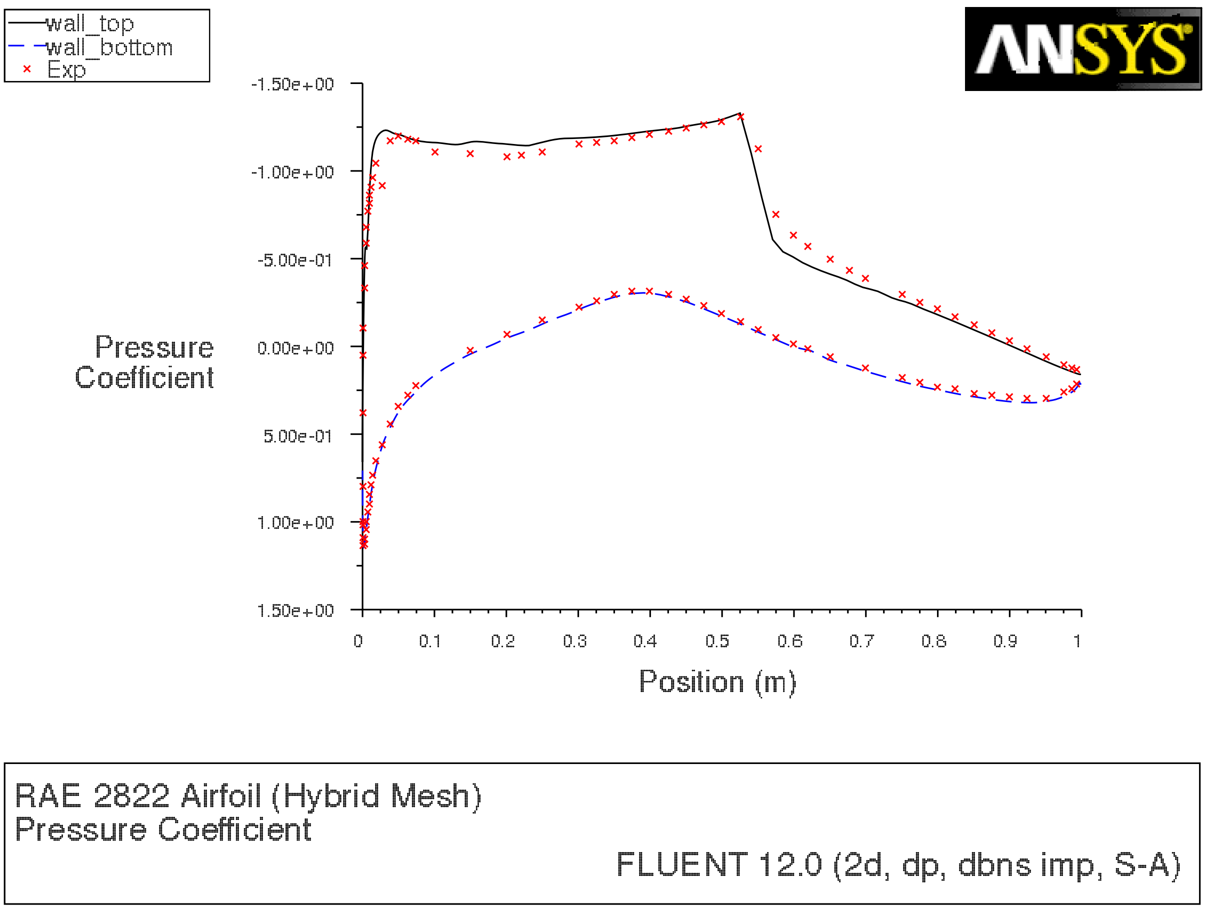


Figure 10.4.3: Comparison of ANSYS FLUENT's Predictions of the Static Pressure Coefficient C_p With the Experimental Data for the Hybrid Mesh, Spalart-Allmaras Case

Release 12.0 © ANSYS, Inc. January 24, 2009

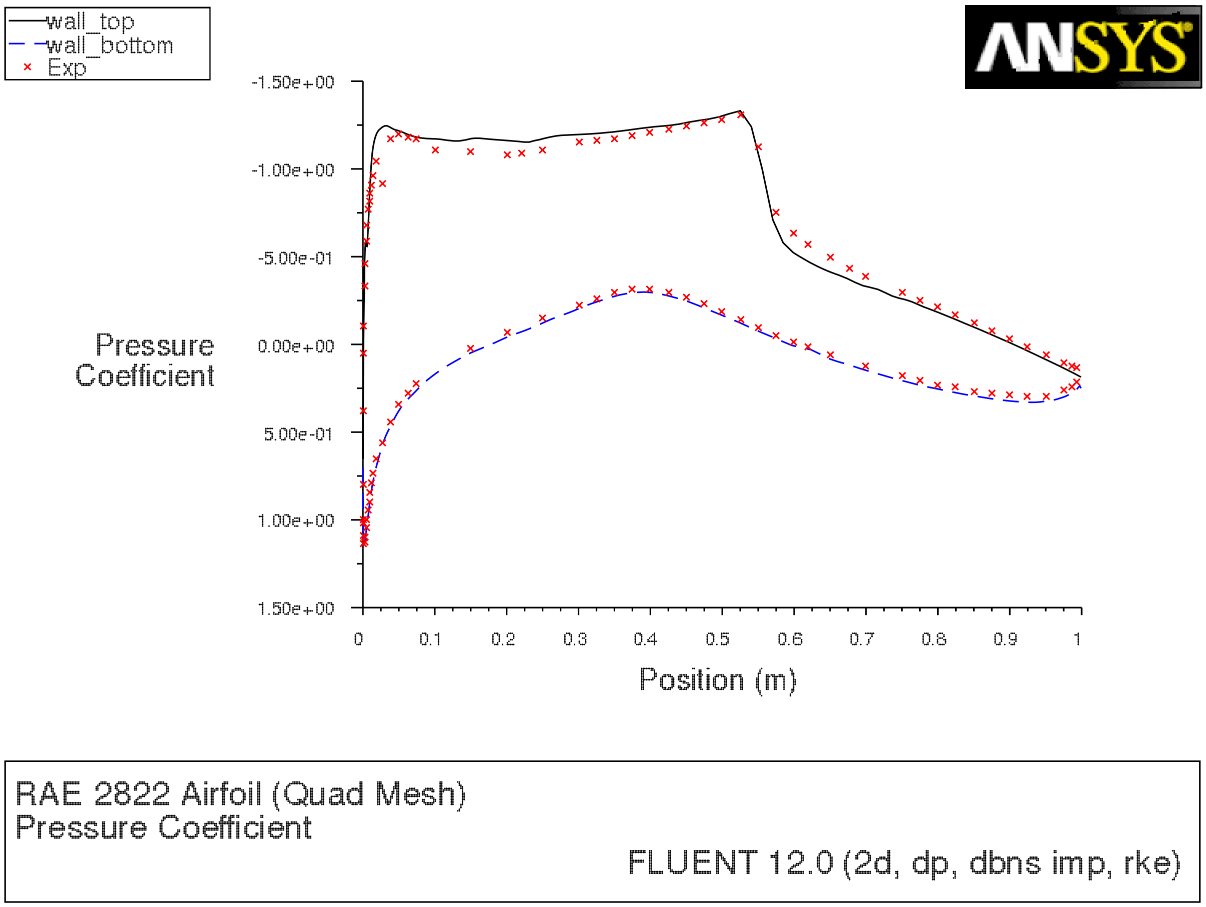


Figure 10.4.4: Comparison of ANSYS FLUENT's Predictions of the Static Pressure Coefficient C_p With the Experimental Data for the Quadrilateral Mesh, Realizable k-ϵ Case

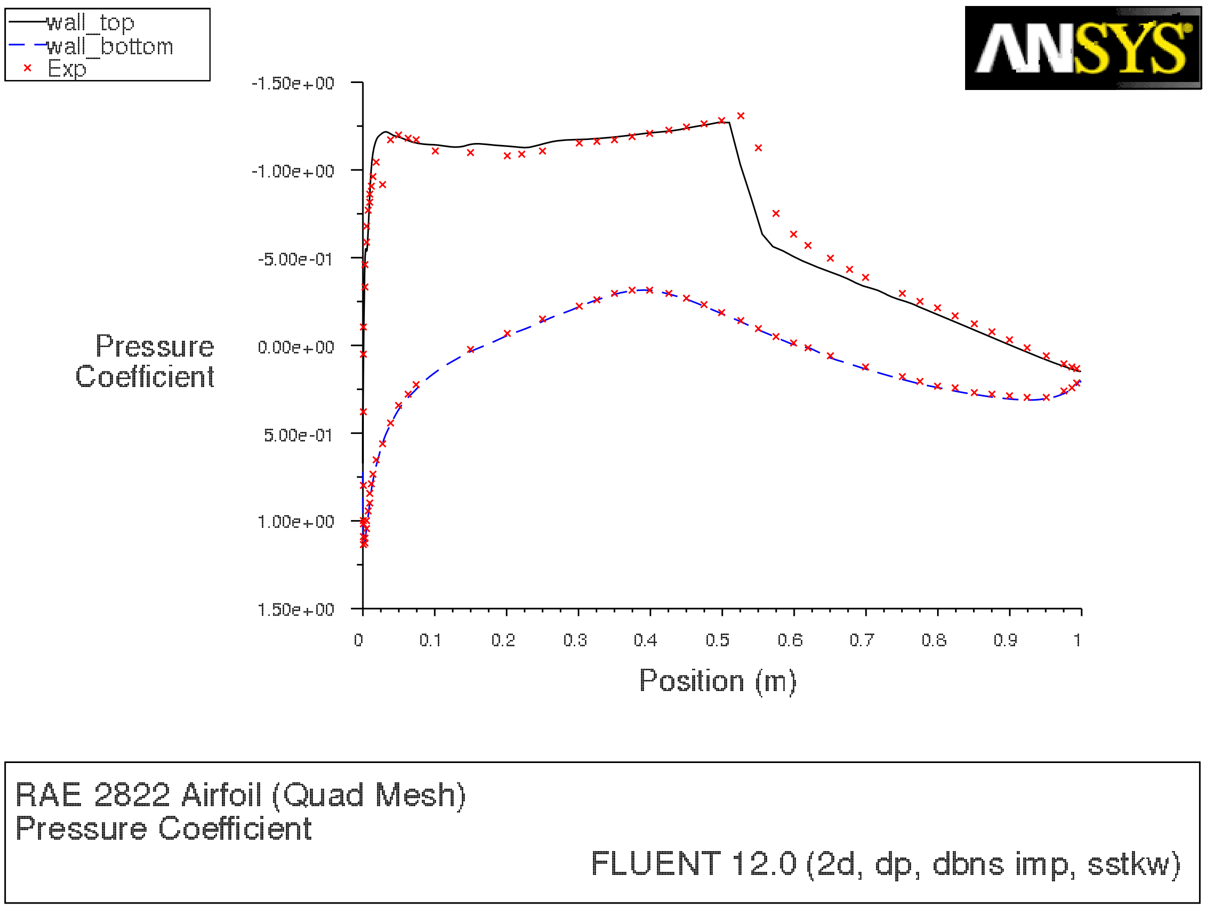


Figure 10.4.5: Comparison of ANSYS FLUENT's Predictions of the Static Pressure Coefficient C_p With the Experimental Data for the Quadrilateral Mesh, SST k-ω Case

Release 12.0 © ANSYS, Inc. January 24, 2009

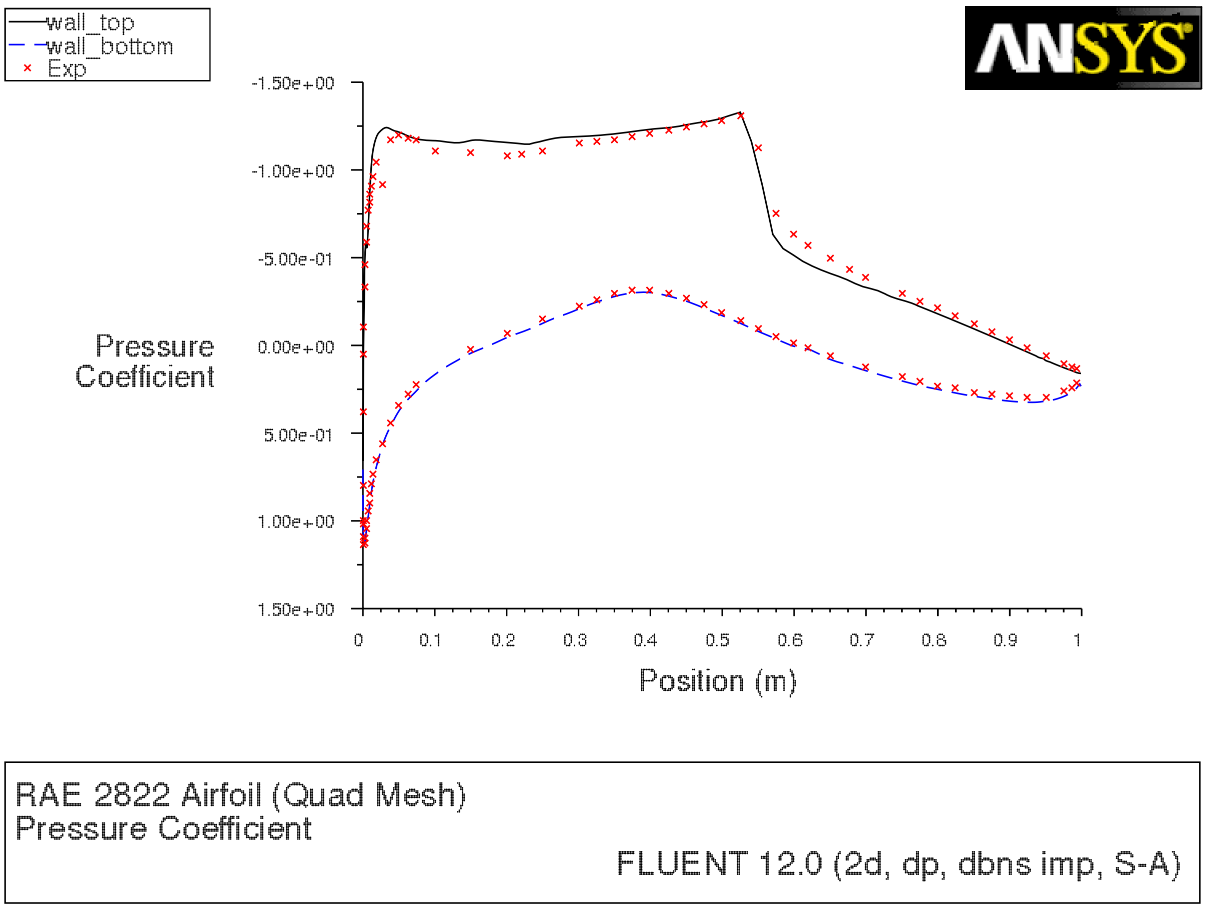


Figure 10.4.6: Comparison of ANSYS FLUENT's Predictions of the Static Pressure Coefficient (C_p) With the Experimental Data for the Quadrilateral Mesh, Spalart-Allmaras Case

Release 12.0 © ANSYS, Inc. January 24, 2009

Validation 11. Mid-Span Flow Over a Goldman Stator Blade

11.1 Purpose

The purpose of this test is to compare ANSYS FLUENT's predictions with the experimental data of Goldman et al.[1]. A comparison is also made between the predictions obtained using the Euler equations and the full Navier-Stokes equations.

11.2 Problem Description

In the present test case, flow over a Goldman stator blade at the mid-span is considered. This 2D analysis provides insight into the accuracy of the discretization scheme and ANSYS FLUENT's ability to predict the complicated flow features typical of turbomachinery applications. The geometry of the domain under consideration is shown in Figure 11.2.1. The inlet and the outlet are located approximately 0.3 m away from the blade's leading and trailing edges, respectively. They are located such that their presence doesn't affect predictions near the blade. The Reynolds number $Re = \rho uh/\mu$ based on the chord length of the blade and the free-stream velocity is $500,000$. Hence the flow is turbulent. The inlet Mach number is approximately 0.2, which implies subsonic flow. Default solver parameters except Green-Gauss Node Based gradient scheme were used in the calculations. The flow field was initialized with the conditions at the inlet. Both the Euler and the full Navier-Stokes equations were used to solve this problem. Moreover, all four solvers available in ANSYS FLUENT were used: density-based explicit, density-based implicit, pressure-based and pressure-based coupled.

11.3 References

1. Goldman, L.G., and McLallin, K.L., Cold-Air Annular Cascade Investigation of Aerodynamic Performance of Core-Engine-Cooled Turbine Vanes: I Solid Vane Performance and Facility Description, NASA Technical Memorandum X-3224, April 1977.

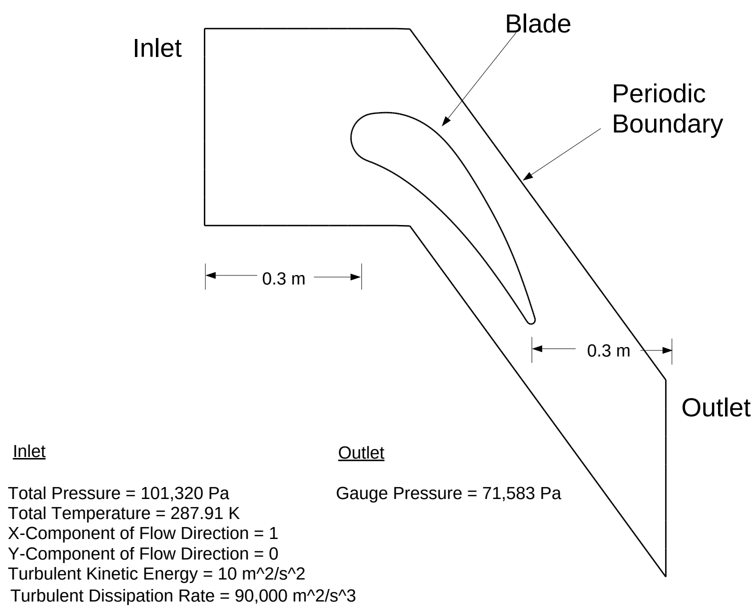


Figure 11.2.1: Geometry of the Goldman Stator Blade

Release 12.0 © ANSYS, Inc. January 24, 2009

11.4 Results

A comparison of the predictions of pressure ratio on the blade (defined as the ratio of static pressure to the inlet total pressure) with the experimental data is shown in Figures 11.4.1 to 11.4.8. ANSYS FLUENT's predictions of pressure distribution at the mid-span of the blade closely match the experimental data of Goldman et al. [1]. The pressure losses at the mid-span due to the presence of end-wall and fluid viscosity are seen to be negligible.

11.4.1 Validation-Specific Information

Solver:	ANSYS FLUENT 2D Double Precision
Version:	6.4.13
Solution Files:	1. `ce_inv.cas.gz`, `ce_inv.dat.gz`
	2. `ce_ke.cas.gz`, `ce_ke.dat.gz`
	3. `ci_inv.cas.gz`, `ci_inv.dat.gz`
	4. `ci_ke.cas.gz`, `ci_ke.dat.gz`
	5. `segr_inv.cas.gz`, `segr_inv.dat.gz`
	6. `segr_ke.cas.gz`, `segr_ke.dat.gz`
	7. `pbcs_inv.cas.gz`, `pbcs_inv.dat.gz`
	8. `pbcs_rke.cas.gz`, `pbcs_rke.dat.gz`

These solution files are available from the User Services Center as described in the Introduction.

11.4.2 Plot Data

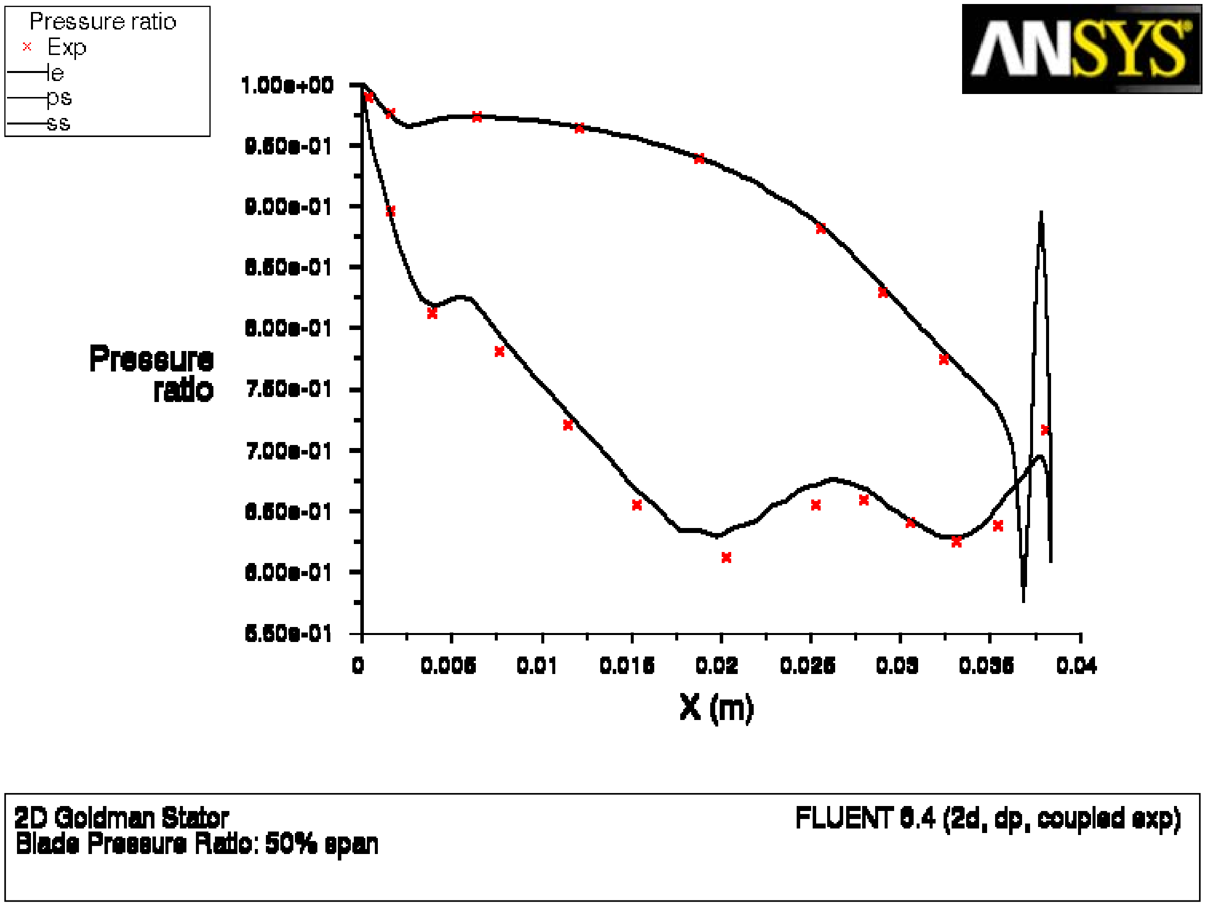


Figure 11.4.1: Pressure Ratio on the Blade (Euler Equations with the Density-Based Explicit Solver)

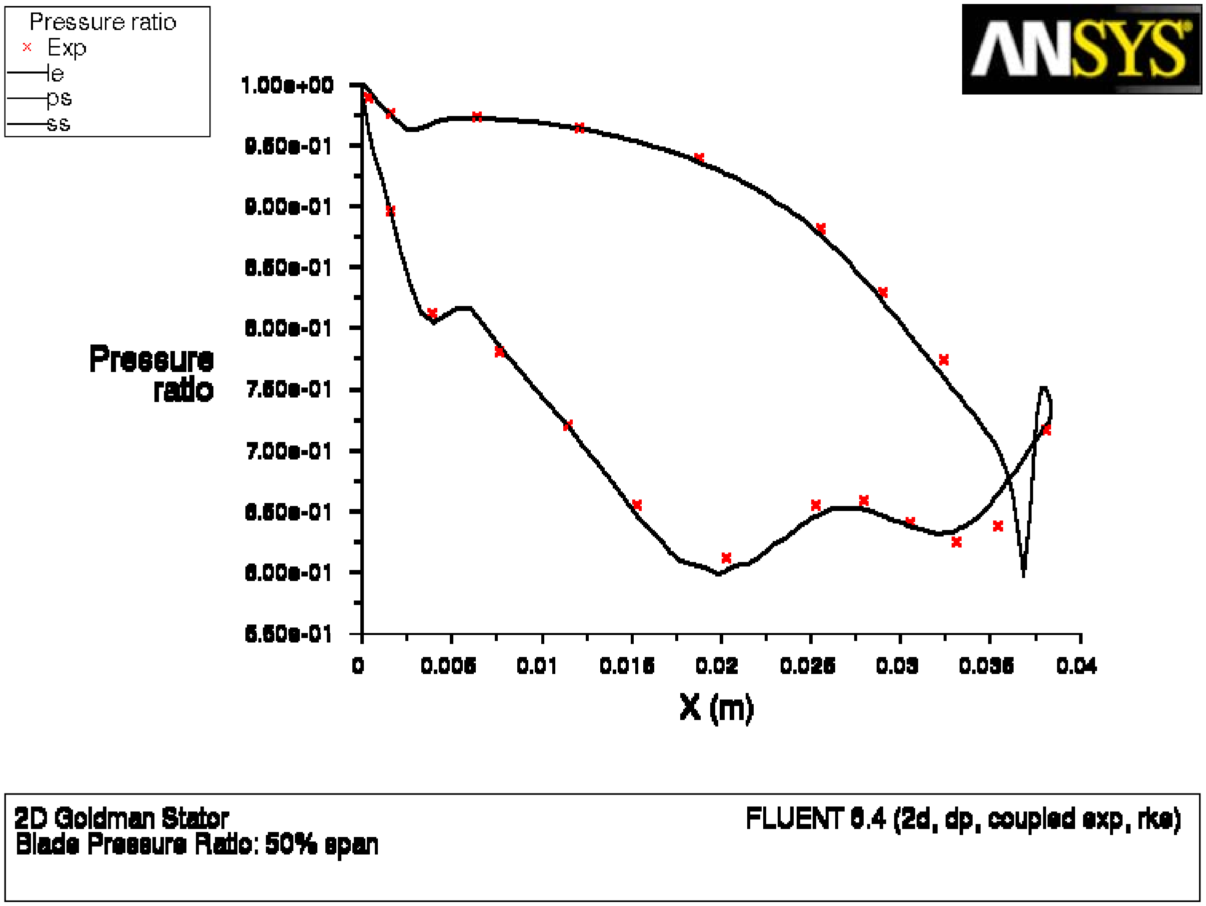


Figure 11.4.2: Pressure Ratio on the Blade (Navier-Stokes Equations with the Density-Based Explicit Solver)

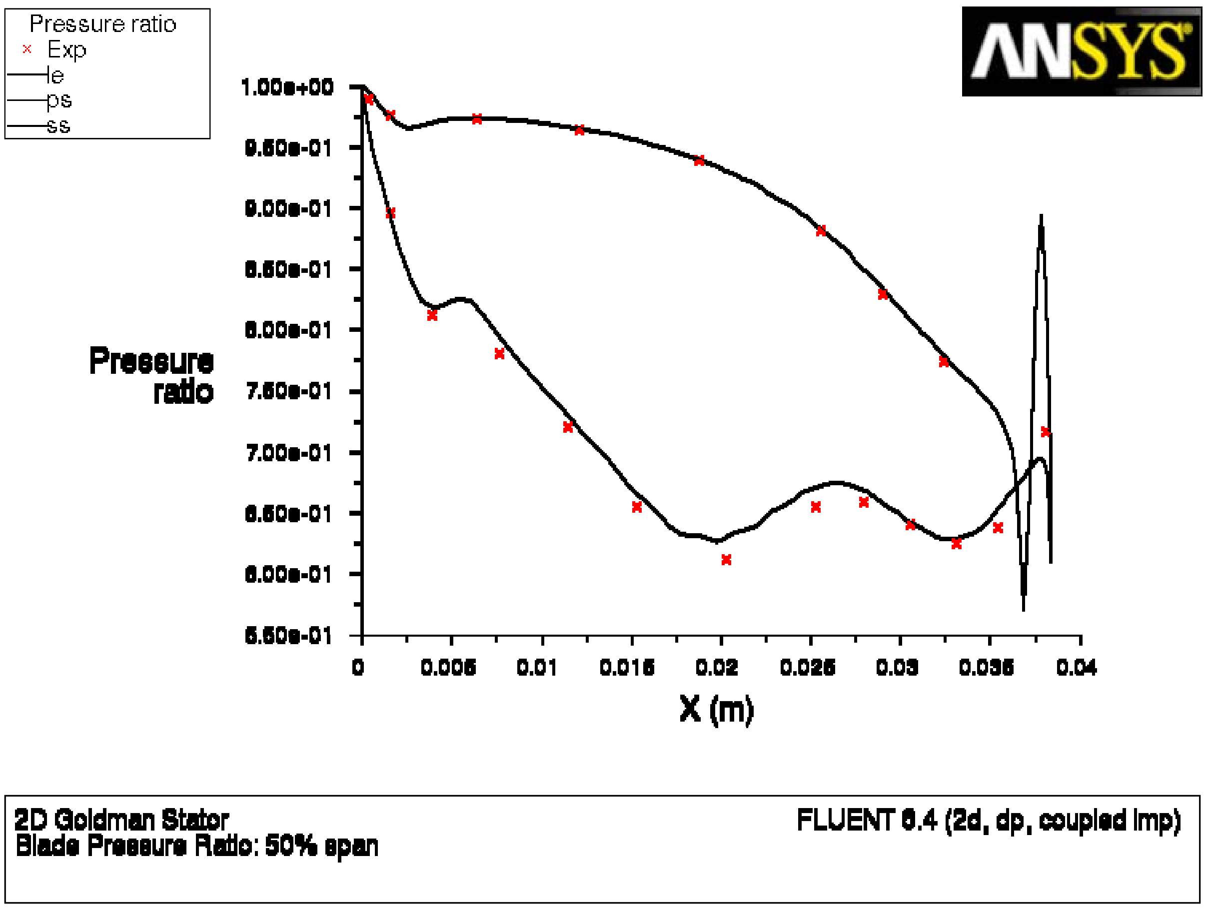


Figure 11.4.3: Pressure Ratio on the Blade (Euler Equations with the Density-Based Implicit Solver)

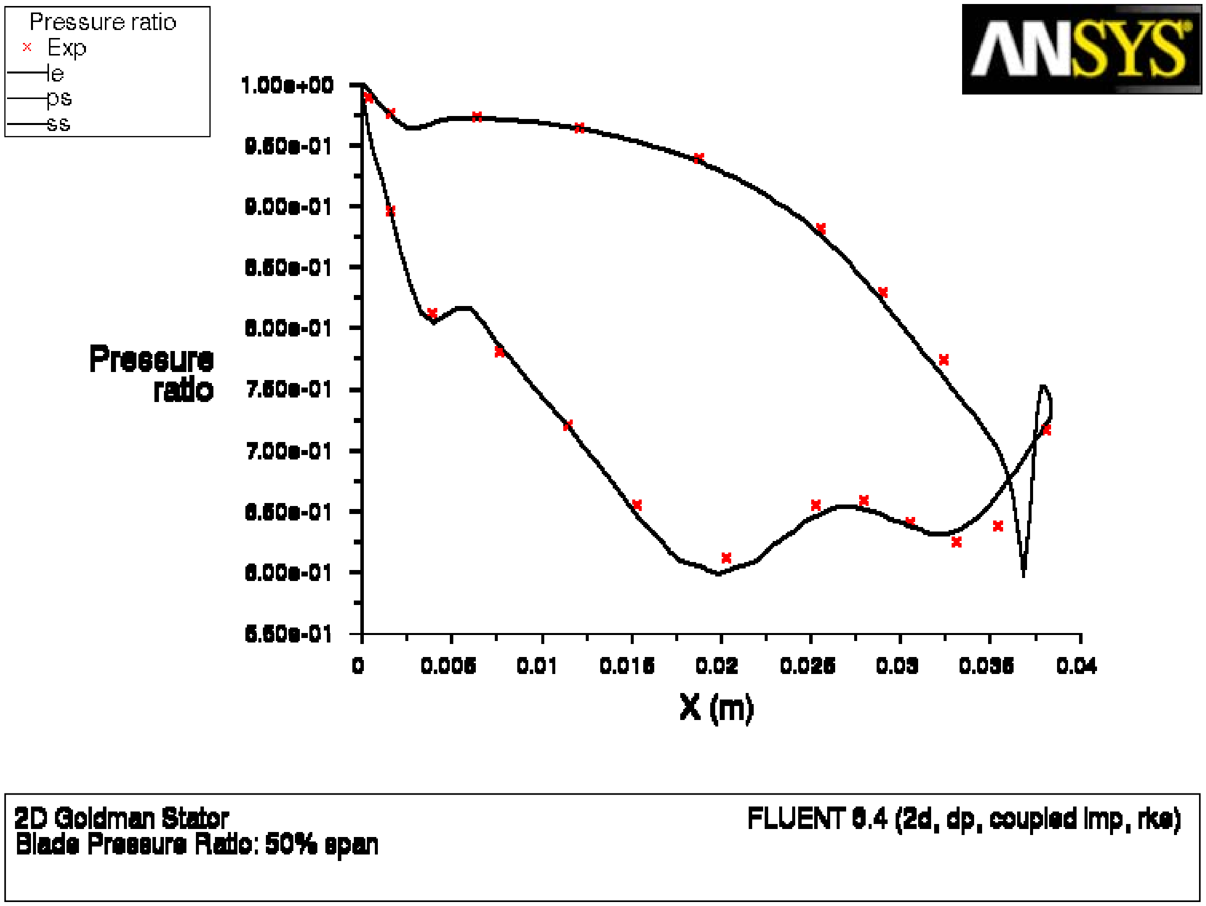


Figure 11.4.4: Pressure Ratio on the Blade (Navier-Stokes Equations with the Density-Based Implicit Solver)

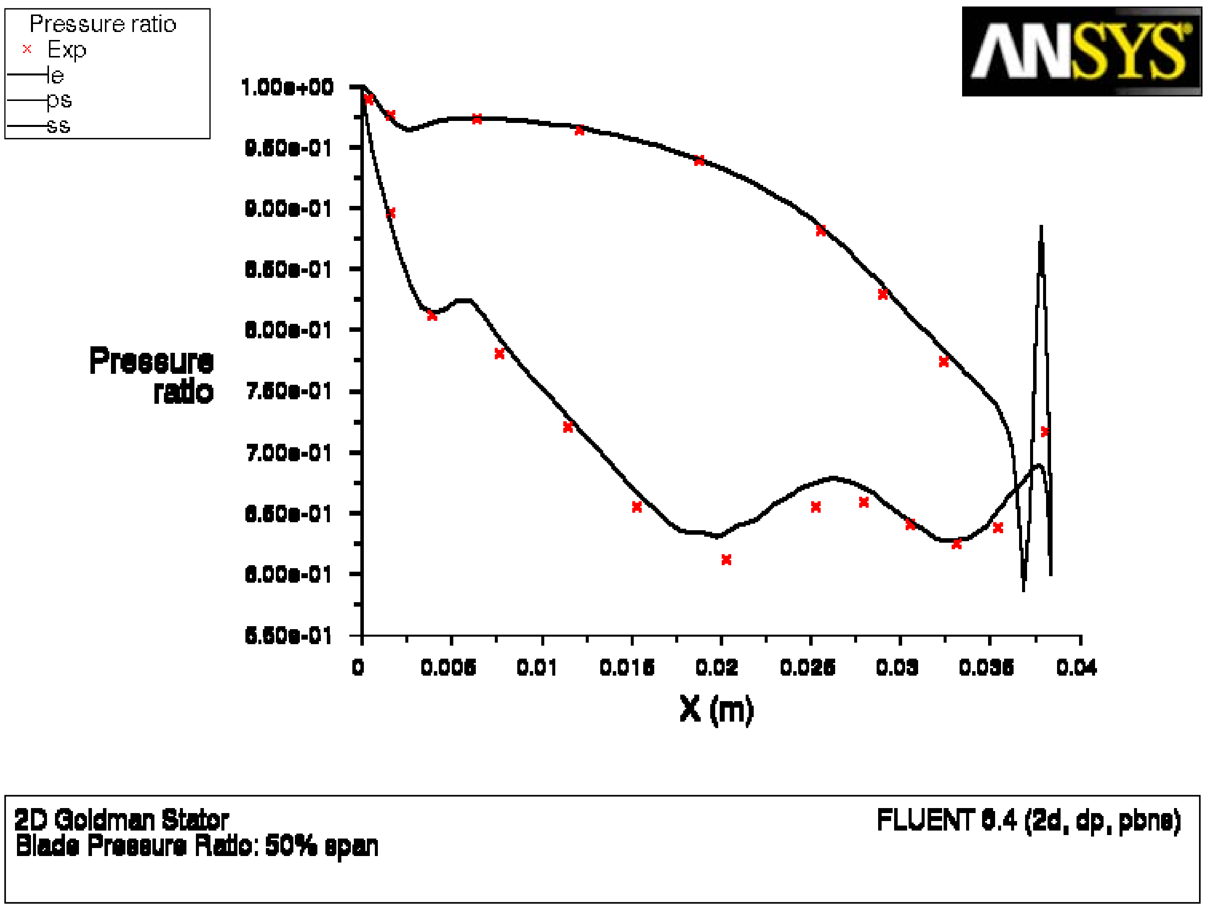


Figure 11.4.5: Pressure Ratio on the Blade (Euler Equations with the Pressure-Based Segregated Solver)

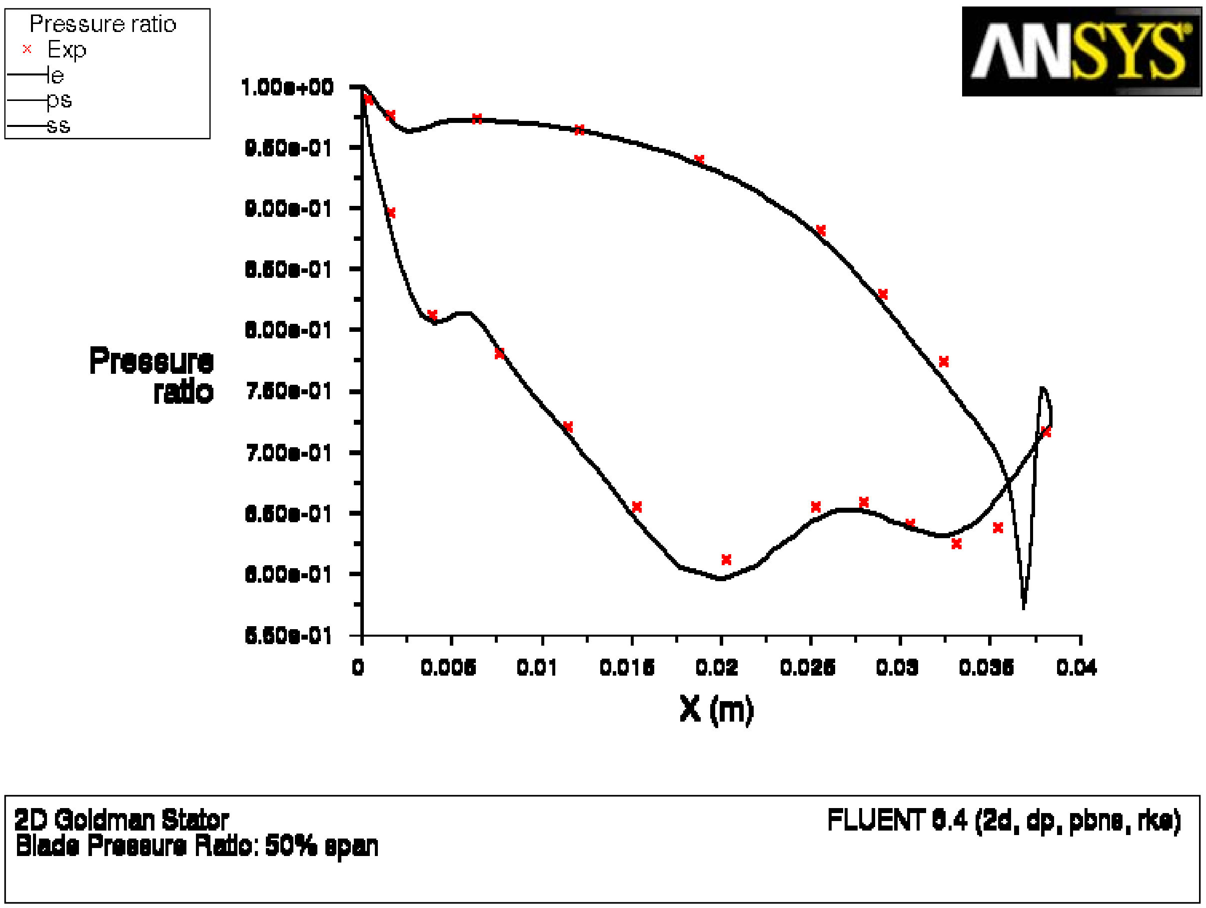


Figure 11.4.6: Pressure Ratio on the Blade (Navier-Stokes Equations with the Pressure-Based Segregated Solver)

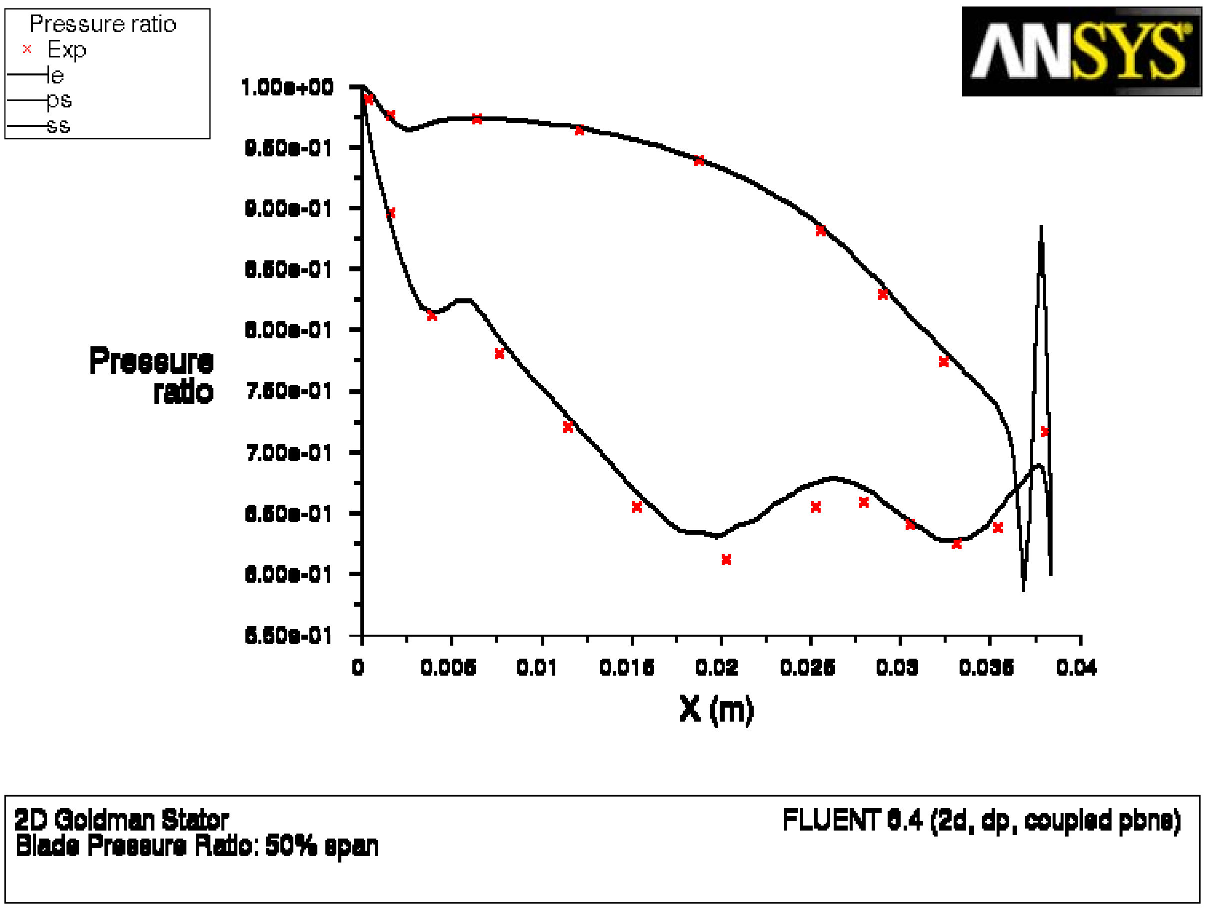


Figure 11.4.7: Pressure Ratio on the Blade (Euler Equations with the Pressure-Based Coupled Solver)

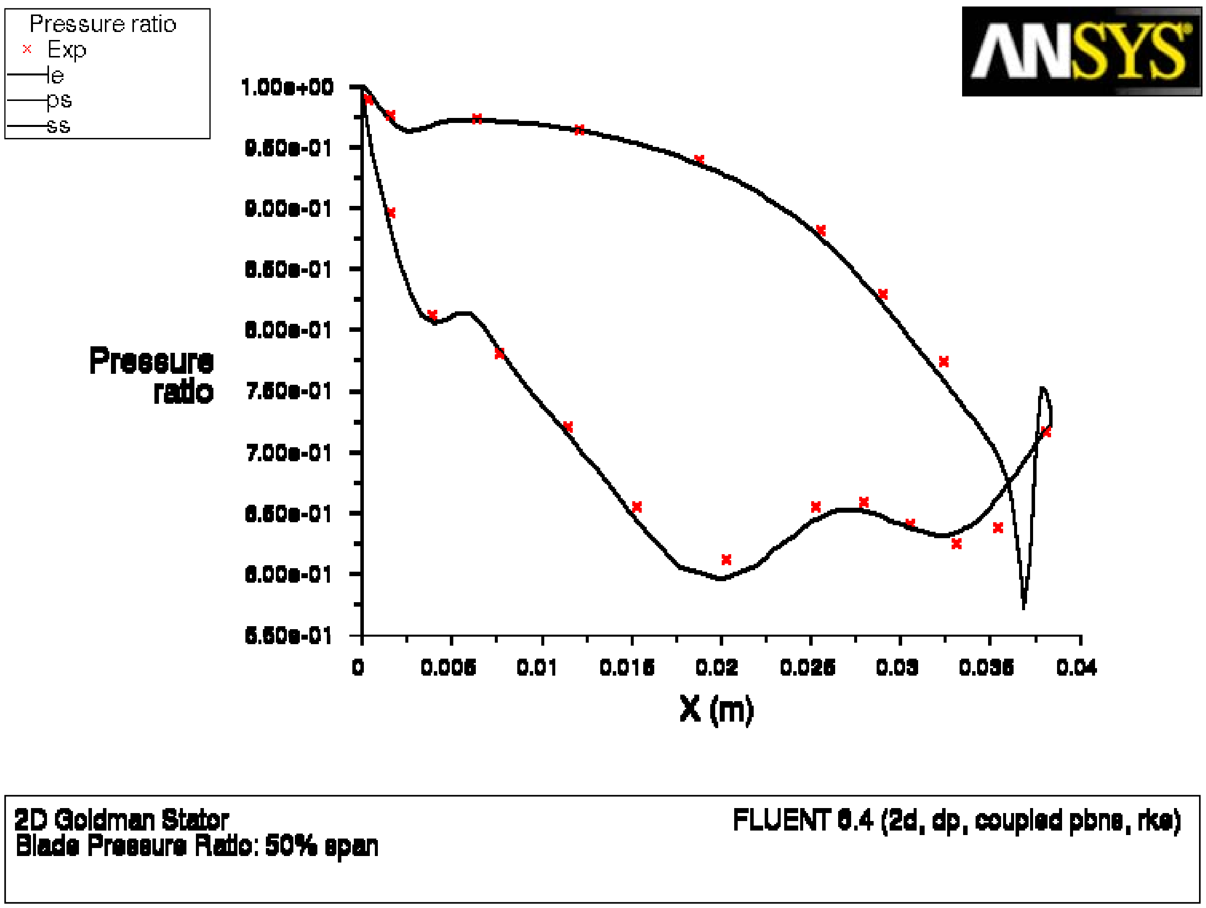


Figure 11.4.8: Pressure Ratio on the Blade (Navier-Stokes Equations with the Pressure-Based Coupled Solver)

Release 12.0 © ANSYS, Inc. January 24, 2009

Validation 12. Reflecting Shock Waves

12.1 Purpose

The purpose of this test is to validate ANSYS FLUENT's ability to predict reflecting shock waves and their effect on wall pressure distribution and heat transfer.

12.2 Problem Description

The flow is considered to be two-dimensional, because the span of the experimental outlet is considerably larger than the height. Both geometries are shown in Figures 12.2.1 and 12.2.2. The flow enters the exhaust section at a Mach number of 1.66. In each case, the cowl wall opposite the afterbody angles initially upward. This is followed by a wedge, inducing a shock that reflects off of the afterbody.

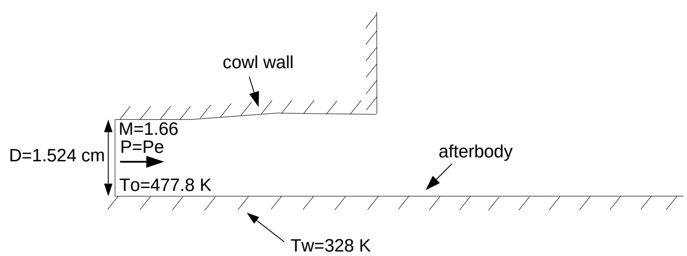


Figure 12.2.1: Problem Description: 0-Degree Afterbody

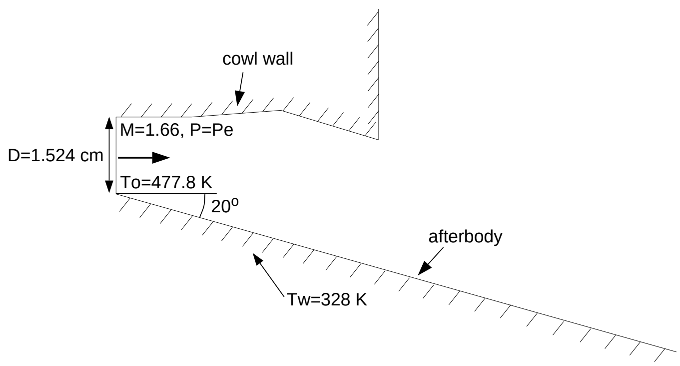


Figure 12.2.2: Problem Description: 20-Degree Afterbody

12.3 References

1. Hopkins, H. B., Konopka, W., and Leng, J. *Validation of scramjet exhaust simulation technique at Mach 6*. NASA Contractor Report 3003, 1979.

12.4 Results

Figure 12.4.1 compares pressure ratio as a function of horizontal distance for the two different meshes (quadrilateral mesh with boundary layer and tri mesh with adaption) for the experimental results [1]. All are in excellent agreement. Pressure is normalized by the entrance value, P_e.

Figure 12.4.3 compares the heat transfer rate for the two 0-degree mesh solutions with the experimental values. Agreement is good for both cases.

Figures 12.4.2 and 12.4.4 show the pressure and heat transfer distributions for the 20-degree afterbody mesh configurations and the comparison with the experiment.

12.4.1 Validation-Specific Information

Solver: ANSYS FLUENT 2D Double Precision
Version: 12.0.5
Solution Files:
1. `quad-bl-impl-0deg_r1.cas.gz`, `quad-bl-impl-0deg_r1.dat.gz`
2. `tri-adapt-impl-0deg_r2.cas.gz`, `tri-adapt-impl-0deg_r2.dat.gz`
3. `quad-bl-impl-20deg_r3.cas.gz`, `quad-bl-impl-20deg_r3.dat.gz`
4. `tri-adapt-impl-20deg_r4.cas.gz`, `tri-adapt-impl-20deg_r4.dat.gz`

 Release 12.0 © ANSYS, Inc. January 24, 2009

These solution files are available from the User Services Center as described in the Introduction.

12.4.2 Plot Data

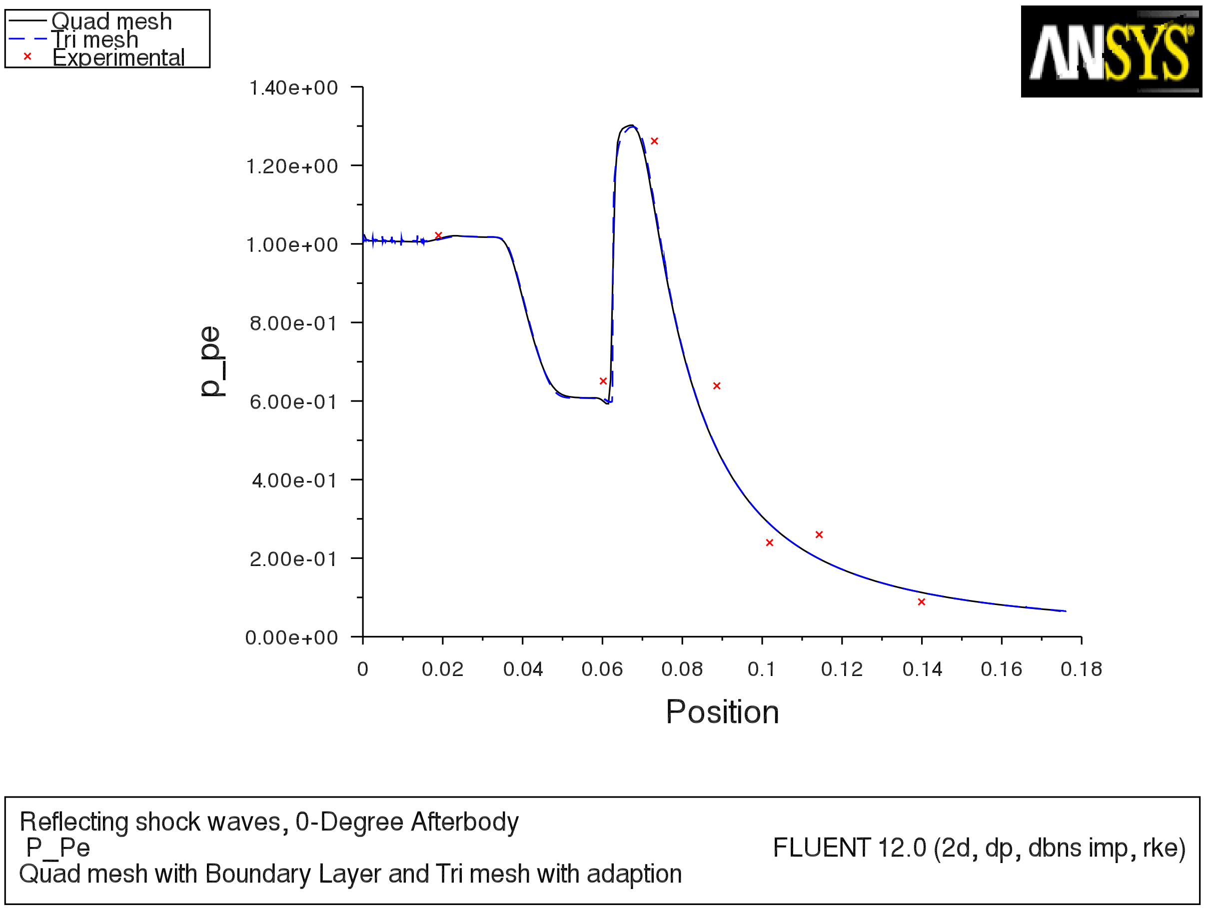


Figure 12.4.1: Normalized Pressure as a Function of Horizontal Distance for the Two 0-Degree Afterbody Mesh Configurations

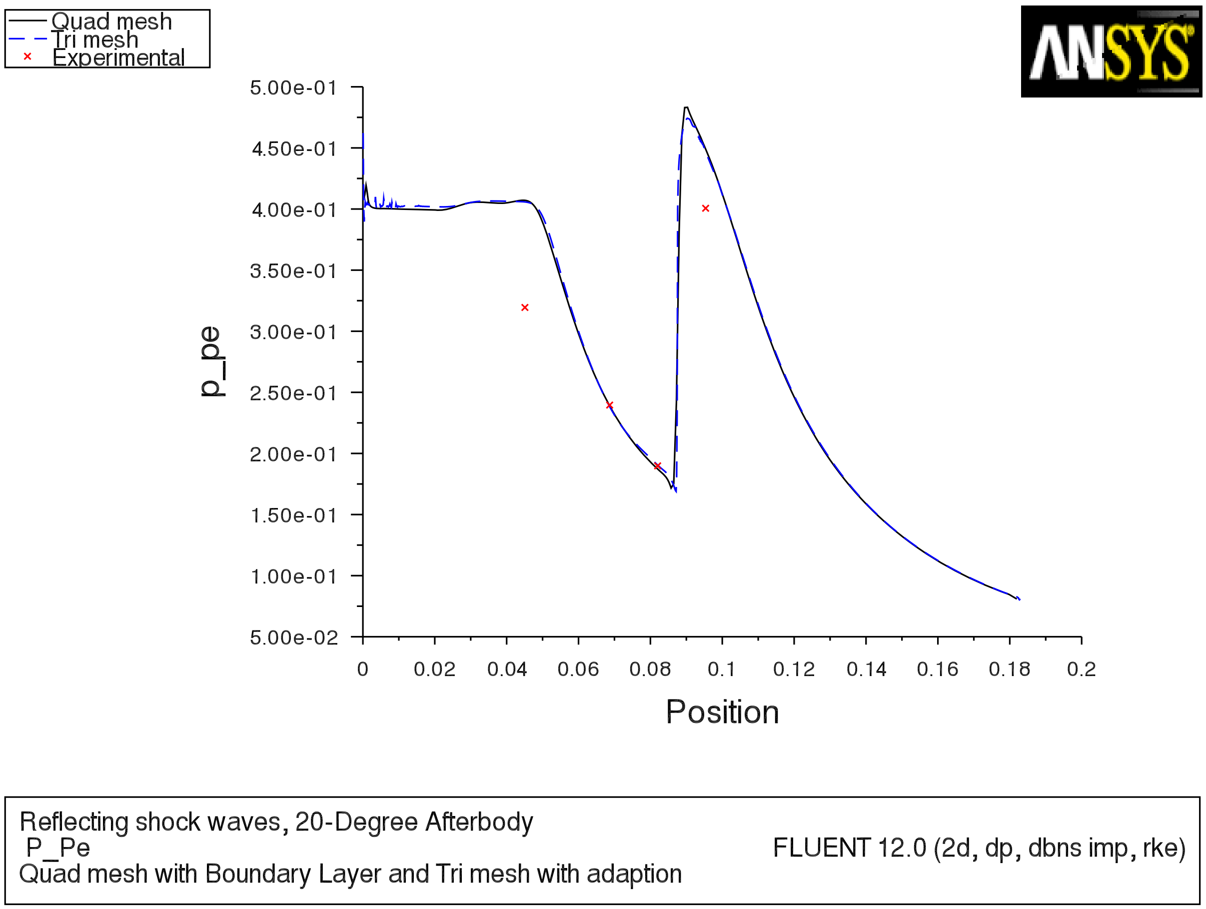


Figure 12.4.2: Normalized Pressure as a Function of Horizontal Distance for the 20-Degree Afterbody Mesh Configurations

Release 12.0 © ANSYS, Inc. January 24, 2009

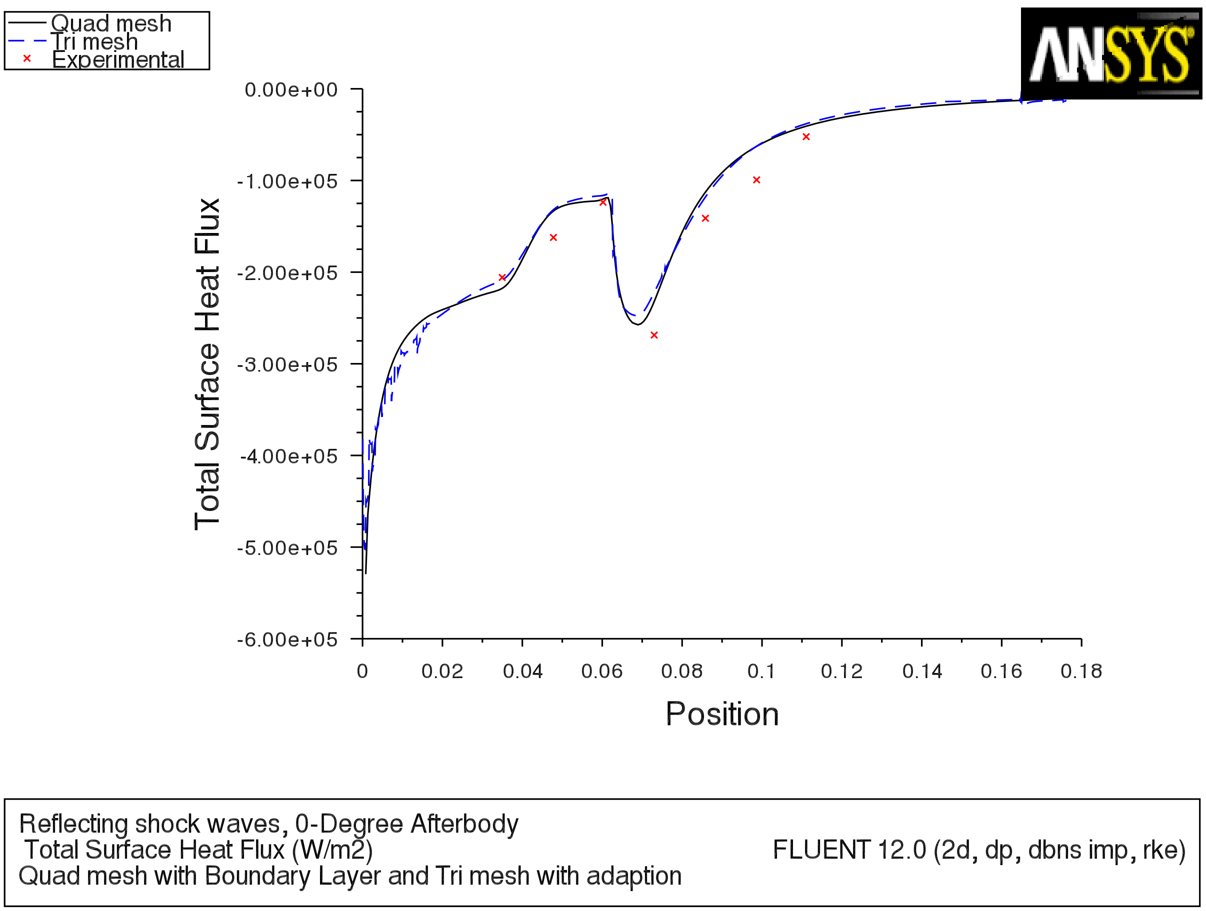


Figure 12.4.3: Heat Transfer Rate as a Function of Horizontal Distance for the Two 0-Degree Afterbody Mesh Configurations

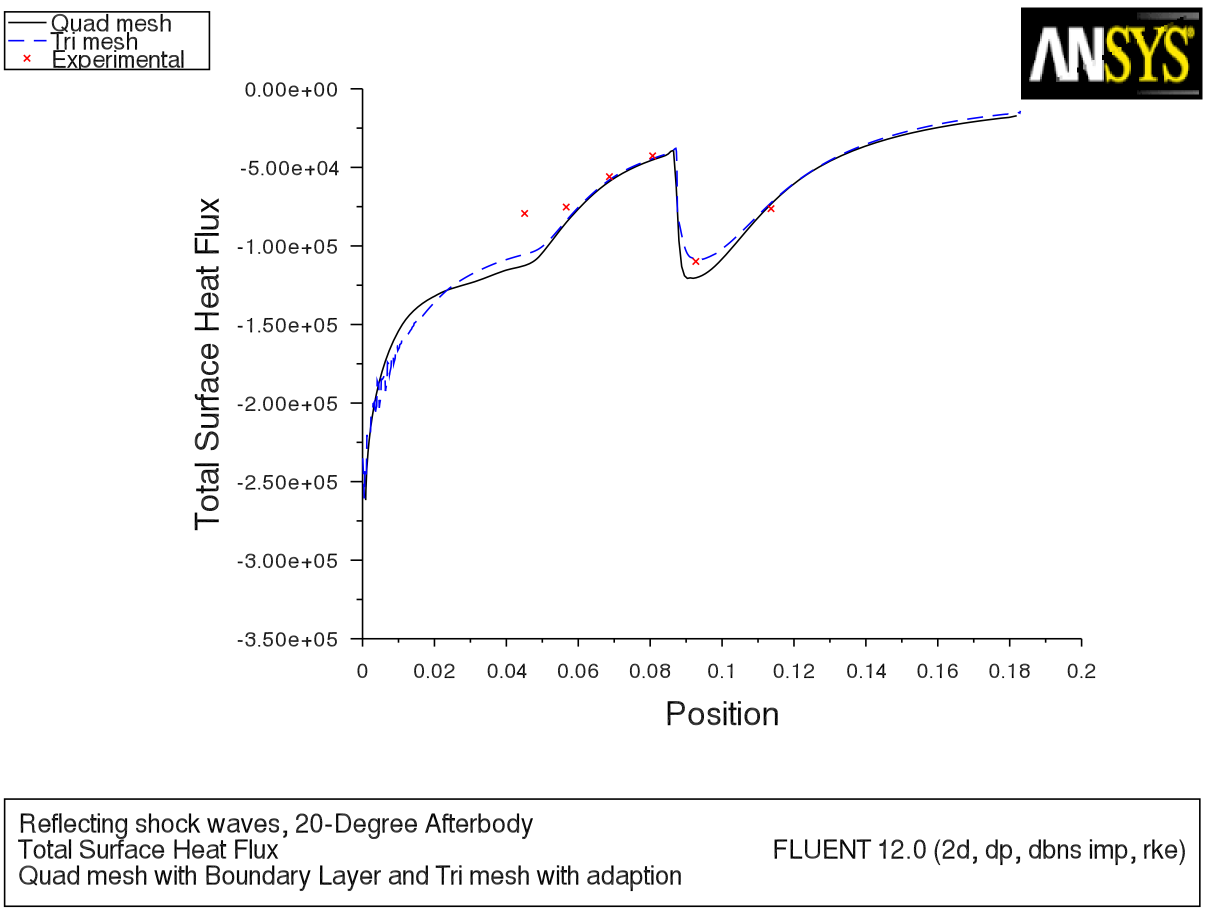


Figure 12.4.4: Heat Transfer Rate as a Function of Horizontal Distance for the Two 20-Degree Afterbody Mesh Configurations

Release 12.0 © ANSYS, Inc. January 24, 2009

Validation 13. Turbulent Bubbly Flows

13.1 Purpose

This validation compares ANSYS FLUENT's predictions of void fraction and axial velocity for bubbly flow in a vertical pipe with experimental data [1,2,3,4,5]. It uses the Eulerian multiphase model with the standard k-ϵ turbulence model.

13.2 Problem Description

The flow considered is an upward, co-current air-water turbulent bubbly flow in a vertical, circular pipe under normal conditions. The pipe has a length $L = 2.5$ m and a diameter of $d = 5.7$ cm. The liquid superficial velocity is 0.495 m/s and the gas superficial velocity is 0.758 m/s. The inlet void fraction of gas is around 0.132. Figure 13.2.1 shows the geometry and the flow conditions used.

13.3 References

1. Moraga, F. J., Bonetto, R.T. and Lahey, R. T. 1999 Lateral forces on spheres in turbulent uniform shear flow. *Int. J.Multiphase Flow* 25, 1321-2372.
2. Wang, S. K., Lee, S. J., Jones, O.C. and Lahey, R. T. 1987 3-D turbulence structure and phase distribution measurements in bubbly two-phase flows. *Int. Multiphase Flow* 13 3, 327-343.
3. A. Troshko, V. Ivanov, S. Vasques, *Implementation of a General Lift Coefficient in the CFD Model of Turbulent Bubbly Flows*, Fluent Inc., Lebanon, NH.
4. Troshko, A. A. 2000 Two-equation, multidimensional model of turbulence in bubbly flows, PhD. dissertation, Texas A&M University.
5. R. Clift, J. R. Grace and M.E. Weber, *Bubbles, drops and particles*, Academic Press, 1978.

13.4 Results

Figures 13.4.1 and 13.4.2 show the comparison between experimental and ANSYS FLUENT's data for the continuous-phase axial velocity and the dispersed-phase volume fraction radial profiles. Note that simulation results at $x = 26$, 35 and 44 d were essentially the same due to the fully-developed nature of the flow at those downstream locations.

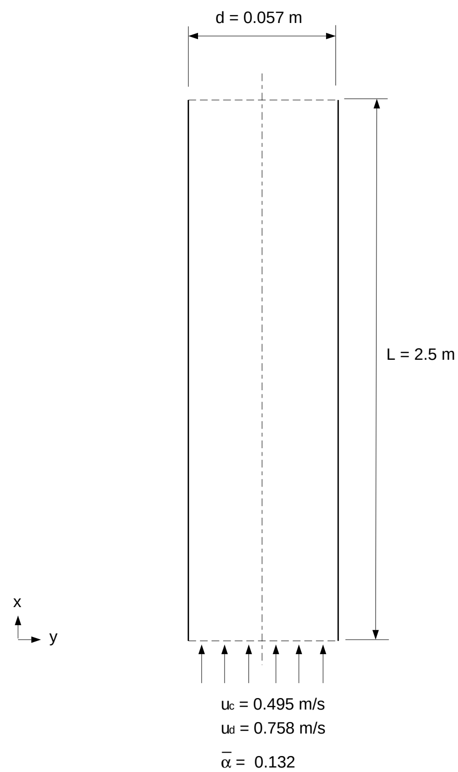


Figure 13.2.1: Problem Description

Release 12.0 © ANSYS, Inc. January 24, 2009

There is a good agreement for the velocity, and excellent agreement for the dispersed-phase volume fraction. Inviscid lift is predominant in the outer layer, pushing bubbles toward the wall, while vortex shedding lift dominates the inner layer, driving bubbles from the wall.

Near the wall, liquid film between the bubble and the wall moves slower than the liquid at the free-stream side of the bubble. This velocity gradient is due to the no-slip condition at the wall, creating a pressure difference driving bubbles from the wall.

13.4.1 Validation-Specific Information

Solver:	ANSYS FLUENT 2D Double Precision
Version:	6.4.13
Solution Files:	`liftch-drag-disp-ke.cas`, `liftch-drag-disp-ke.dat`, `lift.c`

These solution files are available from the User Services Center as described in the Introduction.

13.4.2 Plot Data

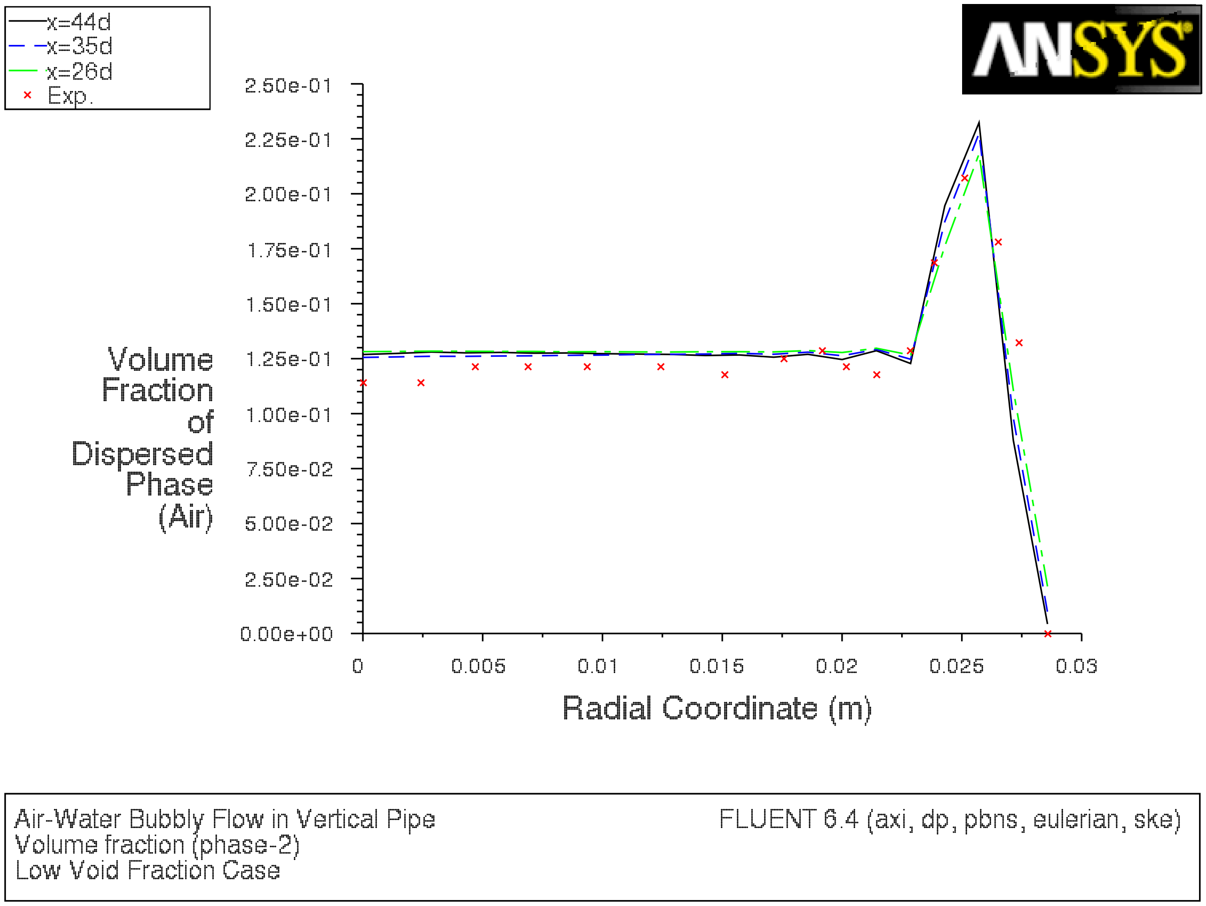


Figure 13.4.1: Radial Profile of Dispersed Phase Volume Fraction (Air)

Release 12.0 © ANSYS, Inc. January 24, 2009

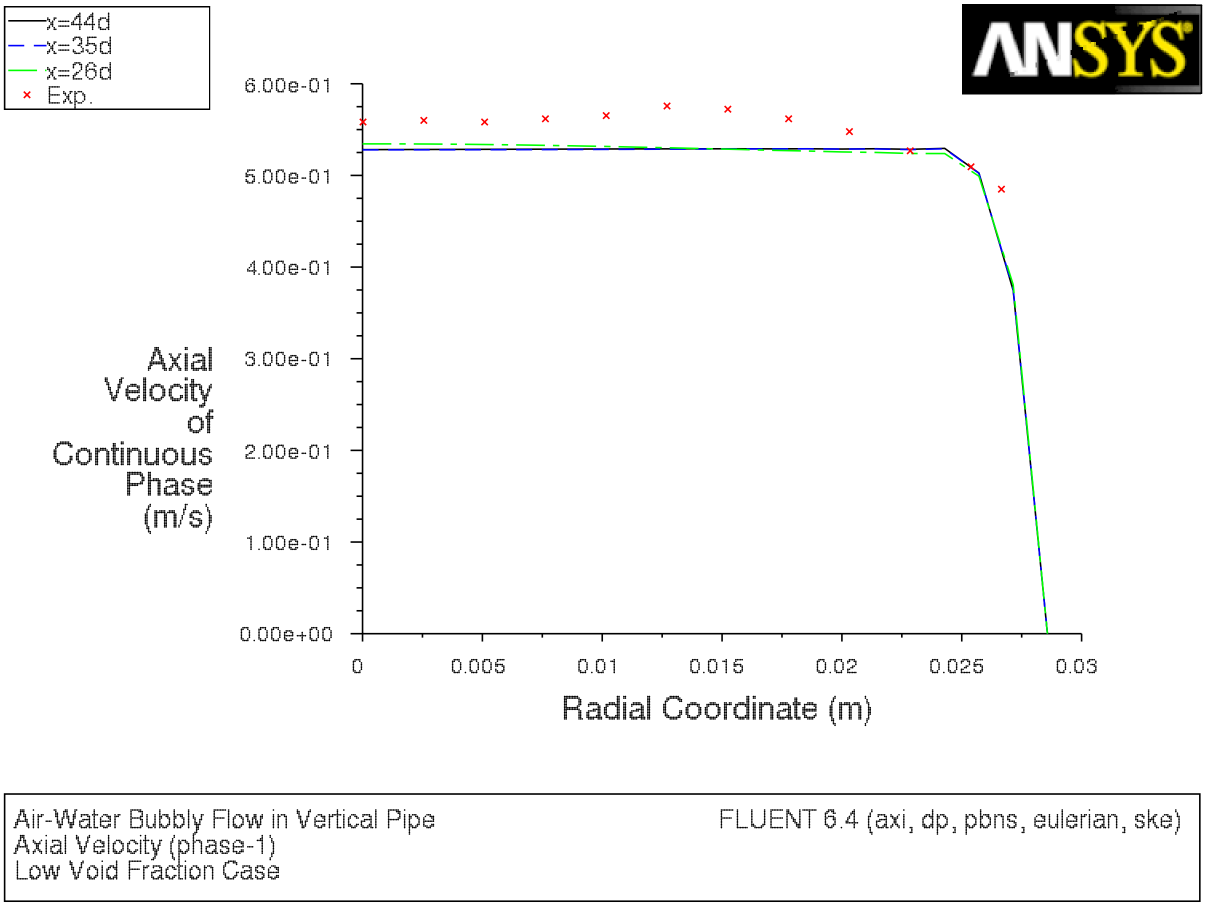


Figure 13.4.2: Radial Profile of Continuous Phase Axial Velocity (Water)

Release 12.0 © ANSYS, Inc. January 24, 2009

Validation 14. Adiabatic Compression and Expansion Inside an Idealized 2D Piston-Cylinder Engine

14.1 Purpose

This validation compares ANSYS FLUENT's predictions for an idealized 2D piston-cylinder engine simulating an adiabatic process against analytical data from isentropic thermodynamic relations. Two different methods are used to model the deforming mesh: dynamic layering and spring-based smoothing with local remeshing.

14.2 Problem Description

A simplified 2D in-cylinder geometry is used, consisting of a 10m x 8m box. The bottom surface represents the piston head. The piston moves up from the bottom dead center (BDC) position, corresponding to a crank shaft angle of 180 degrees, slowly compressing the fluid adiabatically until the volume decreases to 2m x 8m. Once it reaches the top dead center (TDC) position, corresponding to a crank shaft angle of 360 degrees, the piston moves back downward to the initial position, to complete the cycle (see Figures 14.2.1 and 14.2.2).

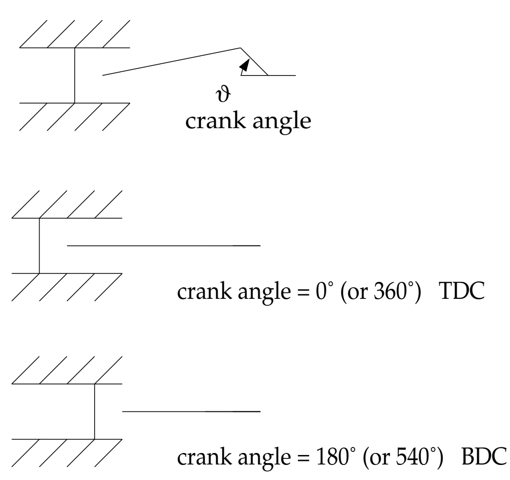


Figure 14.2.1: Problem Specification

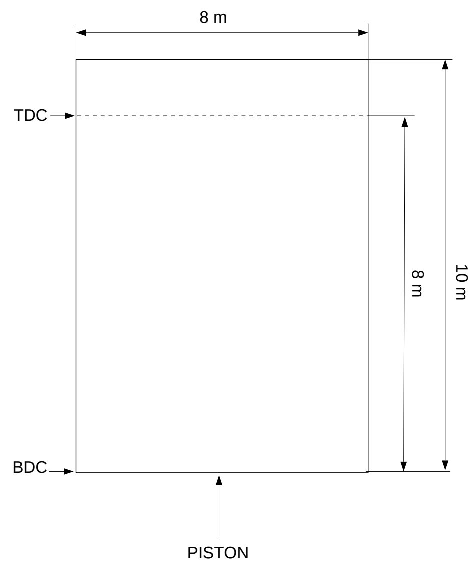


Figure 14.2.2: Problem Geometry

14.3 Results

ANSYS FLUENT results were compared with analytical data from isentropic thermodynamic relations. Pressure and temperature values were obtained through the following expressions:

$$\frac{T_2}{T_1} = \left(\frac{V_1}{V_2}\right)^{\gamma-1} \tag{14.3-1}$$

$$\frac{P_2}{P_1} = \left(\frac{V_1}{V_2}\right)^{\gamma} \tag{14.3-2}$$

where P_1 is the pressure at the volume V_1 and temperature T_1, P_2 is the pressure at the volume $V2$ and temperature T_2 and γ is the specific heat ratio.

Figures 14.3.1 and 14.3.2 compare the temperature and pressure of ANSYS FLUENT results against the analytical data, showing an excellent match of the values for both the layering methods, dynamic layering, and the spring-based smoothing method with local remeshing for the dynamic mesh motion.

Release 12.0 © ANSYS, Inc. January 24, 2009

14.3.1 Validation-Specific Information

Solver:	ANSYS FLUENT 2D Double Precision
Version:	6.4.13
Solution Files:	1. `poly_2d_layer.cas`, `poly_2d_layer.dat`
	2. `poly_2d_remesh.cas`, `poly_2d_remesh.dat`

These solution files are available from the User Services Center as described in the Introduction.

14.3.2 Plot Data

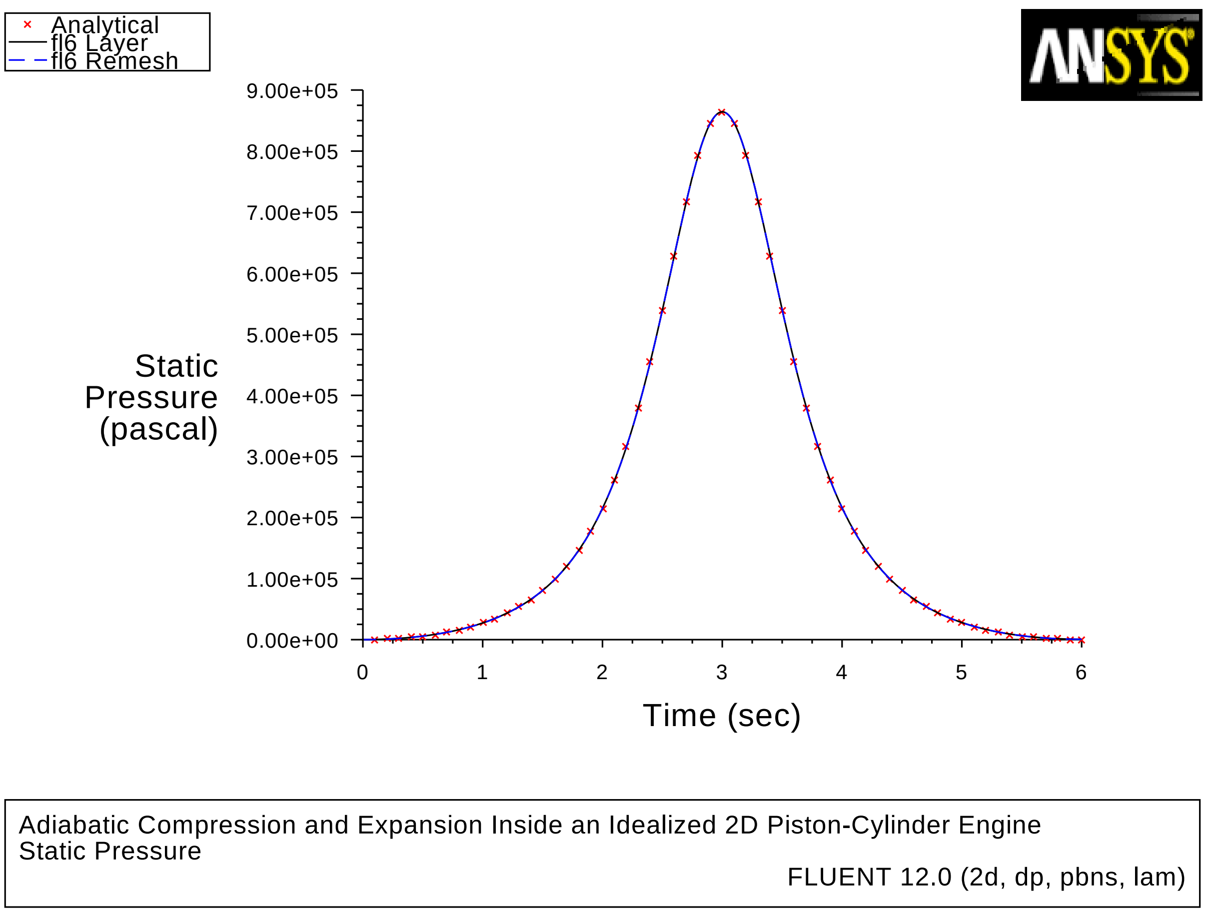


Figure 14.3.1: Static Pressure in the Chamber Area During One Piston Cycle

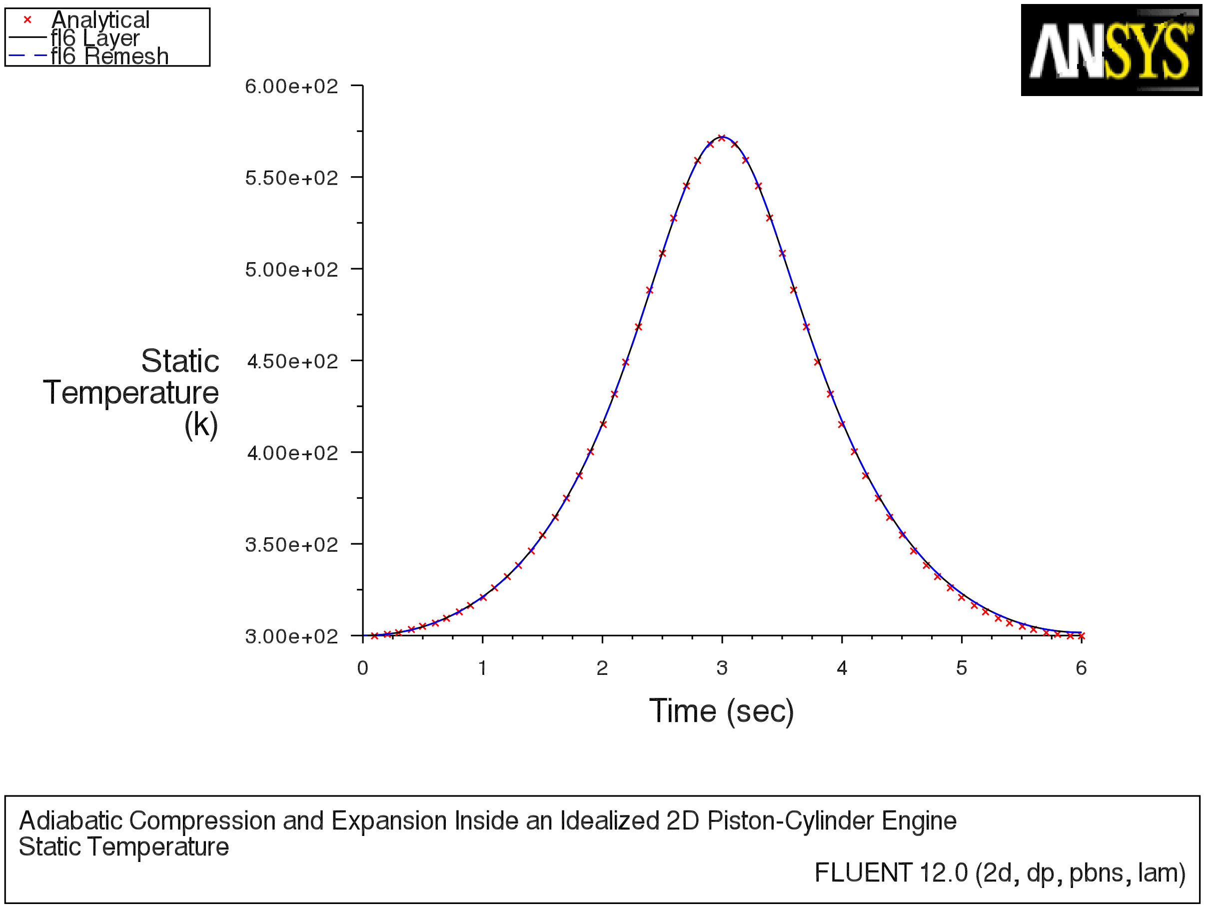


Figure 14.3.2: Static Temperature in the Chamber Area During One Piston Cycle

Release 12.0 © ANSYS, Inc. January 24, 2009

Validation 15. Cavitation Over a Sharp-Edged Orifice

15.1 Purpose

The purpose of this test is to validate the capability of ANSYS FLUENT's cavitation models Schnerr-Sauer, Zwart-Gerber-Belamri and Singhal-Et-al, when applied to a weakly cavitating flow. The strength of the cavitation depends on the inlet pressure. When the inlet pressure is small, cavitation is weak and when pressure goes high, cavitation is strong.

Fourteen (14) test cases were prepared for each of the cavitation models, with the inlet total pressure ranging from 1.9×10^5 to 4×10^8 Pa. The computed discharge coefficients were compared with the experimental correlation by Nurick [1].

15.2 Problem Description

A 2D axisymmetric sharp-edged orifice is considered, as shown in Figure 15.2.1. Its geometric parameters are $R/r = 2.86$ and $L/r = 7.94$, where R, r & L denote the inlet radius, orifice radius and orifice length, respectively. The flow is assumed to be turbulent, and the standard $k - \varepsilon$ model is employed. The specified boundary conditions are the total pressure P_o at the inlet, which varies from 1.9×10^5 to 4×10^8 Pa, and the static pressure $P_{exit} = 95000$ Pa at the exit.

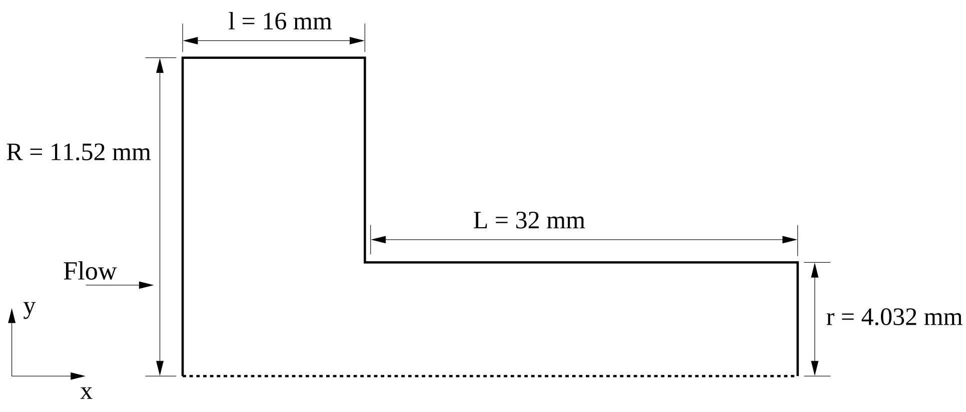


Figure 15.2.1: Problem Description

15.3 References

1. W.H. Nurick, Orifice Cavitation and its Effects on Spray Mixing, *Journal of Fluids Engineering*, Vol. 98, 1976.

15.4 Results

Experimental data is available in the form of discharge coefficient versus inlet pressure, where the discharge coefficient is defined as $\dot{m}/\dot{m}_i$, $\dot{m}$ is the computed mass flow rate, and $\dot{m}_i$ is the ideal mass flow rate through the orifice. The ideal mass flow rate through the orifice is computed as $\dot{m}_i = A\sqrt{2\rho(P_o - P_{exit})}$, where A is the cross-sectional area of the orifice, $A = \pi r^2$, ρ is the density, and P_o and P_{exit} are the inlet pressure and the exit pressure, respectively. ANSYS FLUENT shows excellent agreement with the experimental measurements.

15.4.1 Validation-Specific Information

Solver:	ANSYS FLUENT 2D Double Precision
Version:	12.0.5
Solution Files:	Singhal-Et-al Cavitation model
	1. `1.9bar_n_1_Singhal.cas`, `1.9bar_n_1_Singhal.dat`
	2. `2bar_n_1_Singhal.cas`, `2bar_n_1_Singhal.dat`
	3. `2.25bar_n_1_Singhal.cas`, `2.25bar_n_1_Singhal.dat`
	4. `2.5bar_n_1_Singhal.cas`, `2.5bar_n_1_Singhal.dat`
	5. `3bar_n_1_Singhal.cas`, `3bar_n_1_Singhal.dat`
	6. `3.75bar_n_1_Singhal.cas`, `3.75bar_n_1_Singhal.dat`
	7. `5bar_n_1_Singhal.cas`, `5bar_n_1_Singhal.dat`
	8. `10bar_n_1_Singhal.cas`, `10bar_n_1_Singhal.dat`
	9. `50bar_n_1_Singhal.cas`, `50bar_n_1_Singhal.dat`
	10. `100bar_n_1_Singhal.cas`, `100bar_n_1_Singhal.dat`
	11. `500bar_n_1_Singhal.cas`, `500bar_n_1_Singhal.dat`
	12. `1000bar_n_1_Singhal.cas`, `1000bar_n_1_Singhal.dat`
	13. `2500bar_n_1_Singhal.cas`, `2500bar_n_1_Singhal.dat`
	14. `4000bar_n_1_Singhal.cas`, `4000bar_n_1_Singhal.dat`

Release 12.0 © ANSYS, Inc. January 24, 2009

Solution Files: Schnerr-Sauer Cavitation model

1. `1.9bar_n_1_Schnerr.cas`, `1.9bar_n_1_Schnerr.dat`
2. `2bar_n_1_Schnerr.cas`, `2bar_n_1_Schnerr.dat`
3. `2.25bar_n_1_Schnerr.cas`, `2.25bar_n_1_Schnerr.dat`
4. `2.5bar_n_1_Schnerr.cas`, `2.5bar_n_1_Schnerr.dat`
5. `3bar_n_1_Schnerr.cas`, `3bar_n_1_Schnerr.dat`
6. `3.75bar_n_1_Schnerr.cas`, `3.75bar_n_1_Schnerr.dat`
7. `5bar_n_1_Schnerr.cas`, `5bar_n_1_Schnerr.dat`
8. `10bar_n_1_Schnerr.cas`, `10bar_n_1_Schnerr.dat`
9. `50bar_n_1_Schnerr.cas`, `50bar_n_1_Schnerr.dat`
10. `100bar_n_1_Schnerr.cas`, `100bar_n_1_Schnerr.dat`
11. `500bar_n_1_Schnerr.cas`, `500bar_n_1_Schnerr.dat`
12. `1000bar_n_1_Schnerr.cas`, `1000bar_n_1_Schnerr.dat`
13. `2500bar_n_1_Schnerr.cas`, `2500bar_n_1_Schnerr.dat`
14. `4000bar_n_1_Schnerr.cas`, `4000bar_n_1_Schnerr.dat`

Solution Files: Zwart-Gerber-Belamri Cavitation model

1. `1.9bar_n_1_Zwart.cas`, `1.9bar_n_1_Zwart.dat`
2. `2bar_n_1_Zwart.cas`, `2bar_n_1_Zwart.dat`
3. `2.25bar_n_1_Zwart.cas`, `2.25bar_n_1_Zwart.dat`
4. `2.5bar_n_1_Zwart.cas`, `2.5bar_n_1_Zwart.dat`
5. `3bar_n_1_Zwart.cas`, `3bar_n_1_Zwart.dat`
6. `3.75bar_n_1_Zwart.cas`, `3.75bar_n_1_Zwart.dat`
7. `5bar_n_1_Zwart.cas`, `5bar_n_1_Zwart.dat`
8. `10bar_n_1_Zwart.cas`, `10bar_n_1_Zwart.dat`
9. `50bar_n_1_Zwart.cas`, `50bar_n_1_Zwart.dat`
10. `100bar_n_1_Zwart.cas`, `100bar_n_1_Zwart.dat`
11. `500bar_n_1_Zwart.cas`, `500bar_n_1_Zwart.dat`
12. `1000bar_n_1_Zwart.cas`, `1000bar_n_1_Zwart.dat`
13. `2500bar_n_1_Zwart.cas`, `2500bar_n_1_Zwart.dat`
14. `4000bar_n_1_Zwart.cas`, `4000bar_n_1_Zwart.dat`

These solution files are available from the User Services Center as described in the Introduction.

15.4.2 Plot Data

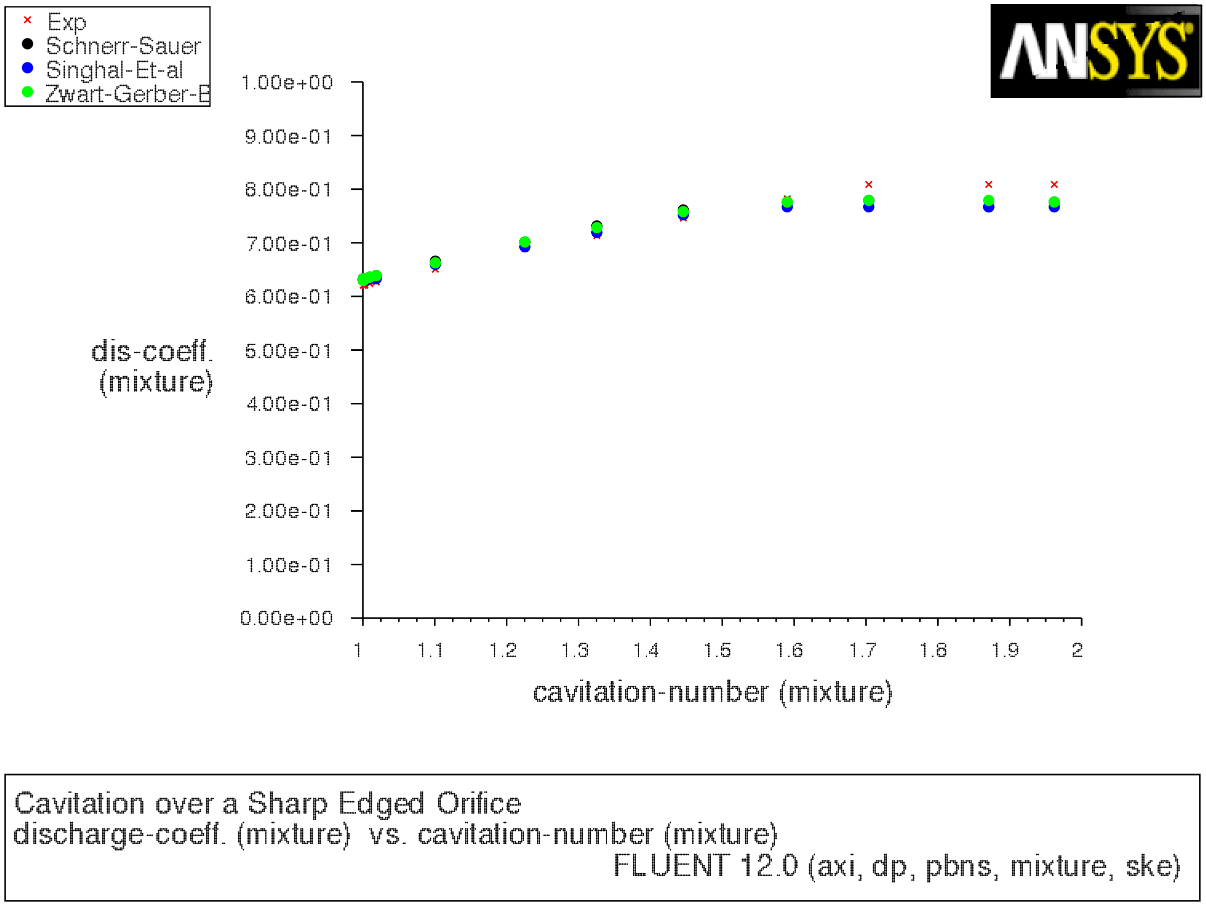


Figure 15.4.1: Comparison of ANSYS FLUENT Prediction of Discharge Coefficient with Schnerr-Sauer, Zwart-Gerber-Belamri, Singhal-Et-al Cavitation Models Over a Range of Inlet Pressure with Experimental Data

Release 12.0 © ANSYS, Inc. January 24, 2009

Validation 16. Oscillating Laminar Flow Around a Circular Cylinder

16.1 Purpose

The purpose of this test is to validate ANSYS FLUENT's ability to predict the flow structure as well as the reattachment length and Strouhal number against experimental results using iterative and non-iterative (NITA) solver. The present calculations are confined to the low-Reynolds-number regime ($Re = 100$), which encompasses unsteady asymmetric flow. The results obtained using the different non-iterative time advancement (NITA) schemes (NITA with PISO and NITA with Fractional Step) are compared to the iterative scheme (PBCS and DBNS solver) and to experimental data [1,2].

16.2 Problem Description

An infinitely long circular cylinder of diameter $D = 2.0\ m$ is placed in an otherwise undisturbed uniform crossflow ($U_\infty = 1.0\ m/s$) as shown in Figure 16.2.1. The lateral boundary and the exit boundary in the far wake are placed at $5D$ and $20D$ from the center of the circular cylinder, respectively.

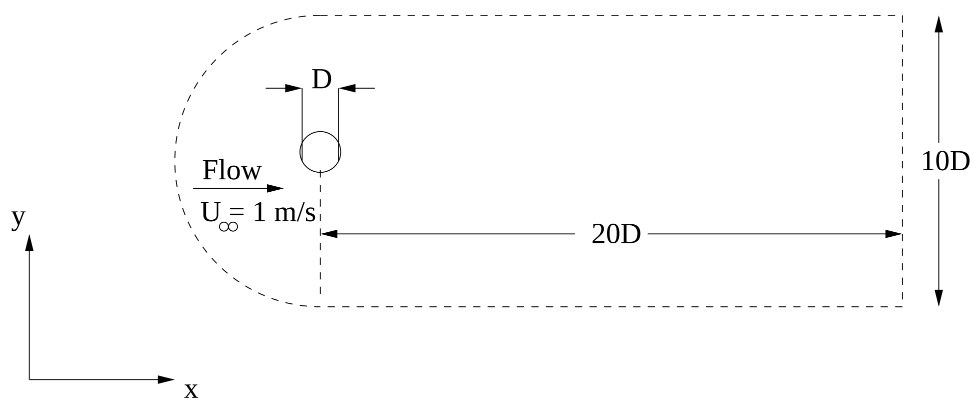


Figure 16.2.1: Problem Description

16.3 References

1. Coutanceau, M. and Defaye, J.R., Circular Cylinder Wake Configurations - A Flow Visualization Survey, Appl. Mech. Rev., 44(6), June 1991.

2. Braza, M., Chassaing, P., and Minh, H.H., Numerical Study and Physical Analysis of the Pressure and Velocity Fields in the Near Wake of a Circular Cylinder, J. Fluid Mech., 165:79-130, 1986.

16.4 Results

The flow seems to demonstrate periodic shedding of vortices downstream of the cylinder. To quantify the periodicity of the flow, the time history of the y velocity, situated at a point that is 1 m behind the cylinder in the near wake, is presented. Also an FFT analysis of the lift coefficient on the cylinder wall is presented to determine the frequency of oscillations. The Strouhal number corresponding to the maximum magnitude of oscillations with different solver schemes are summarized in Table 16.4.1.

Table 16.4.1: Predicted Strouhal Number Using Different Solver Schemes

Method	**Strouhal Number**
Experimental Value	0.165
ITA + PBCS	0.173
ITA + DBNS	0.173
NITA + PISO	0.173
NITA + Fractional Step	0.173

From experimental data, we have a Strouhal number of 0.165. The Formula for the Strouhal number is

$$S = (N * D)/V_\infty \tag{16.4-1}$$

where N is the frequency, D is the diameter of the cylinder, and V_∞ is the freestream velocity. Solving Equation 16.4-1 for the experimental frequency, we get $N = 0.0825s^{-1}$. Computational results yield a frequency of $N = 0.0865s^{-1}$, which are within 5% of the experimental value. Furthermore, the ITA and NITA schemes gave nearly identical solutions.

Release 12.0 © ANSYS, Inc. January 24, 2009

16.4.1 Validation-Specific Information

Solver: ANSYS FLUENT 2D Double Precision
Version: 6.4.13
Solution Files: 1. `cylin_iter-PBCS-2t.cas`, `cylin_iter-PBCS-2t.dat`
2. `cylin_NITA_FS-2t.cas`, `cylin_NITA_FS-2t.dat`
3. `cylin_NITA_PISO_2t.cas`, `cylin_NITA_PISO_2t.dat`
4. `cylin_iter-DBNS-2t.cas`, `cylin_iter-DBNS-2t.dat`

These solution files are available from the User Services Center as described in the Introduction.

16.4.2 Plot Data

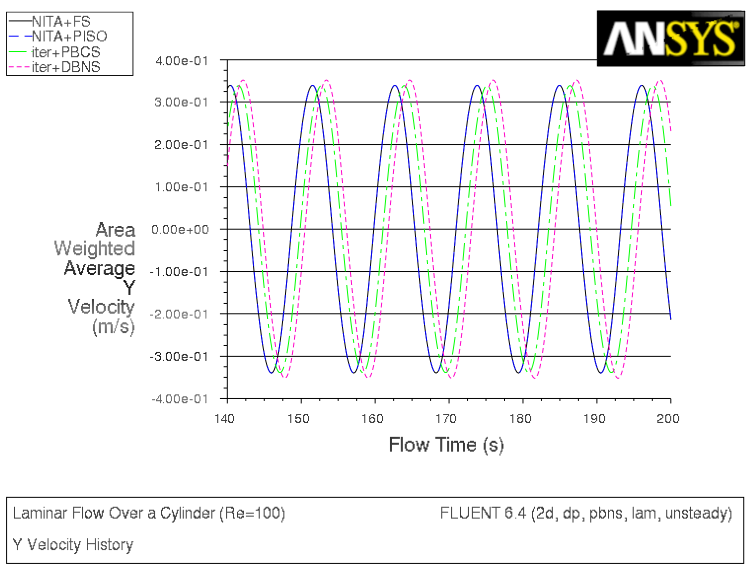


Figure 16.4.1: Comparison of Monitor of y Velocity at History Point Between Iterative Solver and Different NITA Schemes

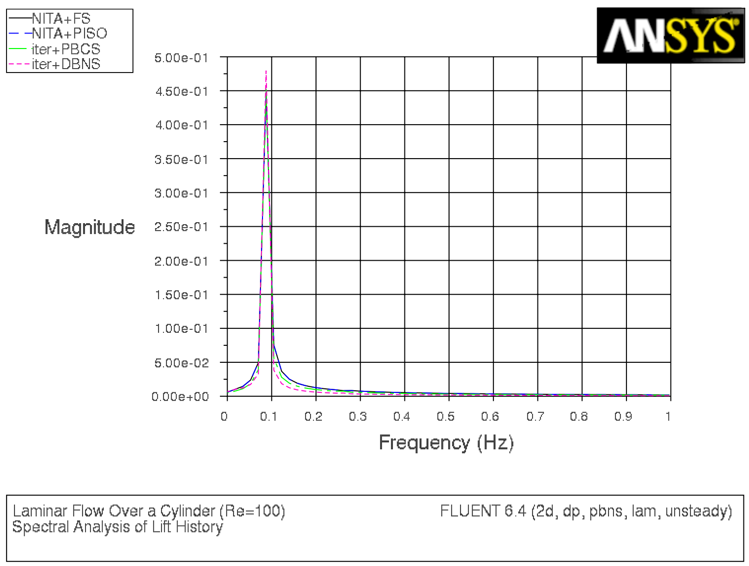


Figure 16.4.2: Comparison of FFT Analysis of Monitor of Lift Coefficient on the Cylinder Wall Between Iterative Solver and Different NITA Schemes

Release 12.0 © ANSYS, Inc. January 24, 2009

Validation 17. Rotation of Two Immiscible Liquids

17.1 Purpose

The purpose of this test is to validate ANSYS FLUENT's Volume of Fluid (VOF) model for rotational flow of immiscible liquids. ANSYS FLUENT's predictions of swirl velocity and displacement of the interface between the liquids are in close agreement with the experimental data of Sugimoto and Iguchi [1].

17.2 Problem Description

A vertical cylindrical vessel containing immiscible silicone oil and water is initially at rest. The silicone oil layer rests on top of the water due to its lower density. The top of the cylindrical vessel is sealed. The vessel is set into rotation with a constant angular velocity, ω. The diameter and height of the vessel are 46 mm and 120 mm, respectively. The following equations are definitions of the dimensionless parameters:

$$Re_\omega = R(\frac{\omega}{\nu_w})^{\frac{1}{2}} \tag{17.2-1}$$

$$VR = \frac{V_w}{V_{so}} \tag{17.2-2}$$

where, R is the radius of the vessel, ω is the angular velocity of the vessel, ν_w is the kinematic viscosity of water, V_w is the volume of water, V_{so} is the volume of silicone oil, Re_ω is the rotation Reynolds number, and VR is the volume ratio.

Dimensionless swirl velocity is defined as $V_{sw}/(R\omega)$, where V_{sw} is the swirl velocity of water, and R and ω are the radius of the cylinder and the angular velocity of the cylindrical vessel, respectively.

Development of the flow field as a function of time, and the behavior of the interface between the two liquids are numerically studied using the VOF model. A geometric reconstruction scheme is used for the entire unsteady run. Due to the symmetrical nature of the flow, a 2D axisymmetric calculation is performed.

17.3 References

1. Sugimoto, T. and Iguchi, M., Behavior of Immiscible Two Liquid Layers Contained in Cylindrical Vessel Suddenly Set in Rotation, ISIJ Int., 42, pp. 338-343, 2002.

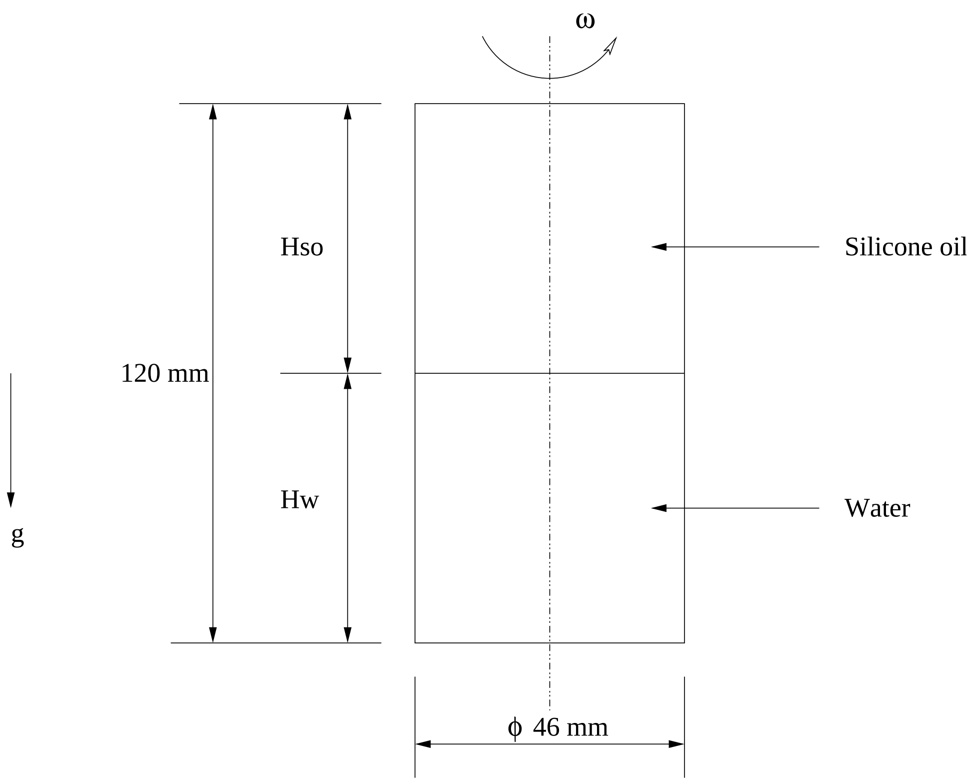


Figure 17.2.1: Problem Description

Release 12.0 © ANSYS, Inc. January 24, 2009

17.4 Results

Experimental data is available in the form of

- Dimensionless swirl velocity of water vs. time.
- Vertical displacement of the interface h vs. time.

Dimensionless swirl velocity is defined as

$$\frac{V_{sw}}{Re_{\omega}}$$

where V_{sw} is the swirl velocity of water. The displacement (h) of the interface on the axis of the vessel is calculated from the initial horizontal interfacial plane. Time histories of dimensionless swirl velocities of water are compared with experimental results for a Re_{ω} = 35.6 and a VR of 0.5. The axial (x) and radial (r) coordinates of the locations where the profiles are computed are shown in Figures 17.4.1–17.4.3. The axial distance is measured from the bottom of the cylinder. For Re_{ω} = 74.9 and VR=1, the variation of the interface height (h) with time is measured from the intermediate data files (see Figure 17.4.4). The results show strong agreement with experimental results.

17.4.1 Validation-Specific Information

Solver:	ANSYS FLUENT 2D Double Precision
Version:	12.0.9
Solution Files:	1. `Rew35.6_VR0.5-swirl_t80.cas.gz`, `Rew35.6_VR0.5-swirl_t80.dat.gz` (for $Re_{\omega} = 35.6$ and VR=0.5, final solution at 80 seconds)
	2. `Rew74.9_VR1-Interface_t60.cas.gz`, `Rew74.9_VR1-Interface_t60.dat.gz` (for $Re_{\omega} = 74.9$ and VR=1, final solution at 60 seconds)

These solution files are available from the User Services Center as described in the Introduction.

17.4.2 Plot Data

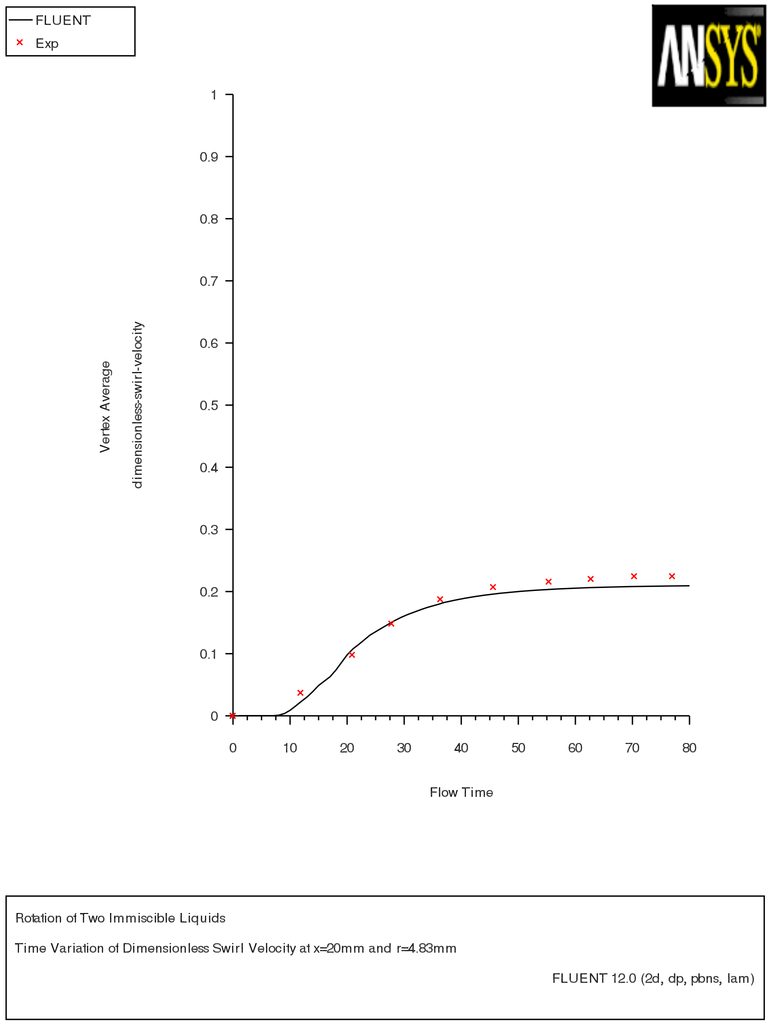


Figure 17.4.1: Time Variation of Dimensionless Swirl Velocity at $x = 20$ mm and $r = 4.83$ mm for $Re_\omega = 35.6$ and $VR = 0.5$

Release 12.0 © ANSYS, Inc. January 24, 2009

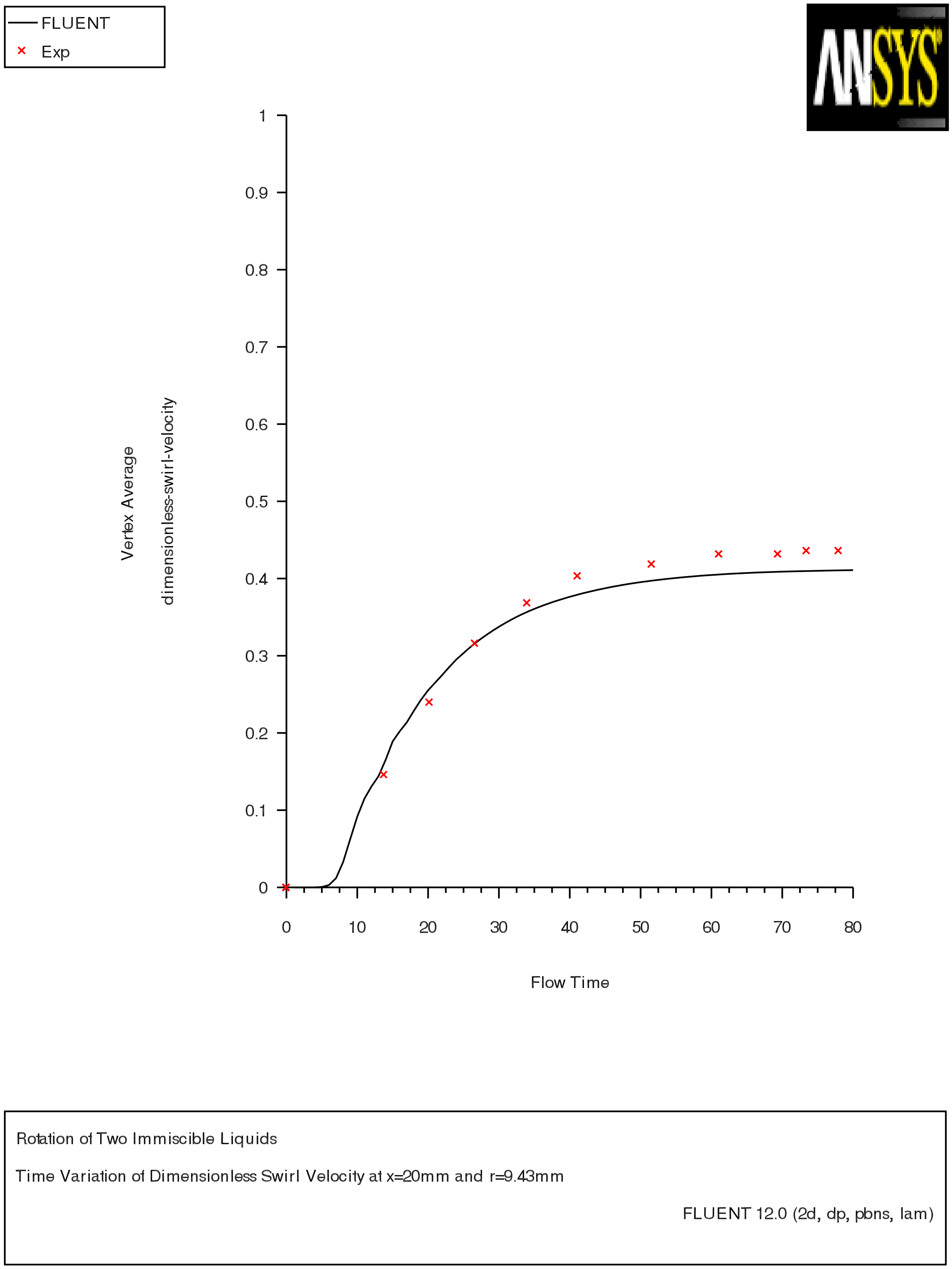


Figure 17.4.2: Time Variation of Dimensionless Swirl Velocity at $x = 20$ mm and $r = 9.43$ mm for $Re_\omega = 35.6$ and $VR = 0.5$

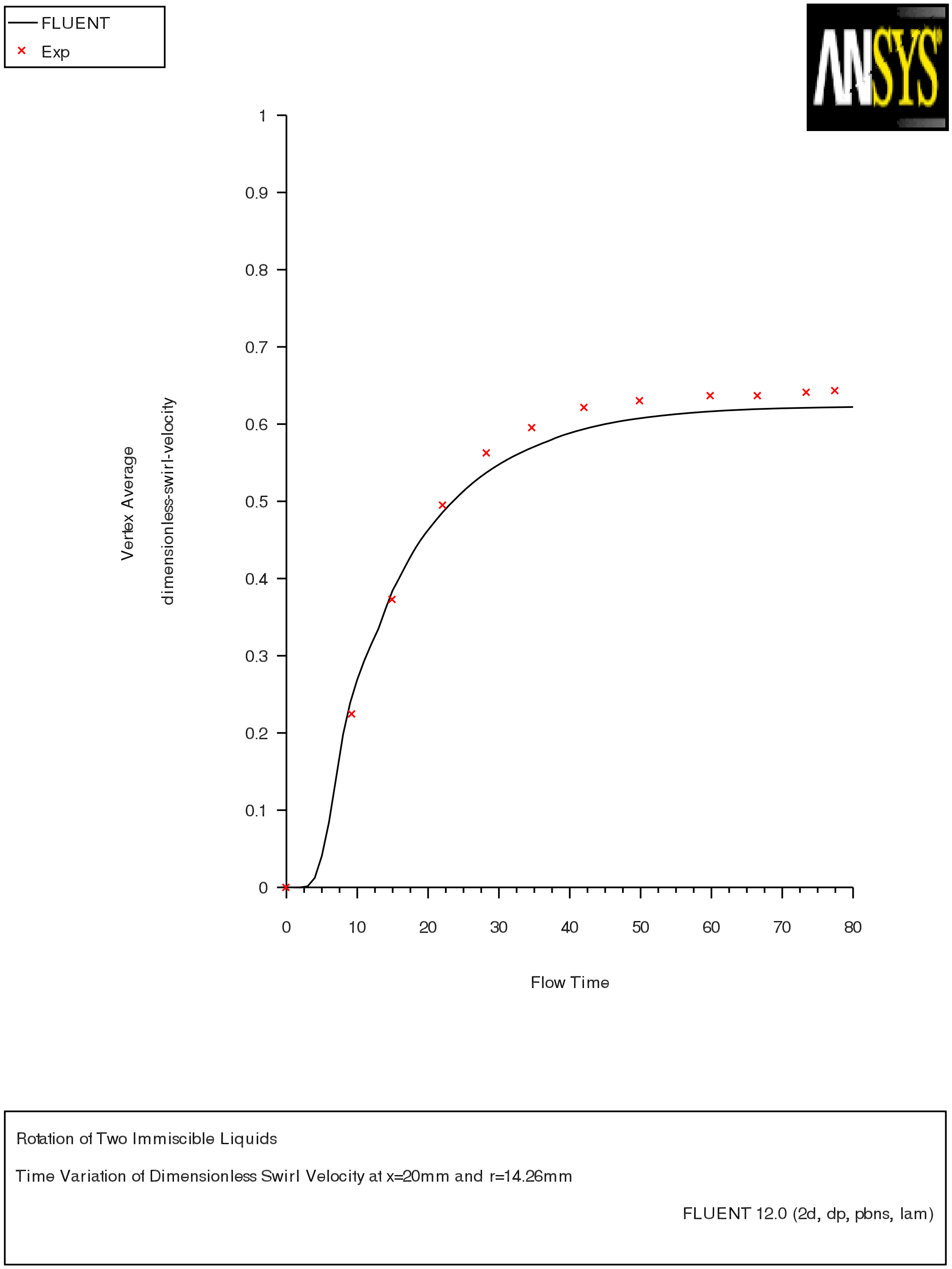


Figure 17.4.3: Time Variation of Dimensionless Swirl Velocity at $x = 20$ mm and $r = 14.26$ mm for $Re_\omega = 35.6$ and $VR = 0.5$

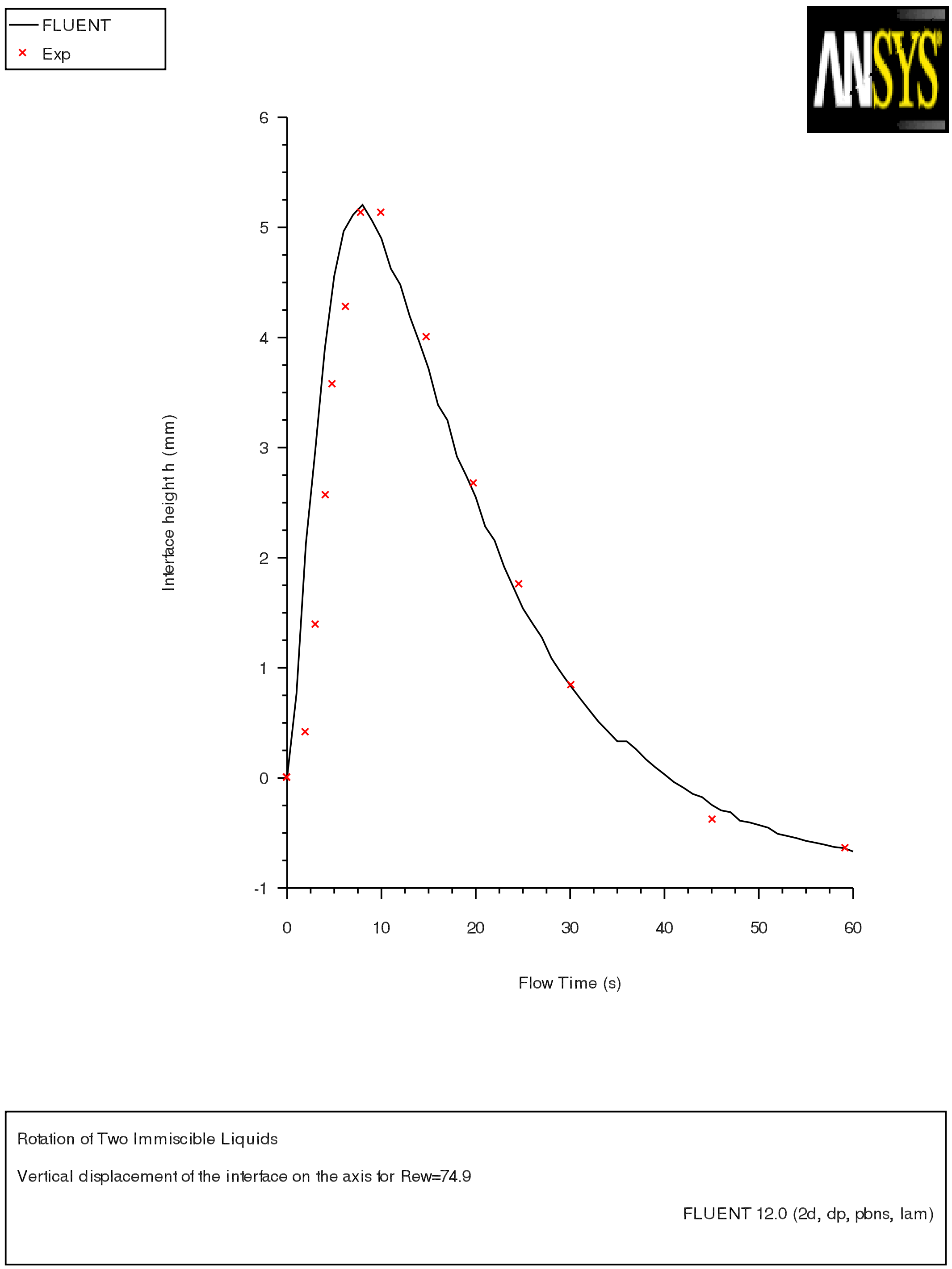


Figure 17.4.4: Vertical Displacement of the Interface on the Axis for $Re_\omega = 74.9$ and $VR = 1.0$

Release 12.0 © ANSYS, Inc. January 24, 2009

Validation 18. Polyhedral and Tetrahedral Mesh Accuracy

18.1 Purpose

The purpose of this test is to validate the accuracy of second-order discretization schemes for the pressure-based solver, with tetrahedral and polyhedral meshes.

18.2 Problem Description

The laminar incompressible flow in a 3D driven cavity is solved at Reynolds number = 1000. A half domain is modeled with height = 1m, length = 1m and breadth = 0.5m, using symmetry boundary conditions. The top of the domain is modeled using a moving boundary condition. The flow is solved with both pressure based and density based solvers. The flow is solved with second order discretization schemes for pressure and momentum. Coupled scheme is used for pressure-velocity coupling for pressure based solver. For density based solver implicit formulation, Roe-FDS are used along with second order discretization scheme.

18.3 References

1. Roache, P. J., *Verification and Validation in Computational Science and Engineering*, Hermosa Publishers, Albuquerque, New Mexico, 1998.
2. Wirogo, S., *Flux Corrected Method: An accurate approach to fluid flow modeling*, Ph.D thesis, Iowa State University, Ames, Iowa, 1997.

18.4 Results

The problem is solved for five sets of tetrahedral and polyhedral meshes, with increasing mesh density. For tetrahedral meshes only pressure based coupled solver is used and for polyhedral meshes both pressure based coupled solver and density based solver are used. A baseline is established for the velocity distribution along a line at the center of the symmetry plane in the direction of flow by obtaining a solution on a very fine, uniform size hexahedral mesh. This baseline is used to calculate the percent relative L2 norm (a measurement of error) for each of the tetrahedral and polyhedral meshes.

A logarithmic plot is then generated that shows how the L2 norm results change for each of the mesh types as the cell count increases (see Figure 18.4.5). Such a plot makes it possible to visually compare the difference in the cell count of polyhedral meshes and

tetrahedral meshes for the same level of accuracy. Also plotted are two lines for first and second order accuracy. For 3D meshes, a first-order accurate solution can be represented by $y = x^{(-1/3)}$ and a second-order accurate solution can be represented by $y = x^{(-2/3)}$, where x is the cell count. Comparison to this plot validates the second order accuracy for the two mesh types.

18.4.1 Validation-Specific Information

Serial Number	Tetrahedral Mesh Cell Count	Tetrahedral Mesh Face Count	Polyhedral Mesh Cell Count	Polyhedral Mesh Face Count
1	12290	25658	2621	17224
2	29000	59808	5787	38608
3	57789	118427	11114	74858
4	241041	489263	43839	299647
5	1592404	3213634	279894	1930755

Release 12.0 © ANSYS, Inc. January 24, 2009

Solver: ANSYS FLUENT 3D Double Precision
Version: 6.4.13
Solution Files: Tetrahedral Meshes

1. `drv-cav-tet-pbcs-1.cas.gz`, `drv-cav-tet-pbcs-1.dat.gz` (pressure based)
2. `drv-cav-tet-pbcs-2.cas.gz`, `drv-cav-tet-pbcs-2.dat.gz` (pressure based)
3. `drv-cav-tet-pbcs-3.cas.gz`, `drv-cav-tet-pbcs-3.dat.gz` (pressure based)
4. `drv-cav-tet-pbcs-4.cas.gz`, `drv-cav-tet-pbcs-4.dat.gz` (pressure based)
5. `drv-cav-tet-pbcs-5.cas.gz`, `drv-cav-tet-pbcs-5.dat.gz` (pressure based)

Polyhedral Meshes

1. `drv-cav-poly-pbcs-1.cas.gz`, `drv-cav-poly-pbcs-1.dat.gz` (pressure based)
2. `drv-cav-poly-pbcs-2.cas.gz`, `drv-cav-poly-pbcs-2.dat.gz` (pressure based)
3. `drv-cav-poly-pbcs-3.cas.gz`, `drv-cav-poly-pbcs-3.dat.gz` (pressure based)
4. `drv-cav-poly-pbcs-4.cas.gz`, `drv-cav-poly-pbcs-4.dat.gz` (pressure based)
5. `drv-cav-poly-pbcs-5.cas.gz`, `drv-cav-poly-pbcs-5.dat.gz` (pressure based)
6. `drv-cav-poly-dbns-6.cas.gz`, `drv-cav-poly-dbns-6.dat.gz` (density based)
7. `drv-cav-poly-dbns-7.cas.gz`, `drv-cav-poly-dbns-7.dat.gz` (density based)
8. `drv-cav-poly-dbns-8.cas.gz`, `drv-cav-poly-dbns-8.dat.gz` (density based)
9. `drv-cav-poly-dbns-9.cas.gz`, `drv-cav-poly-dbns-9.dat.gz` (density based)
10. `drv-cav-poly-dbns-10.cas.gz`, `drv-cav-poly-dbns-10.dat.gz` (density based)

These solution files are available from the User Services Center as described in the Introduction.

18.4.2 Plot Data

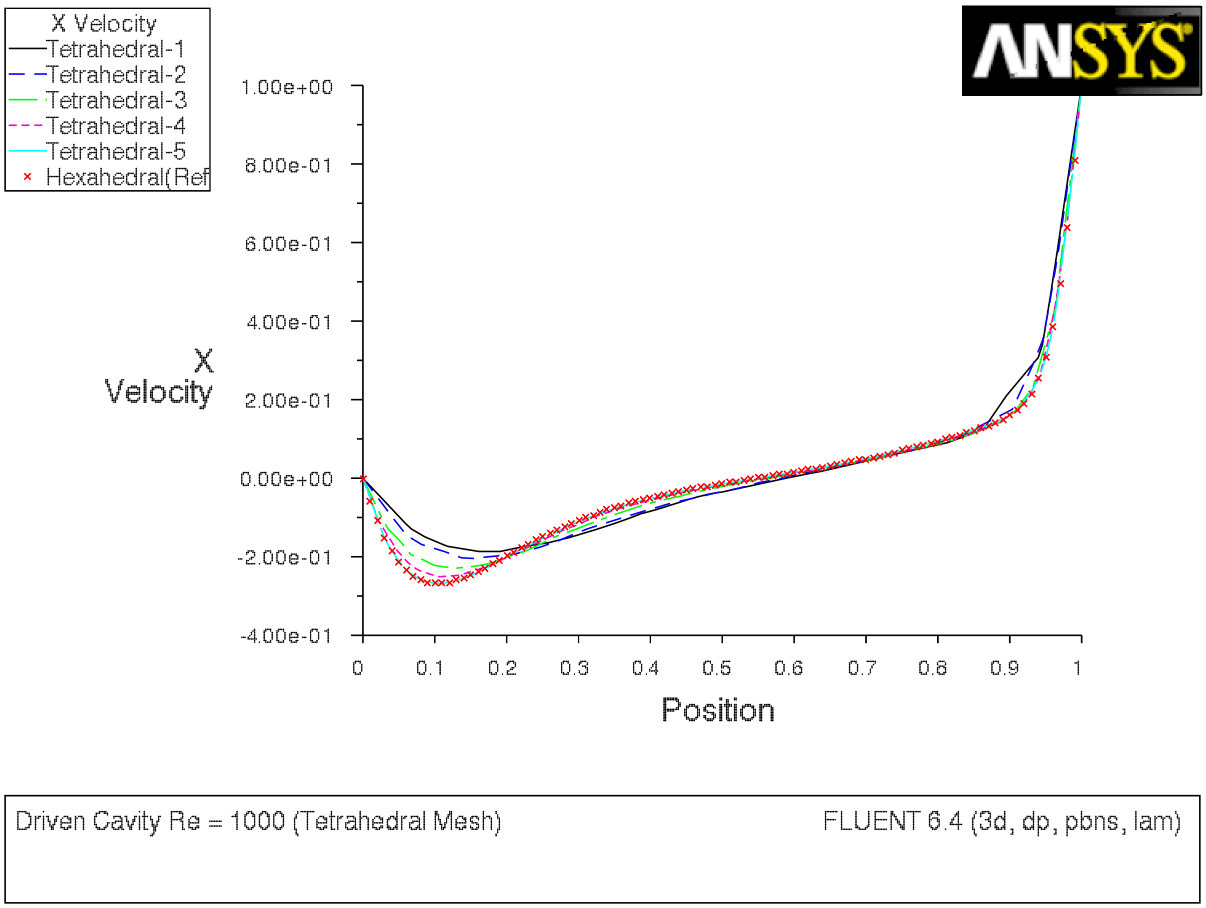


Figure 18.4.1: Velocity Distribution for Tetrahedral Meshes with PBCS

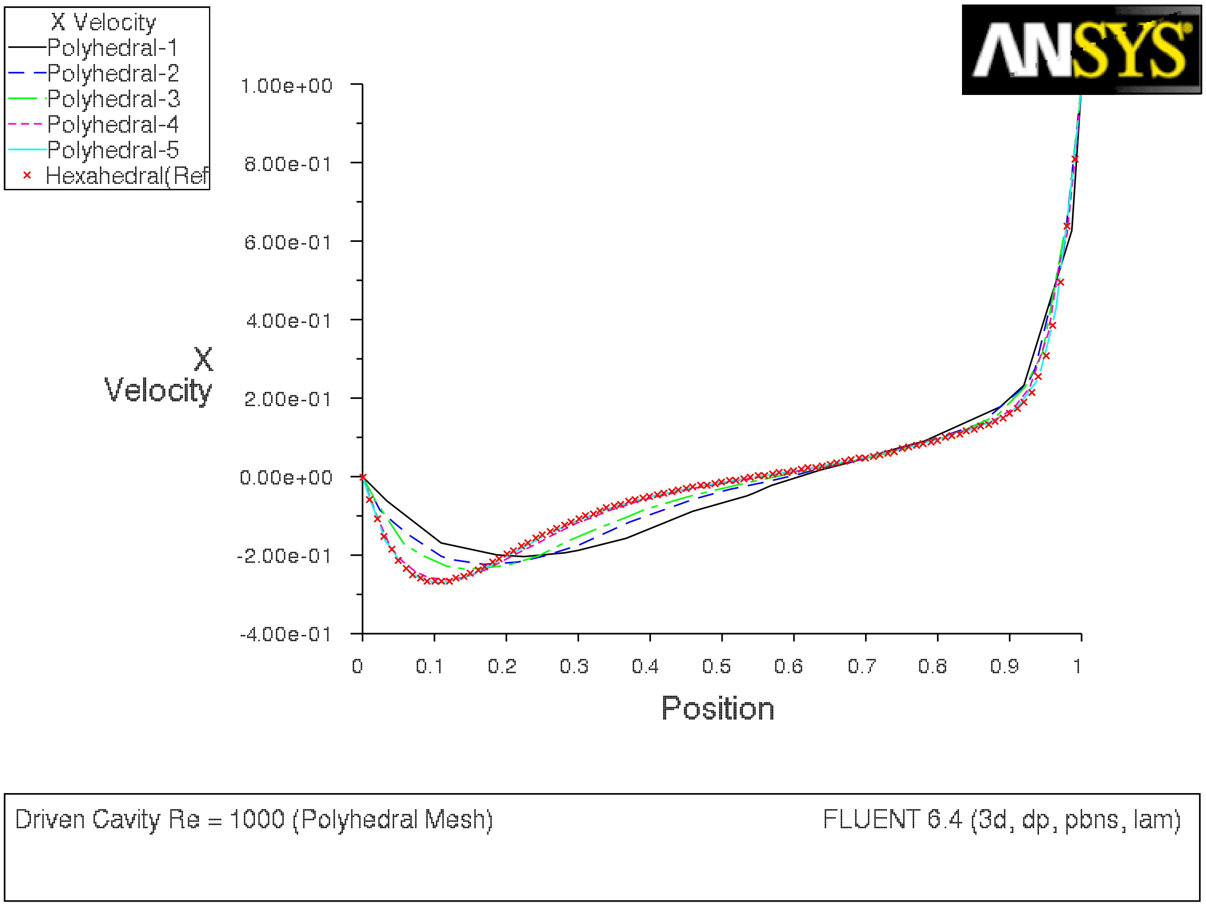


Figure 18.4.2: Velocity Distribution for Polyhedral Meshes with PBCS

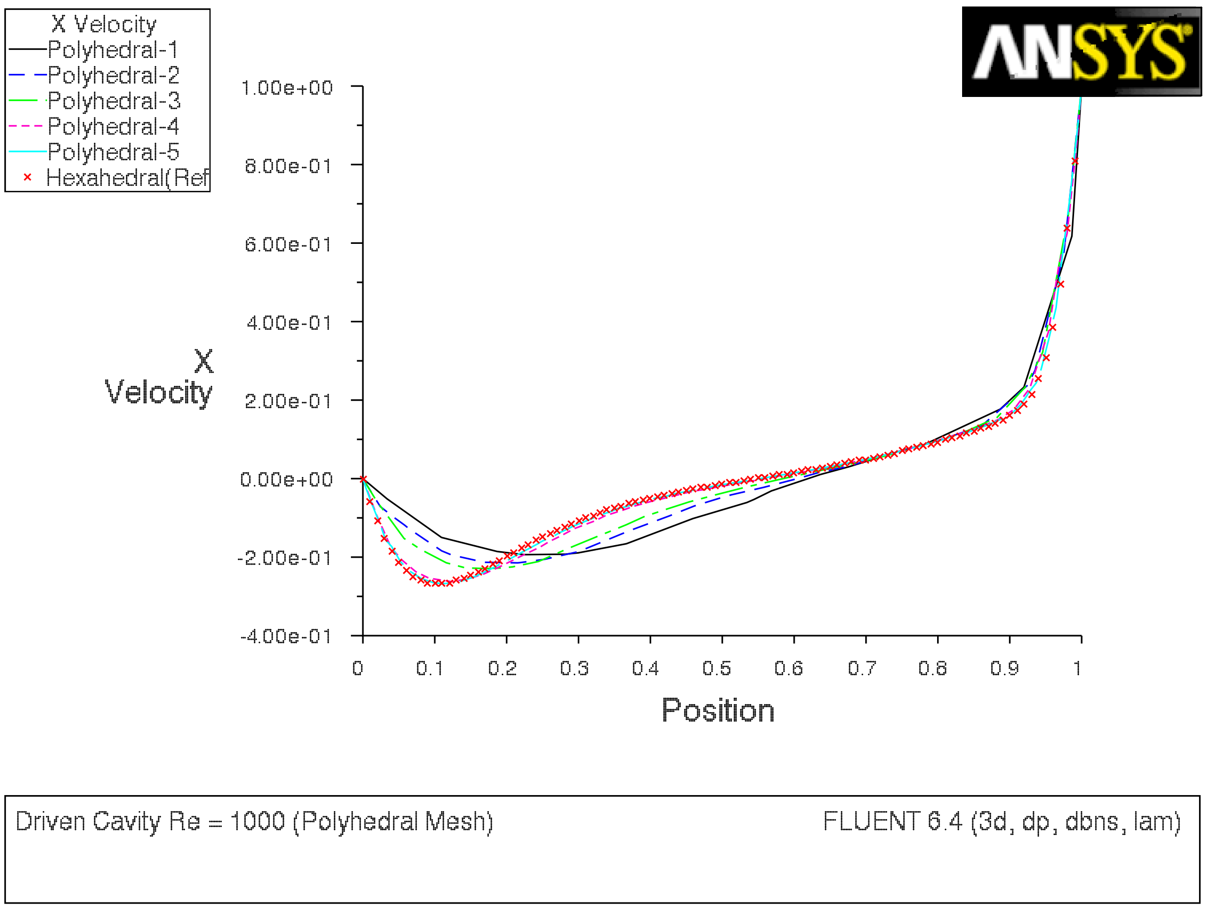


Figure 18.4.3: Velocity Distribution for Polyhedral Meshes with DBNS

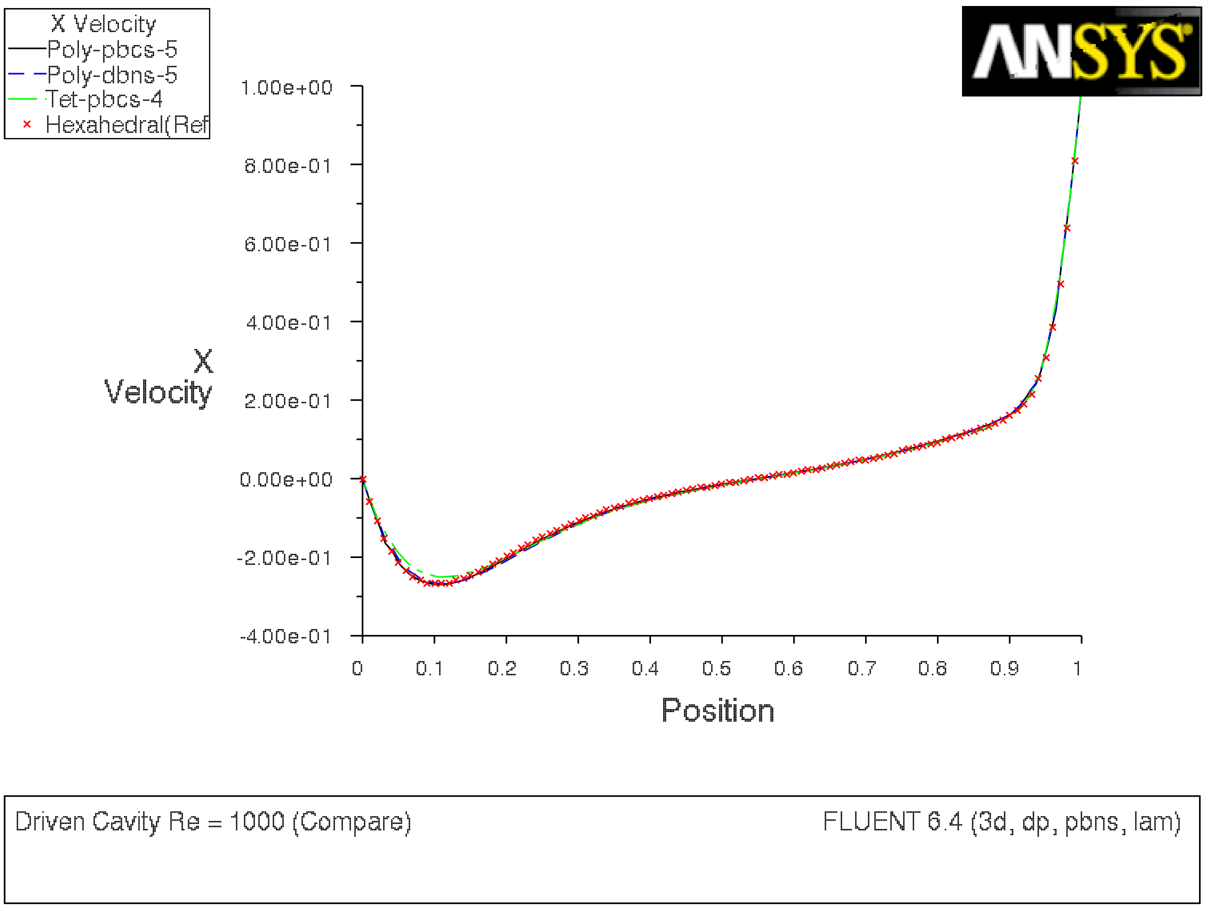


Figure 18.4.4: Comparison of Velocity Distributions by Mesh Type and Solver Type

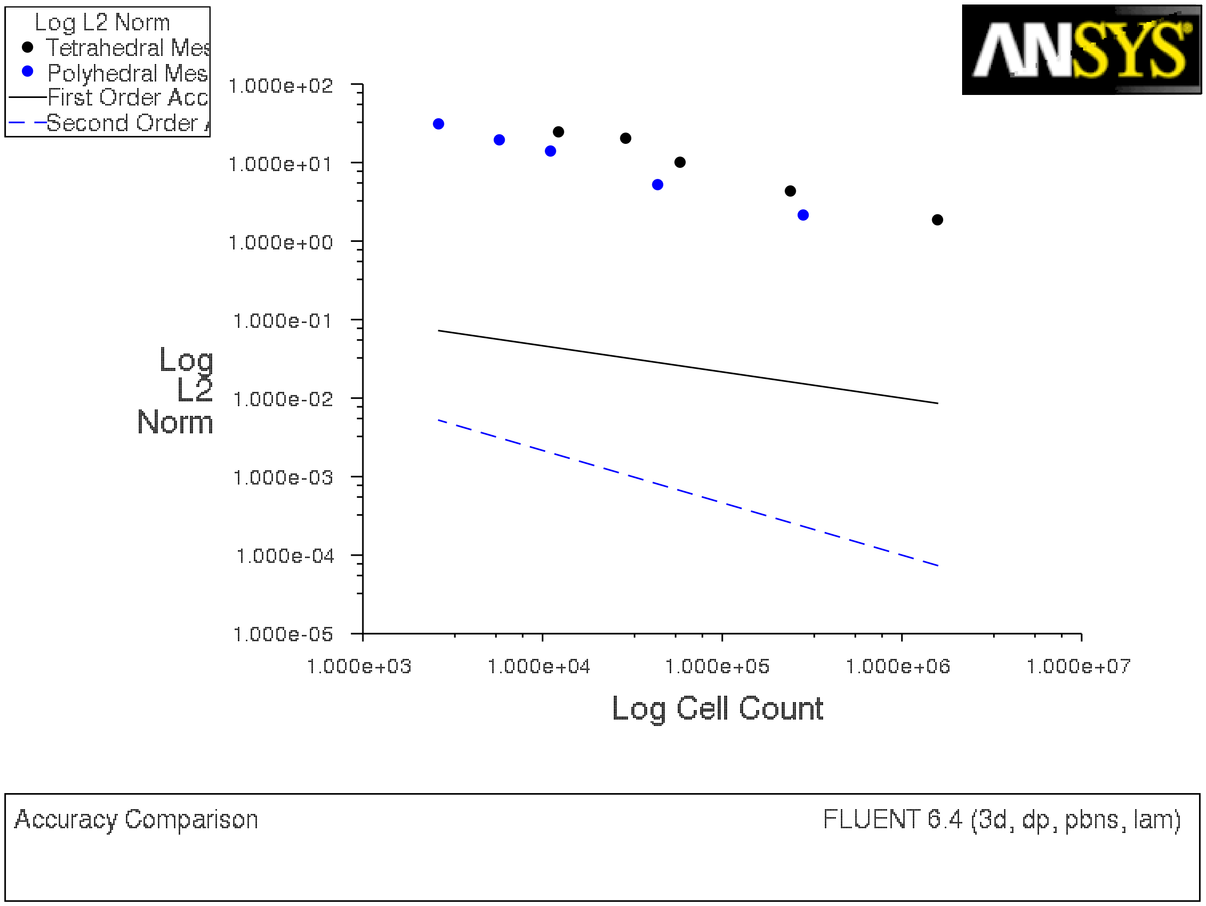


Figure 18.4.5: Accuracy Comparison

Release 12.0 © ANSYS, Inc. January 24, 2009

Validation 19. Methane Jet Combustion in a Swirling Annular Shroud

19.1 Purpose

The aim of this validation is to compare ANSYS FLUENT's predictions of axial velocity, swirl velocity, temperature, and mass-fraction of CO along radial iso-surfaces at several axial stations with the experimental data [1].

The test compares the results from the Non-Premixed Combustion Model with those from the Species Transport Eddy Dissipation Model and experimental data. The same quadrilateral mesh is used for both ANSYS FLUENT models.

19.2 Problem Description

The flow considered is a round reacting turbulent methane jet surrounded by an annular shroud of swirling air. The annular shroud is also surrounded by an air co-flow. The fuel (methane only) inlet has a diameter of 3.6mm and bulk velocity of 32.7 m/s. The air inlet for the annular shroud has an inner diameter of 50mm and an outer diameter of 60mm with a bulk axial velocity of 38.2 m/s and an average swirl velocity of 19.1 m/s.

The annular shroud enters free of methane. The air co-flow is also free of methane, has an average velocity of 20 m/s, and has an outer diameter of 310mm. Air enters the co-flow normal to the boundary. The computational domain, which is composed of 17,000 quadrilateral cells, is axisymmetric with a length of 1.5m. For each case the Realizable K-Epsilon Model is used for turbulence and the Discrete Ordinates Model is used for radiation.

Figure 19.2.1 shows the geometry of the problem.

19.3 References

1. Al-Abdeli, Y.M., and Masri, A.R., *Stability Characteristics and Flow Fields of Turbulent Swirling Jet Flows*, Combust. Theory and Modeling, 7:731-766 (2003). Data is also available online at http://www.aeromech.usyd.edu.au/thermofluids/main_frame.htm

19.4 Results

ANSYS FLUENT's results for both models are compared to the data from [1] in Figures 19.4.1 through 19.4.16, as measured at several axial stations. Figures 19.4.1 to



Figure 19.2.1: Problem Description

Release 12.0 © ANSYS, Inc. January 24, 2009

19.4.4 compare results for axial velocity, Figures 19.4.5 to 19.4.8 compare results for swirl velocity, Figures 19.4.9 to 19.4.12 compare results for temperature, and Figures 19.4.13 to 19.4.16 compare results for mass-fraction of CO. Predictions of axial velocity, swirl velocity, and temperature are good for both runs. Predictions for the mass -fraction of CO generated with the Non-Premixed model show better agreement with experimental results than do the predictions generated with the Species Transport Eddy Dissipation model.

19.4.1 Validation-Specific Information

Solver:	ANSYS FLUENT 2D Double Precision
Version:	6.4.13
Solution Files:	1. `non-premix_17k.cas`, `non-premix_17k.dat`
	2. `spec-transp_17k.cas`, `spec-transp_17k.dat`

These solution files are available from the User Services Center as described in the Introduction.

19.4.2 Plot Data

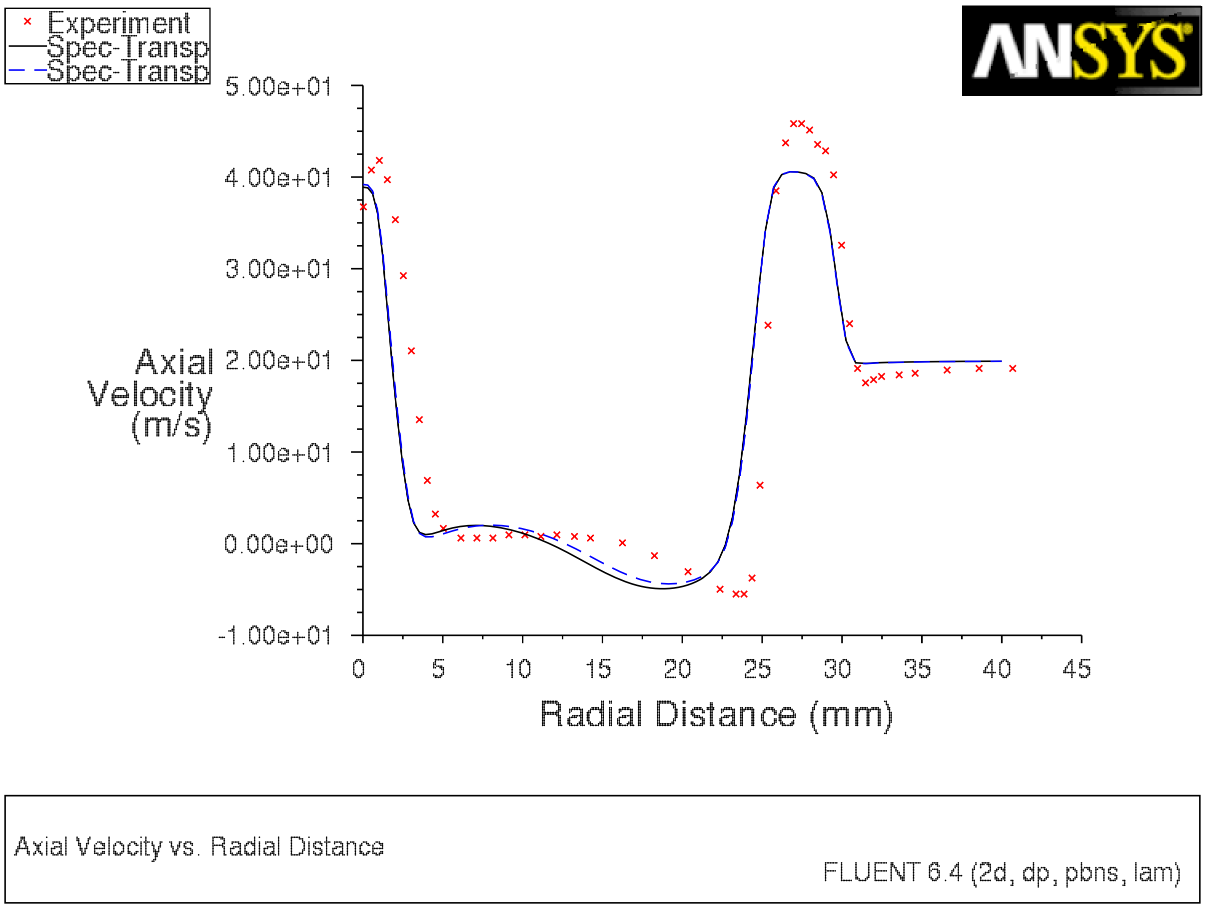


Figure 19.4.1: Axial Velocity vs Radial Distance at an Axial Distance of 6.8mm

Release 12.0 © ANSYS, Inc. January 24, 2009

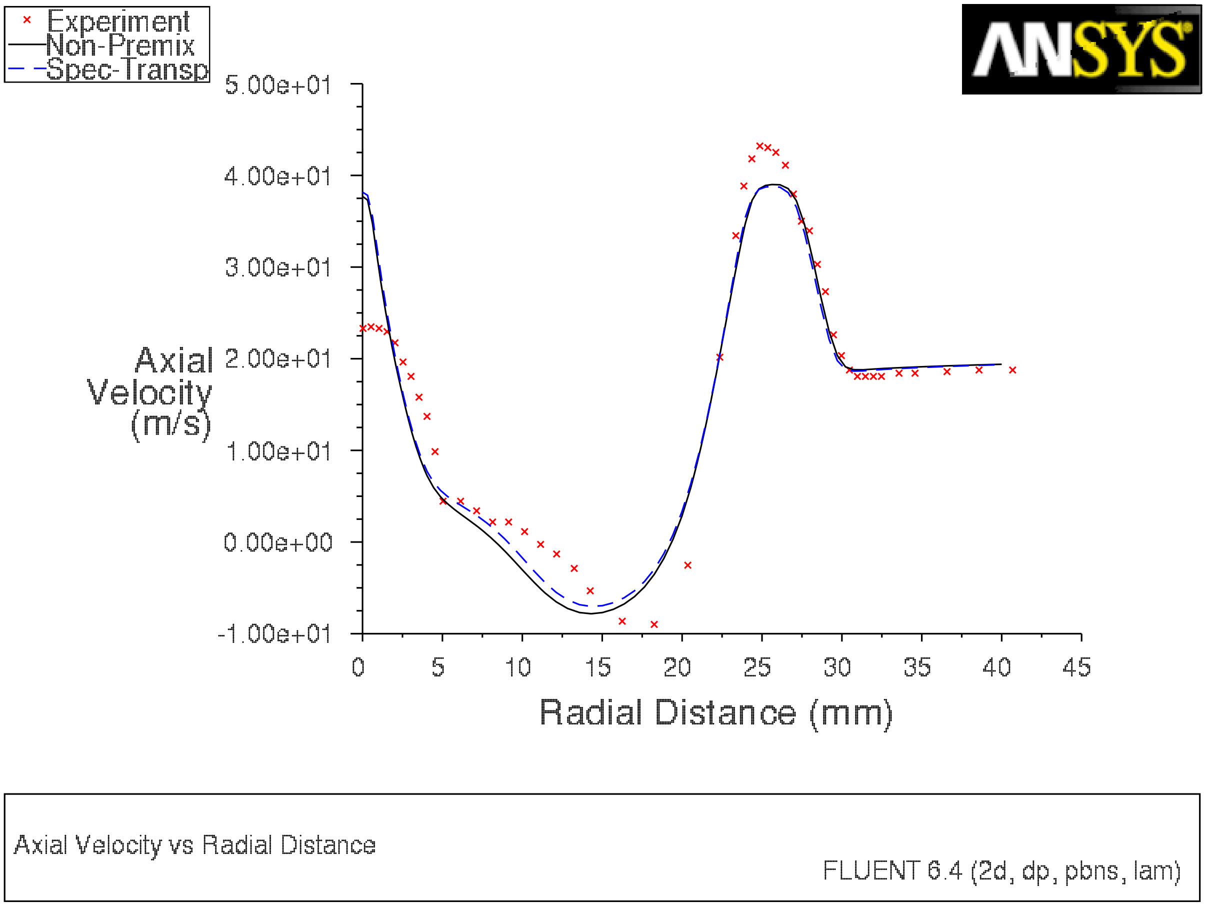


Figure 19.4.2: Axial Velocity vs Radial Distance at an Axial Distance of 20mm

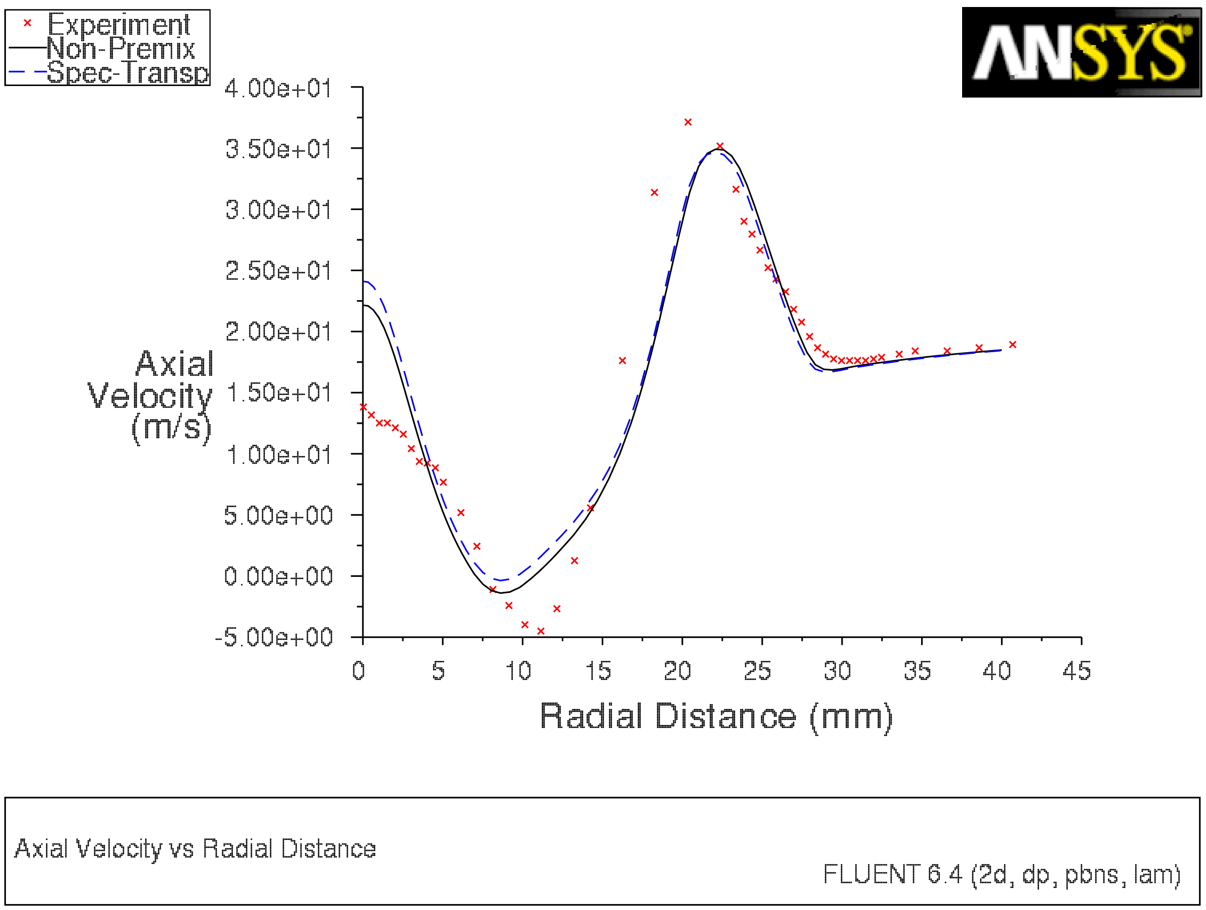


Figure 19.4.3: Axial Velocity vs Radial Distance at an Axial Distance of 40mm

Release 12.0 © ANSYS, Inc. January 24, 2009

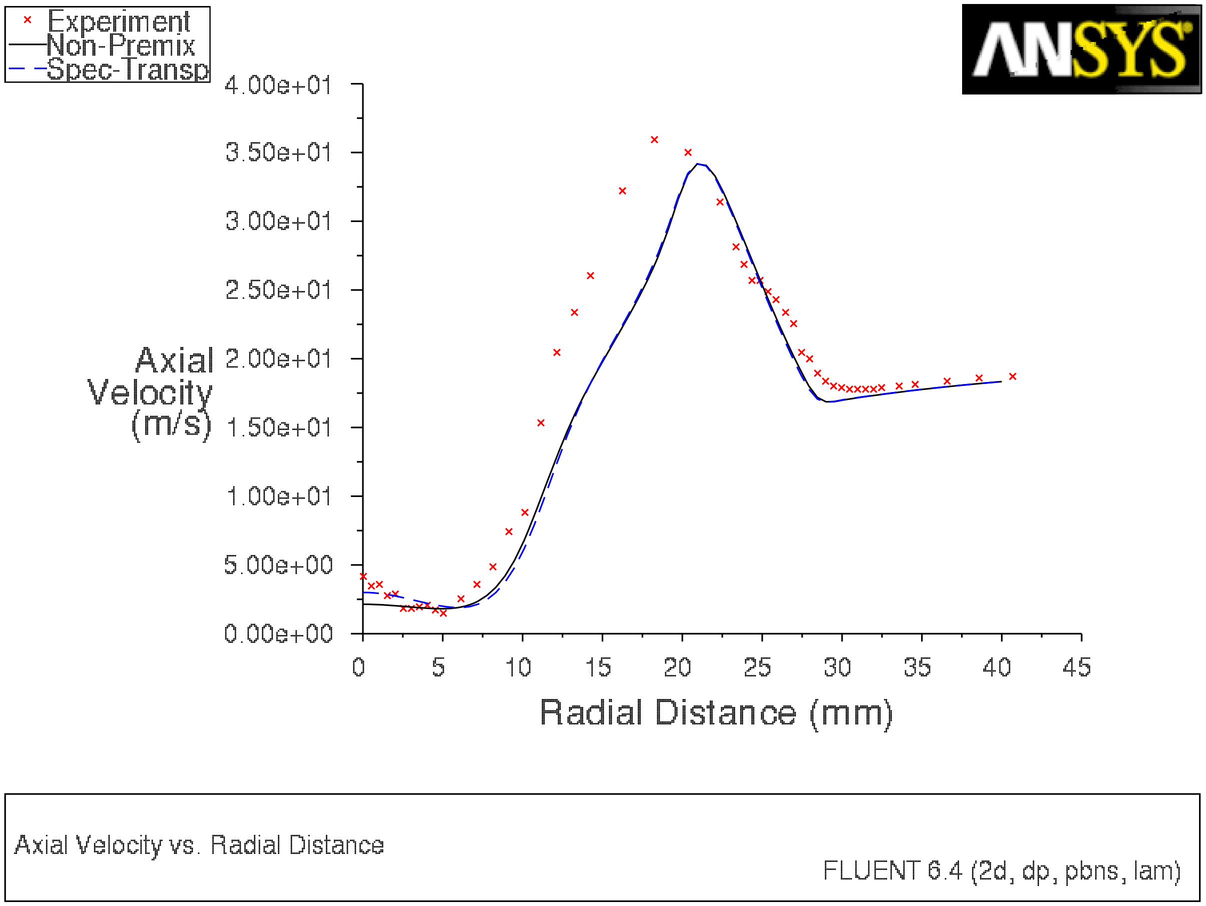


Figure 19.4.4: Axial Velocity vs Radial Distance at an Axial Distance of 60mm

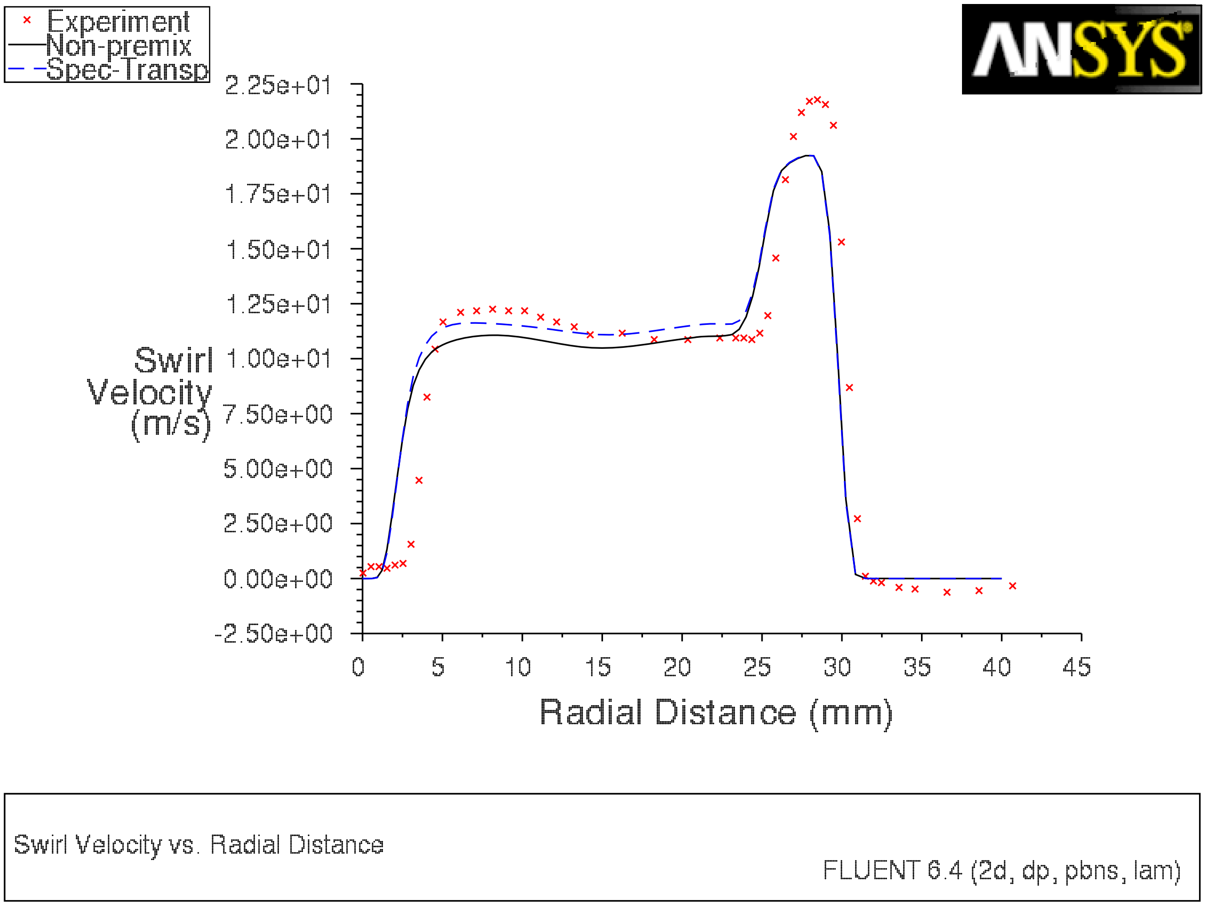


Figure 19.4.5: Swirl Velocity vs Radial Distance at an Axial Distance of 6.8mm

Release 12.0 © ANSYS, Inc. January 24, 2009

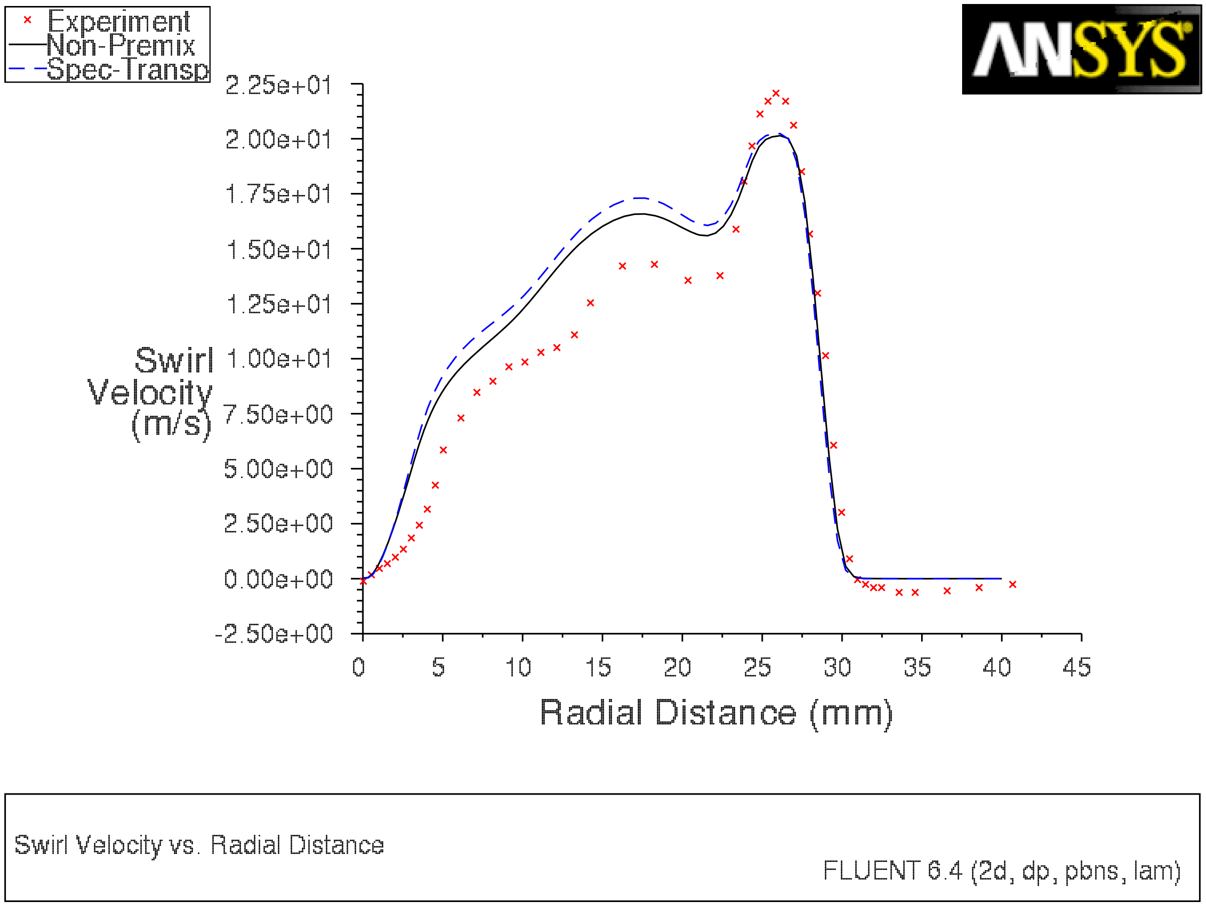


Figure 19.4.6: Swirl Velocity vs Radial Distance at an Axial Distance of 20mm

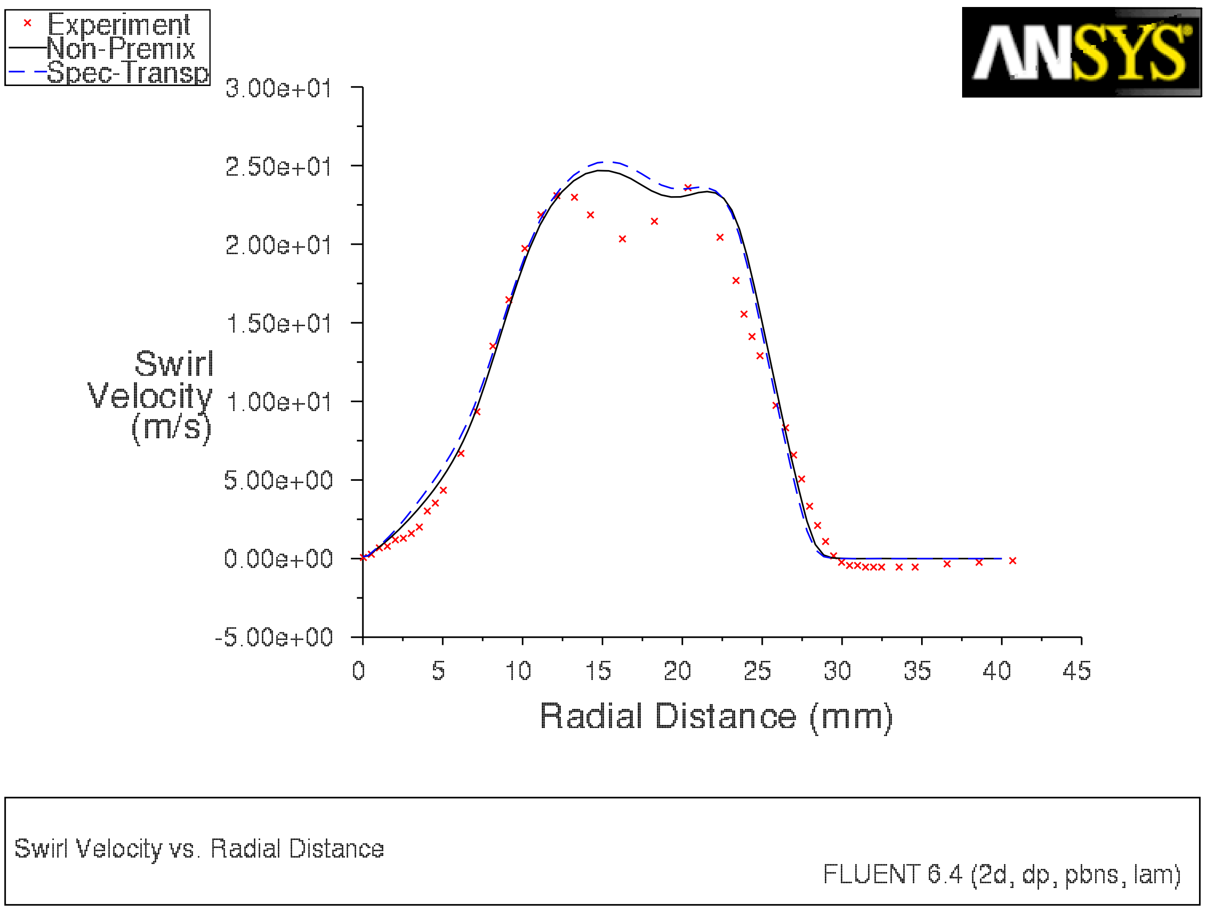


Figure 19.4.7: Swirl Velocity vs Radial Distance at an Axial Distance of 40mm

Release 12.0 © ANSYS, Inc. January 24, 2009

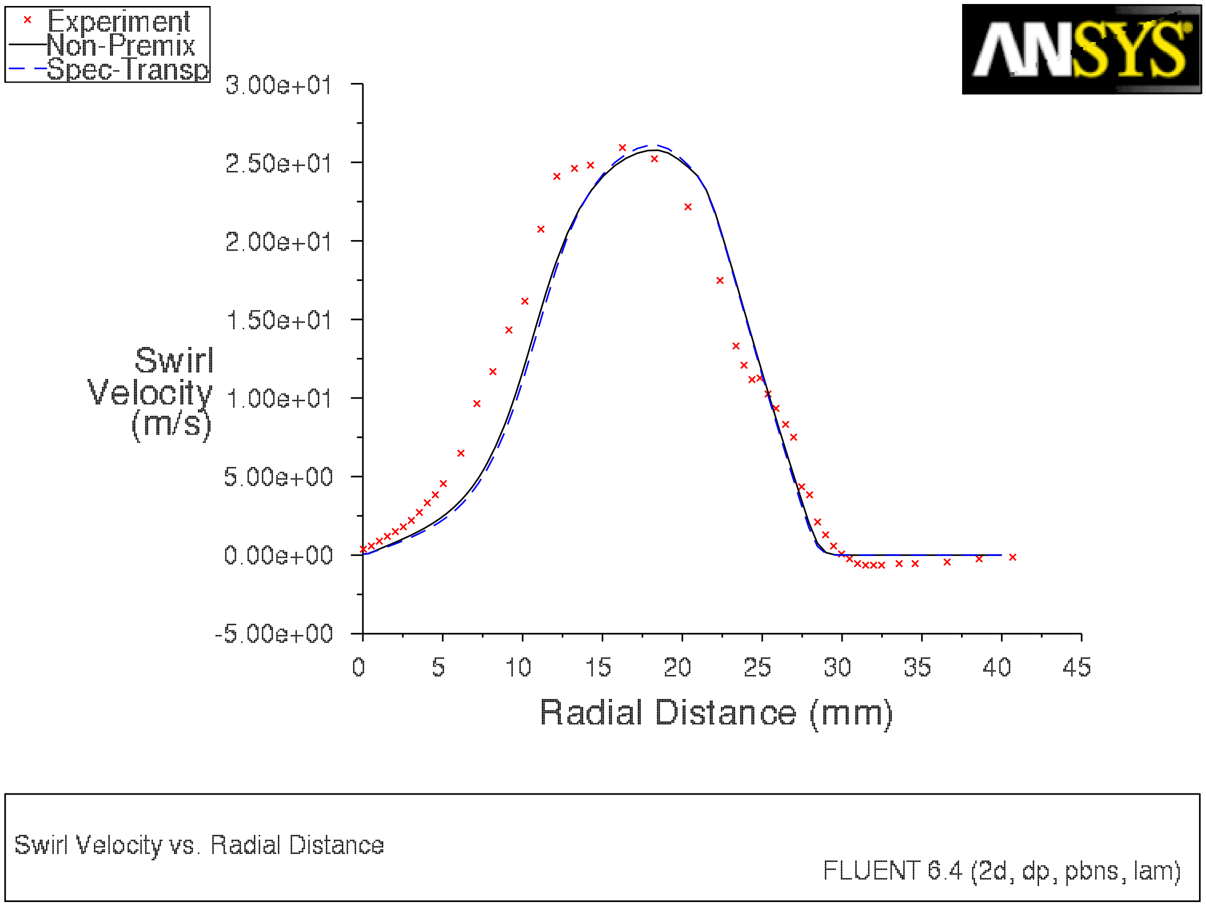


Figure 19.4.8: Swirl Velocity vs Radial Distance at an Axial Distance of 60mm

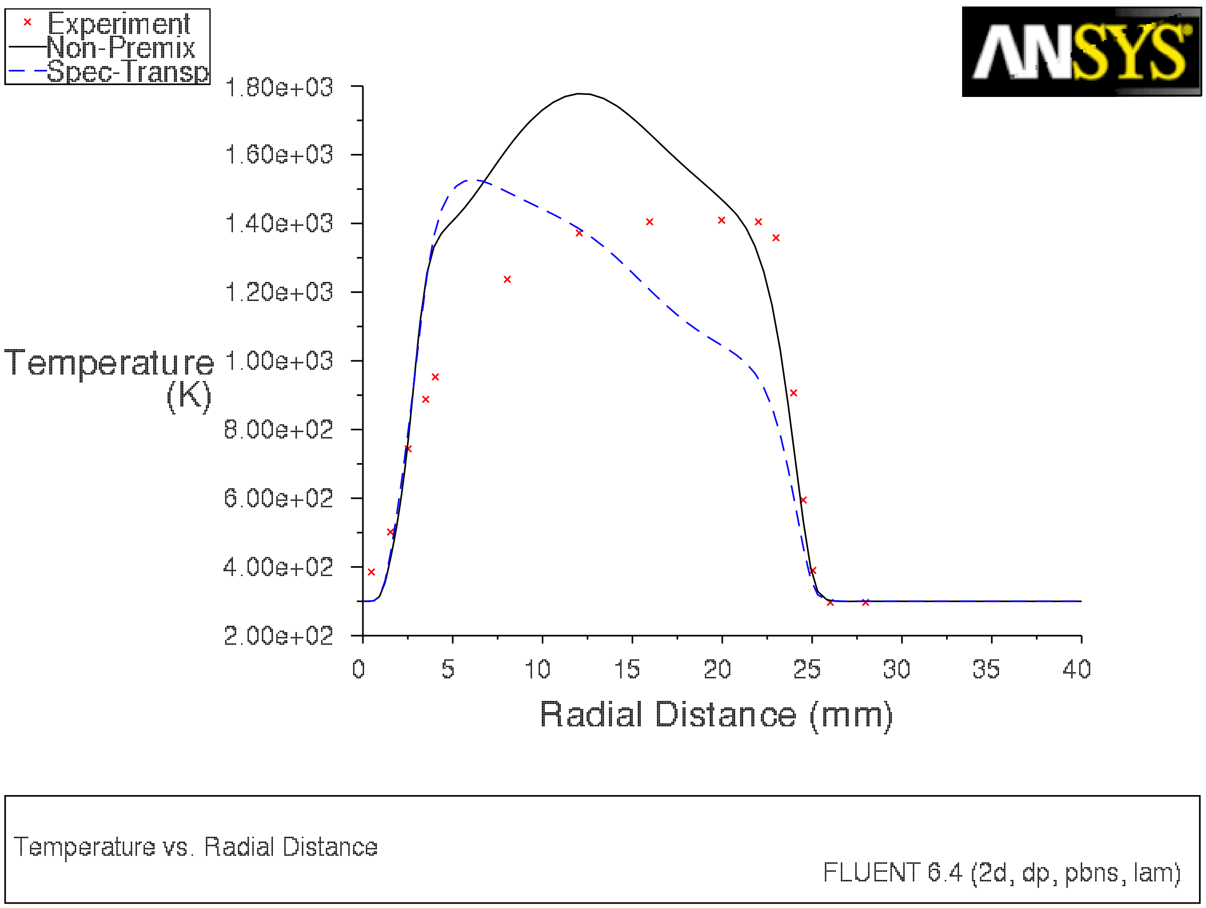


Figure 19.4.9: Temperature vs Radial Distance at an Axial Distance of 10mm

Release 12.0 © ANSYS, Inc. January 24, 2009

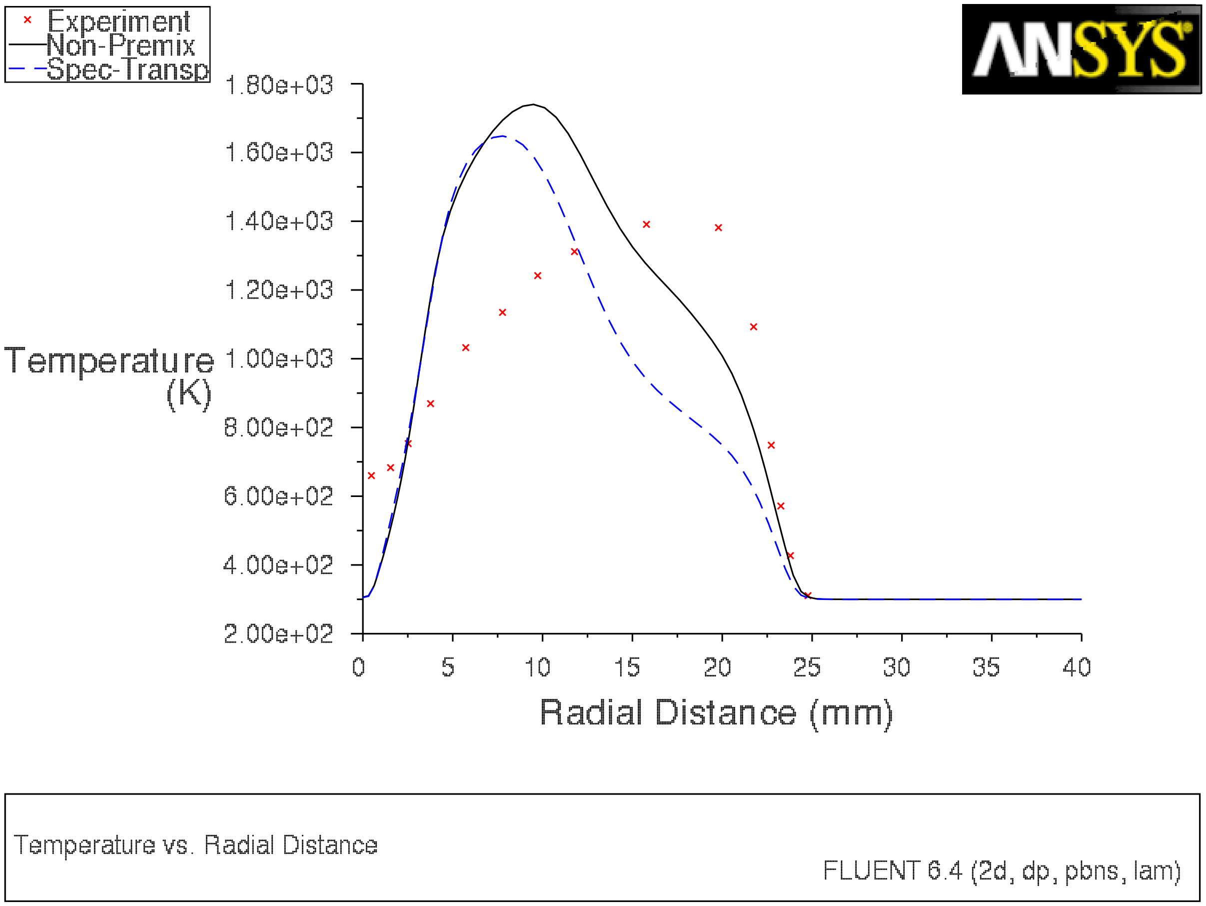


Figure 19.4.10: Temperature vs Radial Distance at an Axial Distance of 20mm

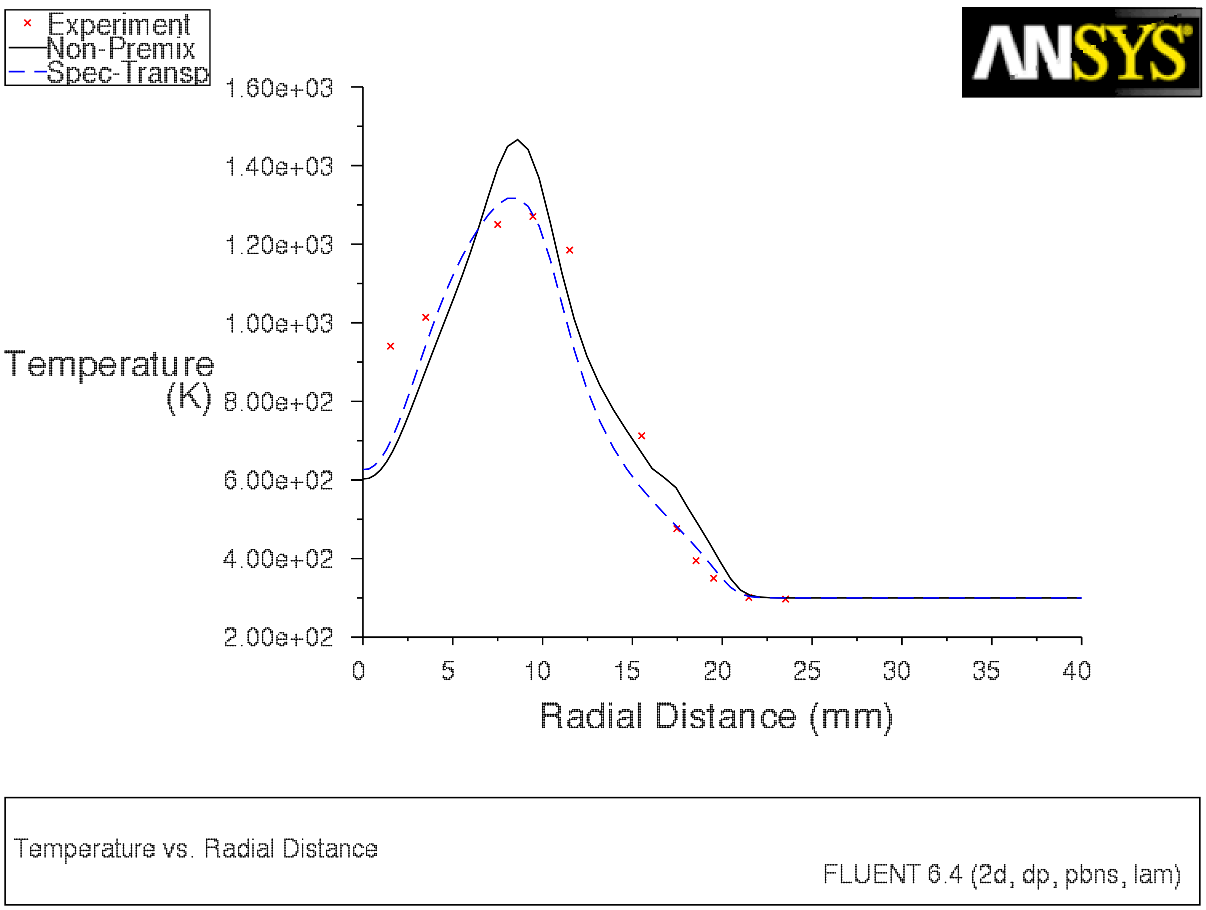


Figure 19.4.11: Temperature vs Radial Distance at an Axial Distance of 40mm

Release 12.0 © ANSYS, Inc. January 24, 2009

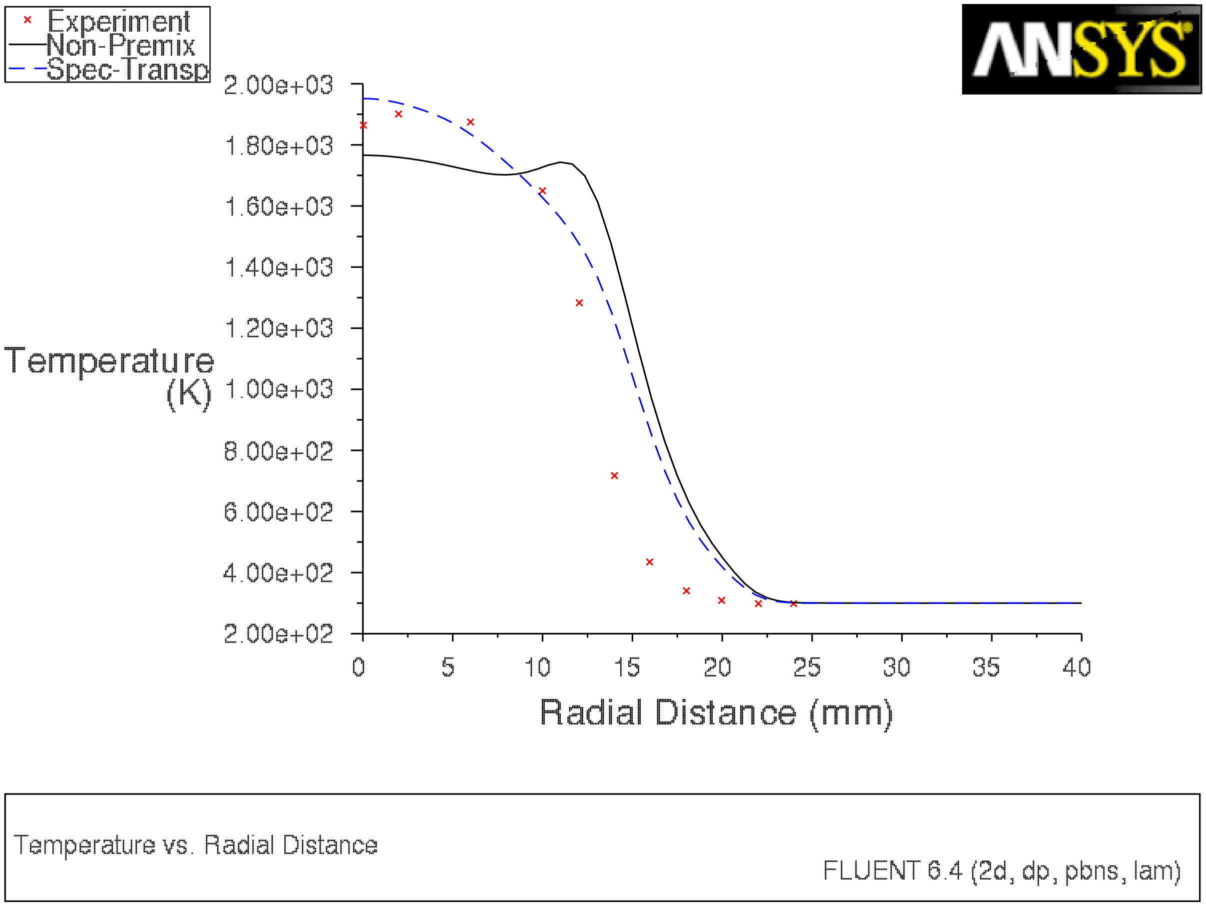


Figure 19.4.12: Temperature vs Radial Distance at an Axial Distance of 75mm

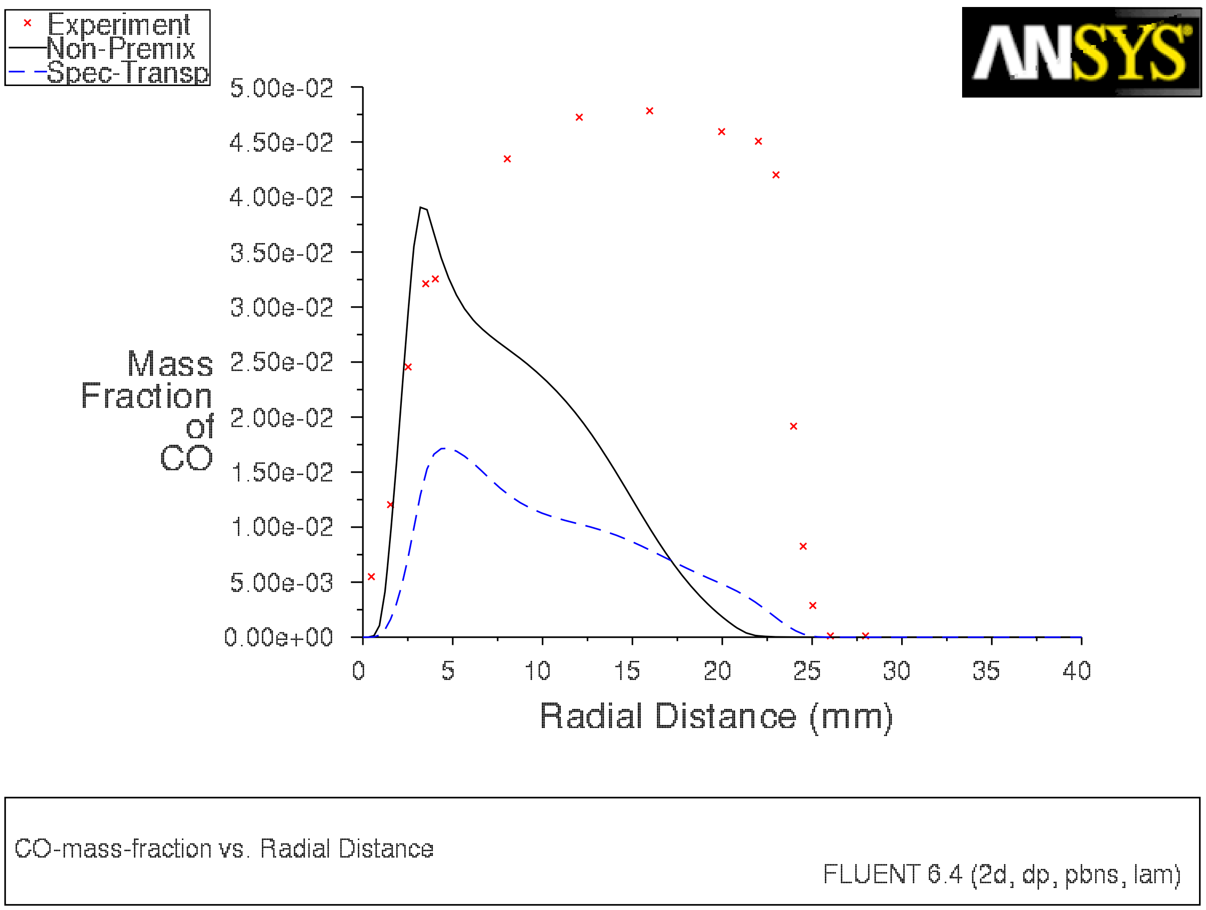


Figure 19.4.13: Mass-Fraction of CO vs Radial Distance at an Axial Distance of 10mm

Release 12.0 © ANSYS, Inc. January 24, 2009

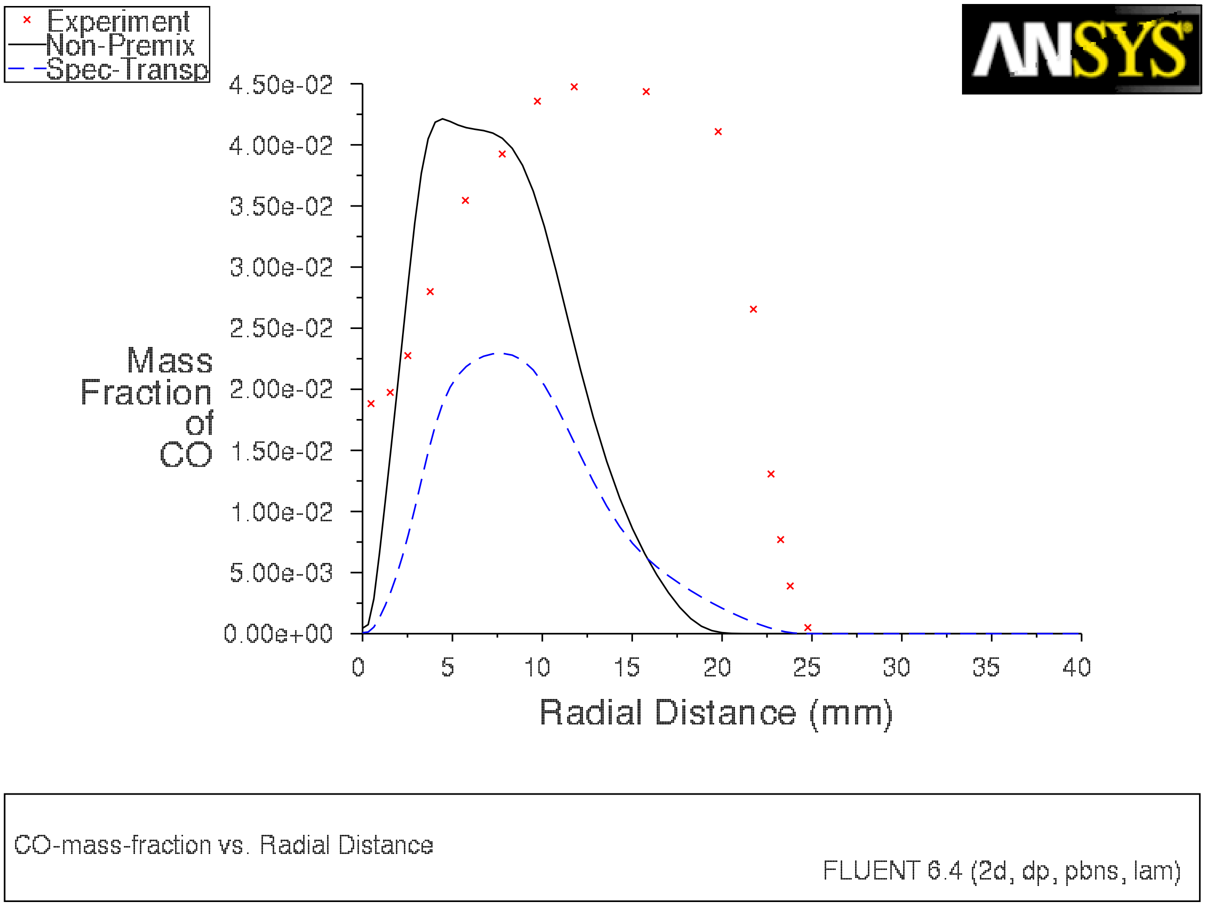


Figure 19.4.14: Mass-Fraction of CO vs Radial Distance at an Axial Distance of 20mm

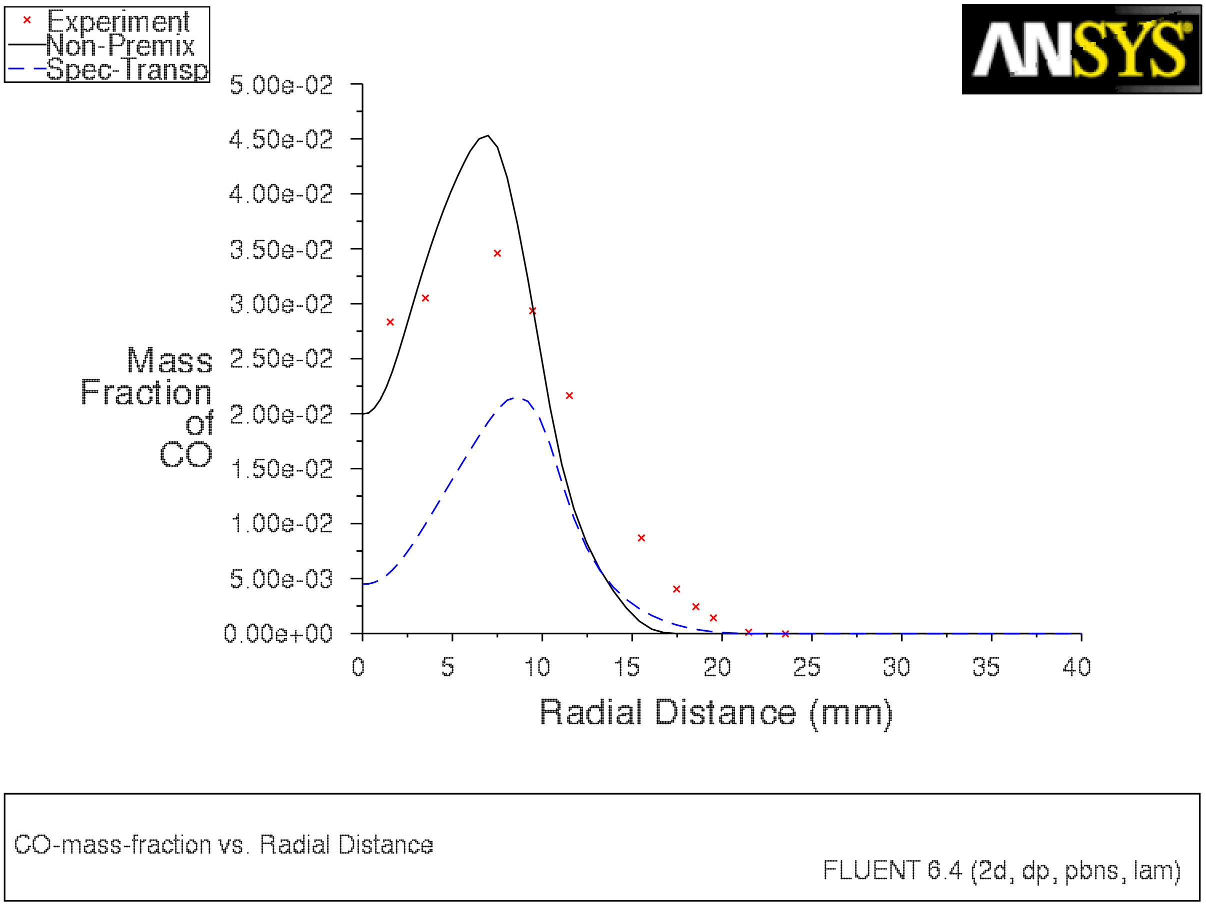


Figure 19.4.15: Mass-Fraction of CO vs Radial Distance at an Axial Distance of 40mm

Release 12.0 © ANSYS, Inc. January 24, 2009

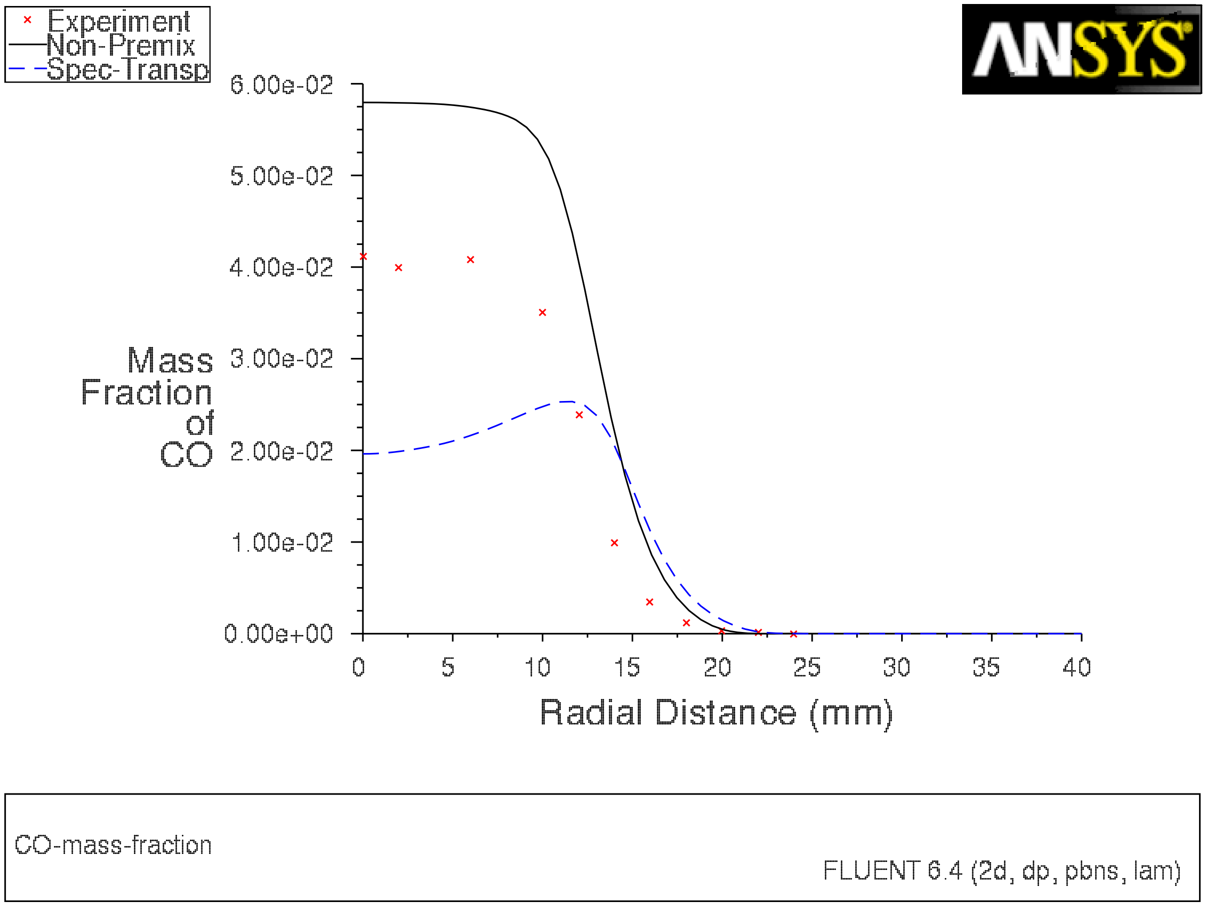


Figure 19.4.16: Mass-Fraction of CO vs Radial Distance at an Axial Distance of 75mm

Release 12.0 © ANSYS, Inc. January 24, 2009

Validation 20. Inviscid High Pressure Hydrogen Flow with Real Gas Effects

20.1 Purpose

The purpose of this test this is to compare ANSYS FLUENT's predictions of pressure, and temperature, using the real-gas model and the pressure-based solver, with the analytical data of Mohamed and Paraschivoiu [1], and with ANSYS FLUENT's predictions using ideal-gas assumptions. The analytical results used are calculated along the center line of the shock tube at a flow time of 6.0e-05 seconds.

20.2 Problem Description

A long hydrogen filled shock tube of L = 1 m, with a cross sectional area, A = 0.01 m^2 is modeled here. Flow is considered to be inviscid. The analytical results were obtained using the Beattie-Bridgeman equation of state [1] to model the real gas effect. The ANSYS FLUENT model is based on the modified Redlich-Kwong equation of state by Aungier [2].

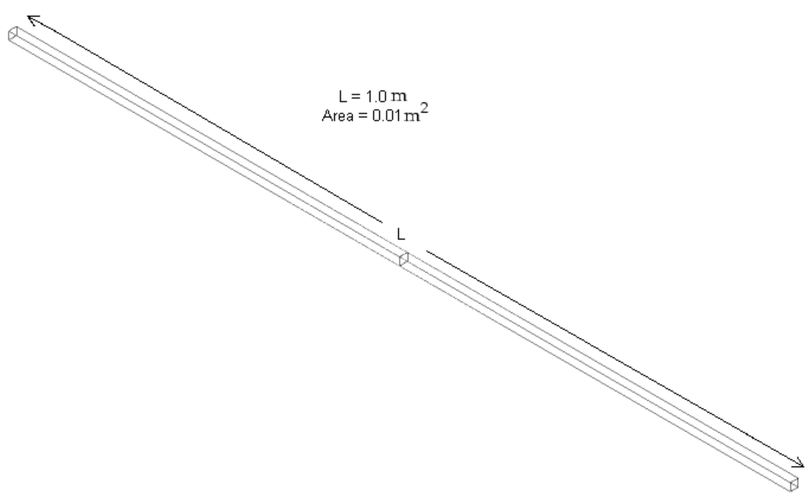


Figure 20.2.1: Problem Description

20.3 References

1. K. Mohamed and M. Paraschivoiu. *Real Gas Numerical Simulation of Hydrogen Flow.* In 2nd International Energy Conversion Engineering Conference, Providence, Rhode Island, Aug. 16-19, 2004.

2. Aungier, R.H. (1995). A Fast, Accurate Real Gas Equation of State for Fluid Dynamic Analysis Applications. *Journal of Fluids Engineering*, 117 (2), 277-281.

20.4 Results

The ANSYS FLUENT predictions of pressure along the center line of the shock tube are compared with the corresponding analytical results from Mohamed and Paraschivoiu [1] in Figure 20.4.1. Figure 20.4.2 shows a comparison of ANSYS FLUENT's predictions of temperature along the center line of the shock tube with the corresponding analytical results from Mohamed and Paraschivoiu [1]. In each case, ANSYS FLUENT predictions generated using ideal-gas assumptions are also included for the purpose of comparison. All ANSYS FLUENT predictions and analytical results are for a flow time of 6.0e-05 seconds.

20.4.1 Validation-Specific Information

Solver:	ANSYS FLUENT 3D Double Precision
Version:	12.0
Solution Files:	1. `realgas_shock-tube.cas`, `realgas_shock-tube.dat`
	2. `idealgas_shock-tube.cas`, `idealgas_shock-tube.dat`

These solution files are available from the User Services Center as described in the Introduction.

Release 12.0 © ANSYS, Inc. January 24, 2009

20.4.2 Plot Data

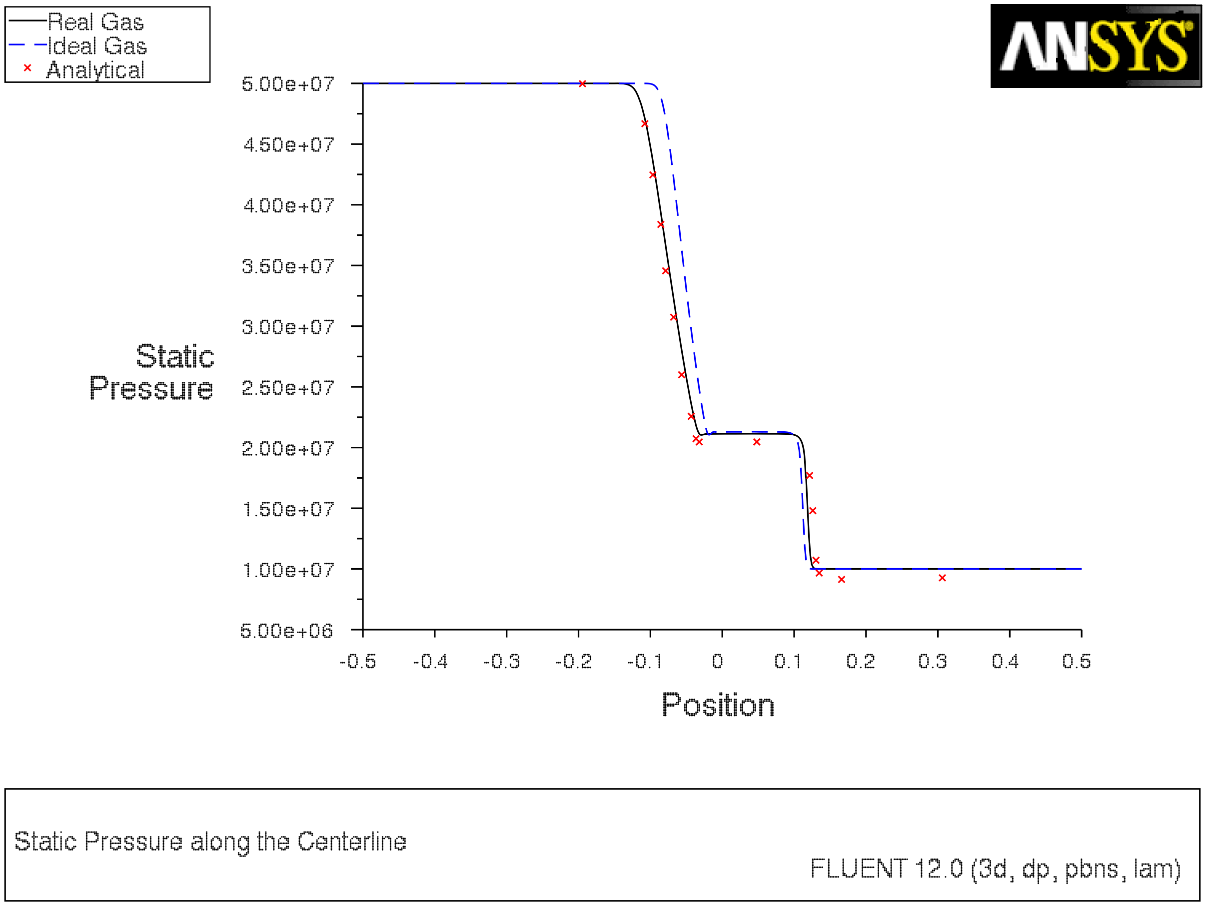


Figure 20.4.1: Pressure vs. Distance Along the Center Line

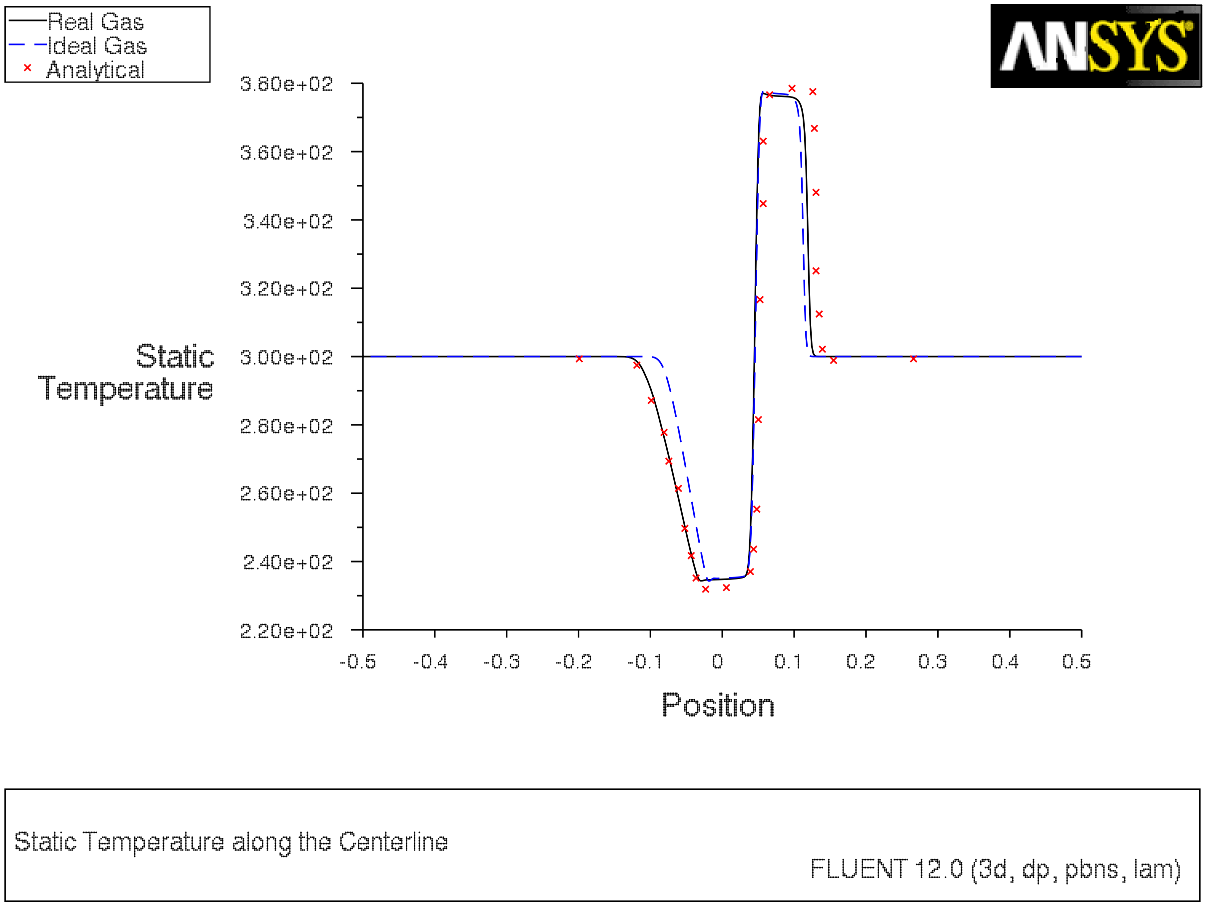


Figure 20.4.2: Temperature vs. Distance Along the Center Line

Release 12.0 © ANSYS, Inc. January 24, 2009